The noisy brain in infancy: A neurobiological marker of normative social development

Meghan Hill Puglia
Charlottesville, VA

B.S., The Pennsylvania State University, 2009
M.A., The University of Virginia, 2015

A Dissertation presented to the Graduate Faculty
of the University of Virginia in Candidacy for the Degree of
Doctor of Philosophy

Department of Psychology

University of Virginia
August 2019

James P. Morris, Ph.D.
Jessica J. Connelly, Ph.D.
Tobias Grossmann, Ph.D.
Brian P. Helmke, Ph.D.

To Luke,

You earned this just as much as I did.

Acknowledgements

First and foremost, I am eternally grateful to my family for their unconditional love, support, encouragement and understanding. To properly acknowledge everyone and all they have given me would require another dissertation. Suffice it to say, without my mother, Sue, nurturing my early curiosity and instilling in me a love of learning, my father, Ken, teaching me that if you love what you do you'll never work a day in your life, and my husband, Luke, selflessly and patiently supporting me on this journey, I would not be here today. I thank my advisors, Jess Connelly and Jamie Morris, for their mentorship, for providing such a unique and collaborative training environment, and for allowing me to explore my scientific curiosities unbridled. I am grateful to all the members of the Social Neuroscience, Connelly, and UVA Baby Labs for sharing stimulating scientific discussion, expertise, ideas, data, and cheesy snacks. Finally, I thank my research assistants and the families and participants who took part in these studies, without whom there would be no data.

Abstract

Humans display a set of perceptual biases to social stimuli that are apparent early in life and set the stage for subsequent social-cognitive development. However, the degree to which different individuals show these perceptual biases and are ultimately successful at advanced social-cognitive processes varies, and in extreme cases may be indicative of disorders like autism. Successful social functioning has strong links to health outcomes; therefore, discovering the neurobiological factors that contribute to optimal social development is an important goal of widespread multidisciplinary interest. Using an individual-differences approach, this dissertation links social-behavioral outcomes to epigenetic differences within the oxytocinergic system and complexity and variability in neural signals, or "neural noise."

It has been hypothesized that oxytocin exerts its effects on social behavior by increasing the salience of social information. This dissertation examines a neural mechanism for this hypothesis – that oxytocin increases the salience of social information by enhancing neural noise in response to social stimuli. In addition to its traditionally understood role regulating social behavior, oxytocin also acts as a neuromodulator that balances neural inhibition and excitation and regulates the signal-to-noise ratio in the brain. Therefore, early-life differences in the oxytocinergic system may trigger variable levels of neural noise during social perception and ultimately set differential developmental trajectories.

Measures of neural noise capitalize upon the inherently fluctuating nature of the brain to quantify moment-to-moment variability and complexity in neural signals. This

work has revealed that neural noise increases during development, is positively associated with behavioral performance, and presents in aberrant levels in neurodevelopmental disorders like autism.

This dissertation encompasses three studies that test the hypothesis that neural noise plays a predominant role in establishing the salience of social information early in life through a process governed by the endogenous oxytocinergic system. Study 1 identifies for the first time that brain signal entropy during social perception is associated with oxytocinergic system function and social-behavioral outcomes during the first year of life. Study 2 establishes that stimuli within the auditory domain, specifically, drive these oxytocinergic-entropy-behavior associations in infancy, and replicates work of others showing an increase in brain signal entropy cooccurs with development. Study 3 demonstrates age-related changes in brain signal entropy across modalities – adults show associations between brain signal entropy and social behavior in both the visual and auditory domains.

These neurobiological markers of normative social development may be used to identify individuals at risk for atypical development before overt clinical behaviors manifest. The results of these studies provide insight into the infant's developing brain and identify molecular and neural signatures reflective of differential developmental trajectories that persist into adulthood.

Table of Contents

1 Introduction

1.1 Background

1.1.1 The continuum of human sociality

Successful organisms must be able to detect and appropriately utilize important environmental cues. For humans, social cues are often particularly relevant and informative, and are typically considered a highly salient class of stimuli[1]. The ability to perceive, interpret, and respond to complex and dynamic social information is critical for the development of adaptive learning and behavior, and ultimately facilitates the formation of important social relationships.

The first year of life constitutes a time of rapid and sweeping changes in behavioral repertoire, cognitive ability, and neural architecture. During this time, developing infants are confronted with the daunting task of making sense of the world as they are bombarded with competing, fluctuating, and often ambiguous external stimuli. Understanding how the brain comes to form accurate models of the external world and generate appropriate behavioral responses is a significant and critical question of widespread multidisciplinary interest.

Infants, and their brains, enter the world primed to take in social information – within the first few hours of life, and potentially even in utero[2], the developing human already displays an attentional bias to socially-relevant cues such as faces[3–5]and voices[6,7]. This attentional bias is posited to reflect a broadly-tuned biological predisposition that sets the stage for subsequent experience-dependent perceptual and neural specialization[8,9].

However, the extent to which social stimuli automatically capture attention varies across individuals. For example, individuals diagnosed with autism spectrum disorder (ASD) often show reduced attention to social stimuli[10–12]. This diminished social attention is apparent very early in life; infants that will go on to receive an autism diagnosis can already be distinguished from typically developing infants by 6 months of age based only on their fixation patterns to social stimuli[13].

While social dysfunction is a hallmark of several disorders including autism, it is increasingly understood that human social behavior is not limited to diagnostic categories, but rather exists on a continuum that is normally distributed[14] and heritable[15] in the general population. For example, in a mixed sample of autistic and typically developing children, it was the amount of time looking at faces that predicted a child's face recognition ability in a separate task, not their diagnostic status[16]. This continuum not only manifests as individual differences in social behavior, but is also reflected in individual differences in the brain's response to social stimuli. For example, we find in a neurotypical, healthy young adult population, that their neural response to biological motion – an important social cue[17] – is explained by the degree to which they display autistic-like traits[18].

Identifying the developmental, neural, and molecular mechanisms that account for individual differences in specific behaviors, such as perceptual bias to social stimuli, across the full range of the social-behavioral continuum will better inform our understanding of the etiology of complex neurodevelopmental disorders[8] and the ontogeny of social behavior.

1.1.2 Oxytocin, social behavior, and neuromodulation

One particularly relevant molecule for regulating social behavior is oxytocin[19,20]. A peripheral hormone and central neuromodulator, oxytocin influences a variety of social and affective processes including affiliative behaviors[21], care-giving[22], and attention to faces[23]. It has been proposed that oxytocin exerts its effects on social behavior via a general effect on basic biological systems that facilitate the detection of and orientation to social information[24,25], thereby increasing the salience of social information.

The actions of oxytocin are dependent upon the expression of its receptor, which is encoded by the oxytocin receptor gene (*OXTR*, hg38_chr3:8,750,409-8,769,614)[26]. Differences in *OXTR* expression likely play a major role in the function of the endogenous oxytocinergic system. Methylation of 5′-Cytosine-phosphate-Guanine-3′ (CpG) dinucleotide pairs in DNA is a highly investigated epigenetic modification that may influence behavioral phenotypes. DNA methylation within the promoter region of *OXTR* is variable within the population[27,28], and methylation of specific *OXTR* CpG sites reduces transcription of the gene[27,29]. Therefore, individuals with lower levels of *OXTR* methylation at these sites are presumed to have an increased ability to use endogenous oxytocin.

Our previous work with this epigenetic modification has provided support that the oxytocinergic system is involved in ascribing salience to social information. We were the first to establish that *OXTR* methylation is associated with differential neural response and functional coupling within regions supporting social perception and emotion processing[28]. We subsequently showed that neurotypical individuals with increased *OXTR* methylation require the recruitment of additional attentional resources to attend to social information

embedded within a complex display[30], suggesting those with presumed diminished ability to use endogenous oxytocin fail to ascribe salience to social information.

Here, we consider a mechanism by which oxytocin might increase the salience of social information. Oxytocin has been shown to directly regulate brain signal variability in rodents[31–34]. We hypothesize that oxytocin increases the salience of social information by increasing neural noise in response to social stimuli.

1.1.3 Neural "noise" is more than just noise

Noise is a fundamental property of neural systems at multiple hierarchical levels, from the dynamics of ion channels to the convergence of multiple independent synaptic inputs[35,36]. Recent work has capitalized on this inherently fluctuating nature of the brain to understand how variability in neural signal, which is often modeled out of analyses as mere "noise," may serve a valuable functional role[35–39].

Neural variability measured via electroencephalography (EEG) and functional magnetic resonance imaging (fMRI) shows significant differences across age groups[40–46], which may reflect changes in synaptic pruning, myelination, and the formation of functional networks that occur during development[41]. Moment-to-moment measures of brain activity have also shown strong associations with behavioral outcomes, such that individuals with increased neural variability produce more consistent and accurate responses[42,47,48].

Stochastic resonance describes the phenomenon in which the addition of a moderate amount of random noise can counterintuitively enhance signal detection by improving the fidelity of an underlying signal (Figure 1-1)[36]. Such variability in brain activity also

facilitates the exchange of information between neurons[49], enhancing neural synchrony and promoting the formation of robust, adaptable networks that are not overly reliant on any particular node and display a greater dynamic range[36,50,51]. Together, these functions suggest that neural variability may act to appropriately weight incoming information such that important stimuli are maximally salient and enable the most flexible behavioral response.

However, inadequate or excessive neural variability provides inconsistent representations of the external world (Figure 1-1), which might result in poorly integrated neural networks and detrimental behavioral outcomes. Indeed, neural variability levels are abnormal in a range of developmental disorders[52] including autism[51,53–58]. Furthermore, infant siblings who are at high risk for developing autism can be distinguished from infants who do not have a sibling diagnosed with autism based on neural variability levels alone, suggesting a genetic predisposition may contribute to both autism and aberrant levels of brain signal variability[59].

Oxytocin has been shown to directly regulate the firing rate of neurons in rodents, enhancing the signal-to-noise ratio, balancing neural inhibition and excitation, and improving information transfer[31–34]. Indeed, when synaptic excitation and inhibition are properly balanced, signal variability is optimal and the neural system displays maximum information capacity, information transmission, and dynamic range[37,49].

1.2 Approach

1.2.1 Quantification of neural noise

Across three studies, we employed two methods for quantifying brain signal variability: standard deviation (SD) to measure overall distributional width (variance) of the signal, and multiscale entropy (MSE) to measure temporal irregularity across time scales in the signal.

Standard Deviation Analysis. Quantifying the variance of a time series simply involves calculating SD either across the time series as a measure of distributional width[60], or across trials as a measure of the reliability of the evoked response[54].

Multiscale Entropy. MSE computation involves 1) coarse graining the time series to scale *s* by averaging together *s* successive, non-overlapping data points, and 2) computing sample entropy[61]. Sample entropy is a measure of signal irregularity which determines how frequently a pattern of length *m* repeats relative to a pattern of length *m*+1. A similarity criterion, *r*, is set as a proportion of the standard deviation of the time series to determine what points are considered indistinguishable. For any data point *u*, all points within $u \pm r$ are considered indistinguishable. Then, the natural log of the ratio of the count of *m* patterns to the count of *m*+1 patterns is computed. Higher sample entropy values therefore indicate higher irregularity in the data because patterns of length *m*+1 reoccur less often than patterns of length m (Figure 1-2).

In Costa's original MSE algorithm[61], *r* is calculated as a percentage of SD of the original time series and remains constant across all scales. However, this method conflates entropy with variance (Figure 1-3)[62,63]. We therefore used a modified algorithm[62] that recalculates *r* at each scale as a percentage of SD of the coarse-grained time series. While many studies consider entropy at a single time scale (typically the native sampling rate),

computing entropy over multiple time scales distinguishes truly complex signals, such as those found in biological systems, from completely random or completely deterministic signals (Figure 1-4) because complexity in biological systems is characterized by variability over many time scales[64]. Computing the area under the MSE curve (MSE_{AUC}) provides a comprehensive picture of the temperodynamic structure of a time series.

Both SD[47,54,55,65] and MSE[41,42,45,59,66,67] have been positively associated with developmental and behavioral outcomes. MSE and SD are considered independent but complementary functions of neural variability. Although it remains unclear exactly how these measures relate[37], MSE and SD typically result in anticorrelated values. Because entropy explicitly incorporates signal SD when defining the similarity criterion *r*, *r* is larger for a signal with greater SD, meaning the entropy algorithm is more likely to identify matches resulting in a lower entropy value[68]. However, only MSE is sensitive to temporal dependencies in a time series (Figure 1-5).

No study to date has directly compared the explanatory power of these two variability measures in a single model, nor considered a role for oxytocinergic system function as an underlying molecular mechanism capable of driving brain signal variability during social perception in humans.

1.2.2 Assay of individual differences in oxytocinergic system function

We used *OXTR* methylation as a measure of individual differences in oxytocinergic system function at CpG site -934 (hg38_chr3:8,769,121-8,769,122). We have previously assayed methylation levels from all CpG sites within two *OXTR* CpG islands and shown that the level of DNA methylation specifically at site -934 is (1) significantly negatively

associated with gene expression in human cortex[27], suggesting a regulatory role in gene transcription, (2) highly variable in the general population and associated with neural response during social-perceptual tasks in neurotypical adults[28,30,69], suggesting it is a viable marker of individual differences in (endo)phenotypes, and (3) elevated in the brain and blood of both individuals with autism[27] and vole pups who experienced lower parental care early in life[70], suggesting this marker is indicative of individual developmental differences that are reflected in both causative (brain) and peripheral (blood) tissue.

1.2.3 Statistical modeling

We employed a multivariate, exploratory approach to develop models of our hypothesized epigene-brain-behavior associations with partial least squares path modeling (PLS-PM). PLS-PM is a prediction-based multivariate method for modeling theorized complex relationships among observed and latent variables[71]. Particularly given the novelty of the present research, PLS is better suited than other multivariate techniques like covariance-based structural equation modeling (CBSEM) because PLS is considered optimal for exploratory, prediction-based research where theory is less developed[71,72]. Complex models with many observed variables and relationships can be estimated with smaller sample sizes with PLS than required by CBSEM[72]. Unlike CBSEM, PLS is a nonparametric technique which makes no assumptions about the normality of the distribution of the data. Furthermore, PLS is well suited to the highly dimensional, highly correlated nature of neuroimaging data (i.e. among many electrodes, voxels)[73]. For these reasons, PLS has become a popular and commonly used modelling technique within neuroimaging[37,41,42,47,48,60,66,74].

1.2.4 Specific aims

This dissertation encompasses three studies that test the hypothesis that neural noise plays a predominant role in establishing the salience of social information early in life through a process governed by the endogenous oxytocinergic system. We aim to identify what metrics of brain signal variability offer the greatest explanatory power for associations between individual differences in the oxytocinergic system and human social behavior, and under what conditions brain signal variability is exploited to benefit social behavior. Finally, this dissertation aims to establish the developmental trajectory of brain signal variability on social behavioral outcomes during the first year of life and into adulthood.

1.3 Figures

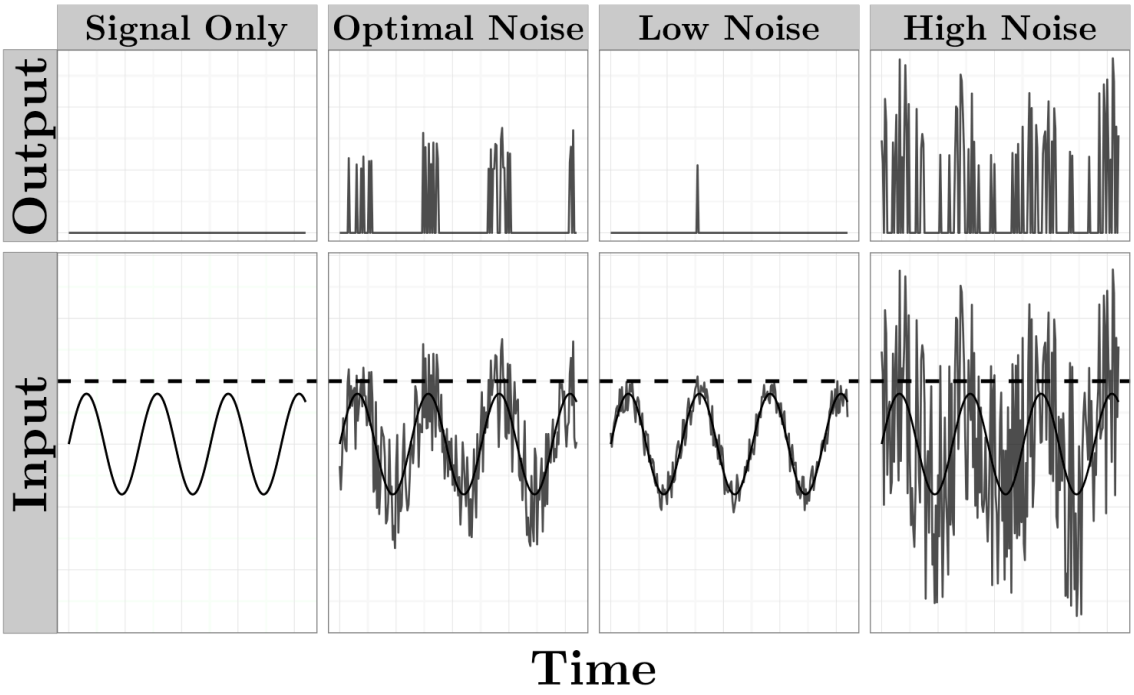

Figure 1-1. Adding random noise to a signal enhances signal detection. A signal that is below the threshold for detection (panel 1) can be enhanced and more accurately represented by the addition of a moderate amount of random noise (panel 2). However, inadequate (panel 3) or excessive (panel 4) noise provides inconsistent representations of the signal.

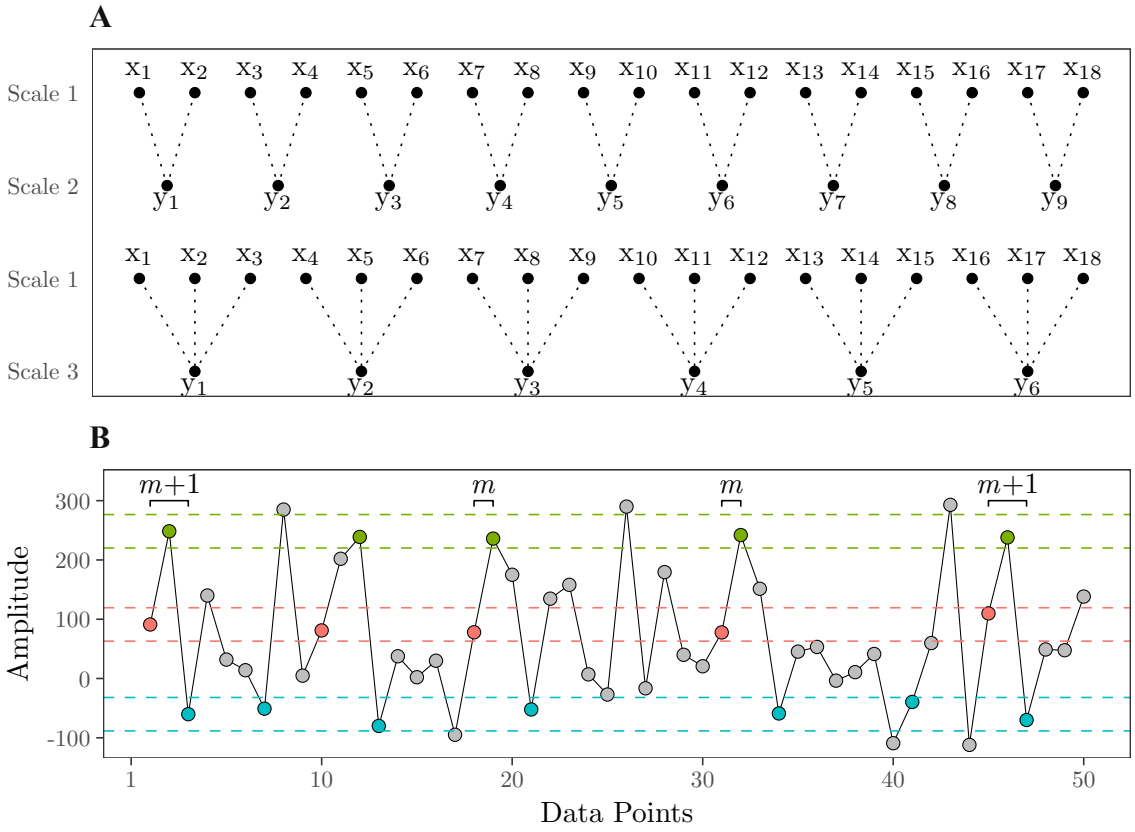

Figure 1-2. The multiscale entropy algorithm illustrated. (A) A coarse-grained time series is first computed for scale *s* by averaging together *s* consecutive, non-overlapping data points of the original time series (Scale 1). Entropy is then calculated on the coarse-grained time series. **(B)** Entropy measures the irregularity in a time series by determining how frequently a pattern of length *m* repeats relative to a pattern of length *m*+1. A similarity criterion, *r*, is set as a proportion of the standard deviation of the time series to determine what points are considered indistinguishable. For any data point *u*, all points within $u \pm r$ (illustrated with dashed lines) are considered indistinguishable. In this example, if $m = 2$, the first pattern of length *m* (points 1 and 2: red, green) repeats 4 times, whereas the first pattern of length *m*+1 (points 1, 2, 3: red, green, blue) repeats 2 times. The pattern template is then shifted forward 1 point such that matches of pattern *m* consisting of points 2 and 3, and pattern *m*+1 consisting of points 2, 3, and 4, are counted, and so on. Entropy is then calculated as the natural log of the ratio of the count of all pattern-length *m* repeats to the count of all pattern-length *m*+1 repeats: $ln\left(\frac{m}{m+1}\right)$. Consequently, low entropy values indicate regularity in a time series; if pattern length *m*+1 occurs as often as pattern length *m*, e.g.: $ln\left(\frac{4}{4}\right) = ln(1) = 0$. Conversely, high entropy values indicate high irregularity because patterns of length *m*+1 occur less often than patterns of length *m*, e.g.: $ln\left(\frac{4}{2}\right) = ln(2) = 0.69$.

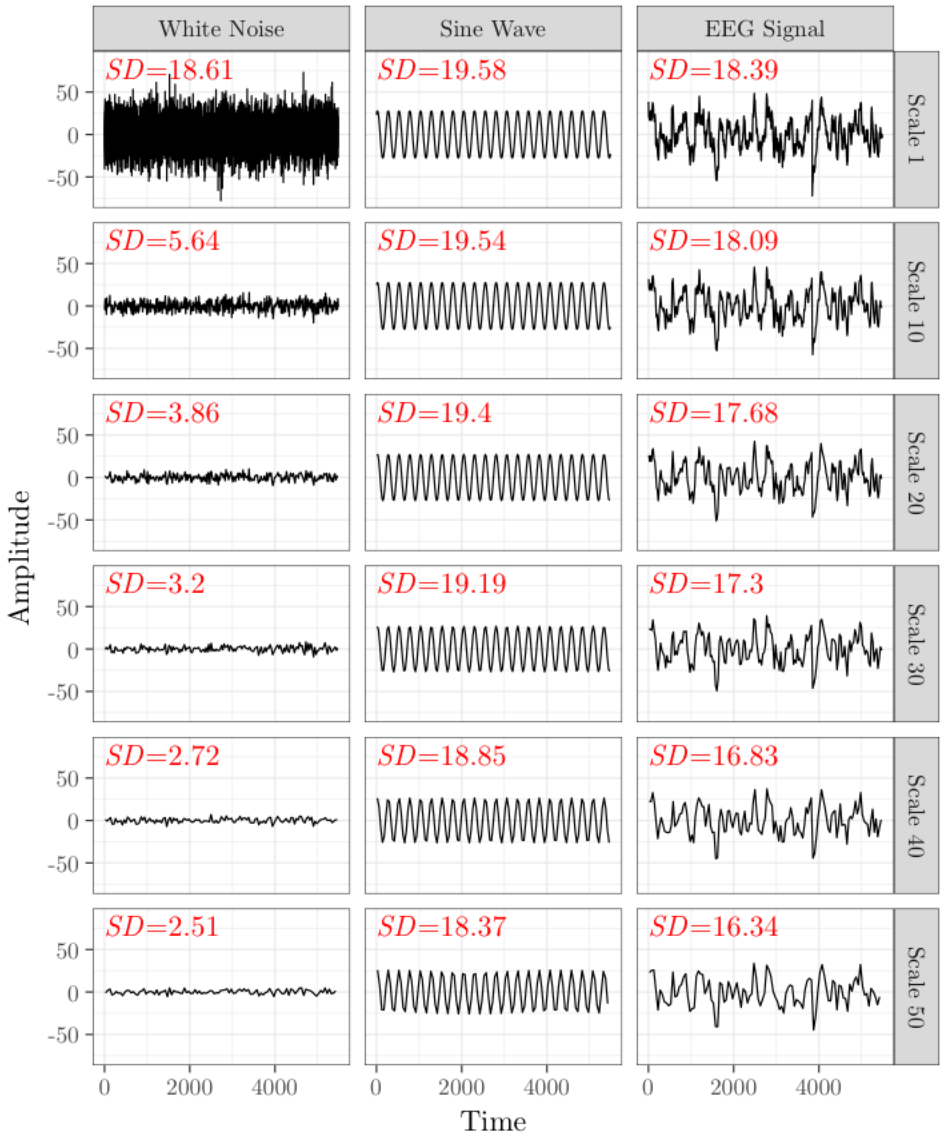

Figure 1-3. Coarse graining differentially impacts standard deviation across signal types. The original multiscale entropy curve involves setting the similarity criterion, *r*, as a proportion of the standard deviation (*SD*) of the native time series (Scale 1) and applying the parameter to all subsequent time scales. However, *SD* will decrease as the scaling factor increases according to the statistical properties of the original time series. Here we plot a time series and its *SD* for simulated white noise (left), a sinusoidal wave (middle), and EEG signal (right) over scales 1, 10, 20, 30, 40, and 50. *SD* decreases most for white noise and least for the sine wave.

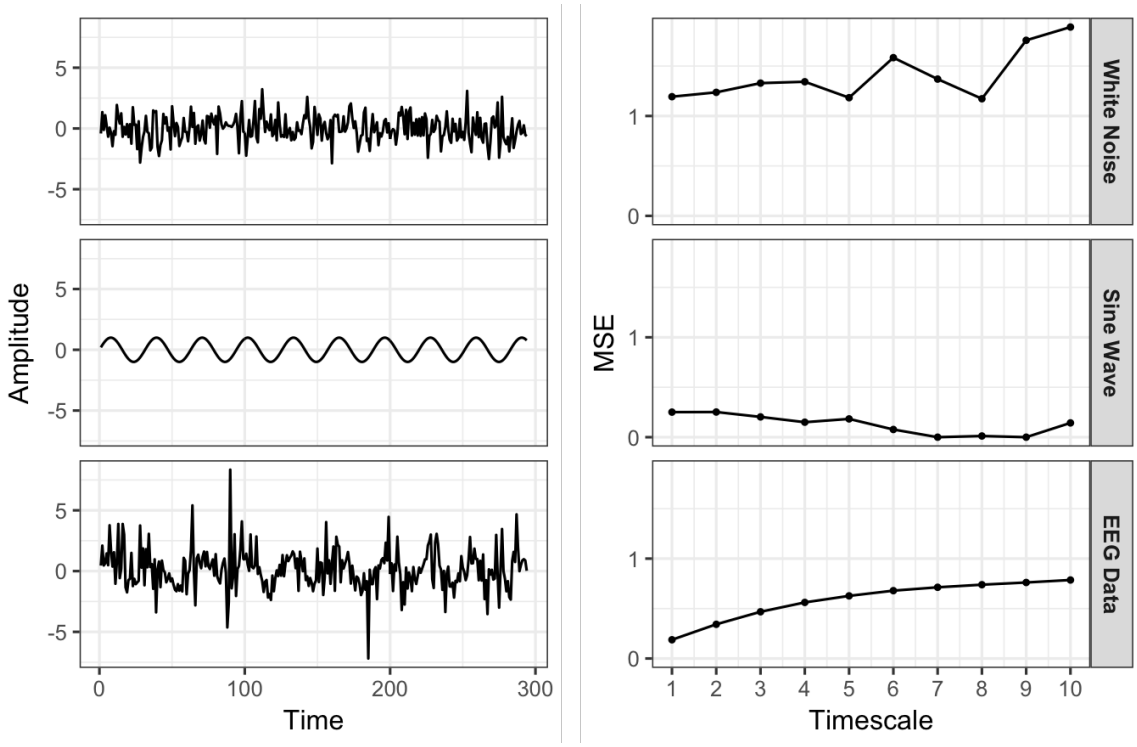

Figure 1-4. Multiscale entropy distinguishes signal types. Multiscale entropy assesses the irregularity of a time series across multiple time scales. (Top) White noise displays a highly irregular pattern across time scales; entropy is therefore high and remains high across the coarse graining procedure. (Middle) A sinusoidal wave is completely regular and deterministic; entropy is therefore low and remains low across the coarse graining procedure. (Bottom) A biological signal, here EEG, contains both random and deterministic properties. Entropy therefore increases across the coarse graining procedure because new information is revealed at all scales.

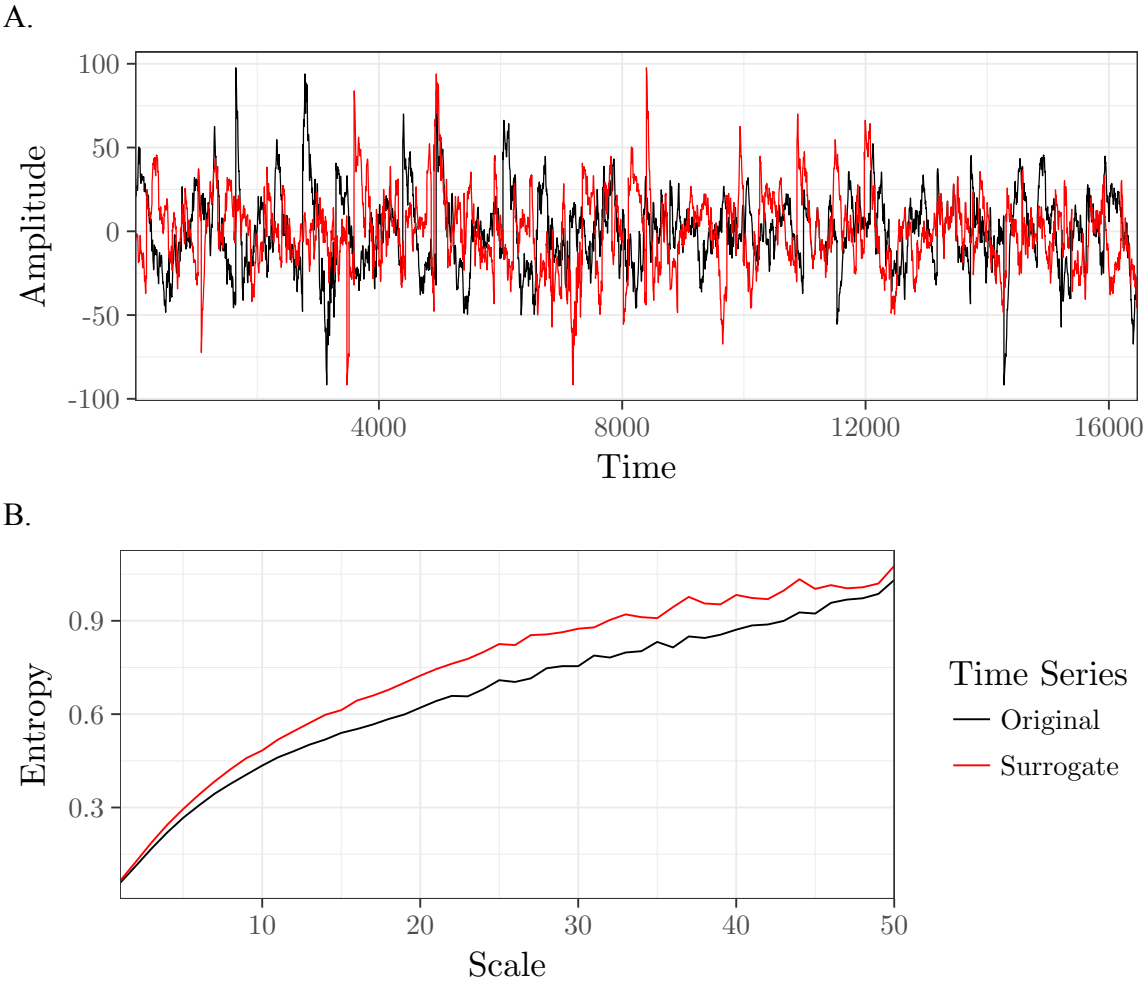

Figure 1-5. Multiscale entropy is sensitive to temporal dependencies in a time series. (A) We created a surrogate time series (red) by randomly shuffling segments of the original time series (black) consisting of actual EEG data from one trial. The standard deviation of the original and surrogate time series are equivalent, 22.63. (B) We find higher entropy for the surrogate time series (red) than the original time series (black) across time scales because the scrambling procedure introduced greater irregularity into the surrogate time series.

2 Study 1: Associations between oxytocinergic system function, neural noise, and infant behavior

2.1 Methods

2.1.1 Participants

We report on a previously-acquired longitudinal dataset in which 96 Caucasian infants (49 female) provided a saliva sample at 5 months of age (M = 147.71 ± 14.75 days) which we subjected to *OXTR* methylation analysis. At 8 months of age (M = 247.85 ± 6.00 days), infants returned to participate in an EEG paradigm in which they were presented with auditory clips of human vocalizations[75] which we subjected to brain signal variability analysis. Infant behavior was assessed using the Revised Infant Behavior Questionnaire (IBQ-R), a widely used and validated measure of infant behavior and temperament across 14 domains based on parental report[76]. Ethical approval was obtained from the University of Leipzig Ethics Committee.

2.1.2 DNA collection and isolation

Infant Samples. Passive drool was collected from infants at five months of age using CS-2 sponges and OG-250 kits (DNA Genotek, Ottawa, Canada), and was stored at room temperature until DNA isolation. Collection kits were incubated at 50°C for 1 hour, then centrifuged for 10 minutes at 200 rcf to release all liquid from sponges. 500 µL of saliva was used to isolate DNA using the manual purification protocol from DNA Genotek. DNA was stored in Hydration Solution (10 mM Tris, 1 mM EDTA, pH 7-8, Qiagen, Hilden, Germany) and quantitated using nanodrop. Insufficient DNA was available from the samples provided by 2 infants. These infants were excluded from the analysis.

Tissue Comparison Study. To determine the reliability of *OXTR* methylation values obtained from saliva, we performed a tissue comparison study in which 207 healthy Caucasian adults (114 females) aged 16 to 81 ($M = 37.74 \pm 22.95$) provided 5 mL passive drool in a Falcon 50mL Conical Centrifuge Tube (Fisher Scientific, Hampton, NH) for assessment of saliva methylation and 8 mL blood in either mononuclear cell preparation tubes (BD Biosciences, Franklin Lanes, NJ) for assessment of mononuclear cell methylation ($n = 142$), or PAXGene Blood DNA Tubes (Qiagen, Valencia, CA) for assessment of whole blood methylation ($n = 182$). One hundred seventeen participants provided all three sample types. Saliva cells were pelleted in 20 mL 1x phosphate-buffered saline (Life Technologies, Carlsbad, CA) by centrifuging at 1800 rcf for 5 mins. Pellets were then transferred into a microcentrifuge tube and frozen at -20°C prior to DNA extraction. We isolated DNA from saliva cells using reagents supplied in the QIAamp DNA Blood Mini Kit (Qiagen, Valencia, CA) following Qiagen's Supplemental Protocol for Isolation of Genomic DNA from Saliva. We isolated DNA from peripheral blood mononuclear cells using reagents and protocol supplied in the Gentra Puregene Blood Kit (Qiagen, Valencia, CA). We isolated DNA from whole blood using reagents and protocol supplied in the PAXgene Blood DNA Kit (Qiagen, Valencia, CA).

2.1.3 Epigenetic analysis

We subjected two hundred nanograms of DNA to bisulfite treatment (Kit MECOV50, Invitrogen, Carlsbad, CA), which converts non-methylated cytosines to uracil for downstream detection of methylated cytosines by sequencing. We amplified a 116-base pair region of *OXTR* containing CpG Site -934 via polymerase chain reaction (PCR) using

12 nanograms of bisulfite-converted DNA, 0.2 μM primers TSL101F (5′-TTGAGTTTTGGATTTAGATAATTAAGGATT-3′) and TSL101R (5′-biotin-AATAAAATACCTCCCACTCCTTATTCCTAA-3′), and reagents supplied in the Pyromark PCR kit (Qiagen, Valencia, CA). Underlined nucleotides in primer set indicate the insertion of an A or C nucleotide at a variable position (C/T) due to a CpG site within the primer. Samples were amplified in triplicate on three identical PCR machines (S1000 Thermal Cycler, Biorad, Hercules, CA) with the following cycling conditions [Step 1: (95°C/15 min)/1 cycle, Step 2: (94°C/30 s, 56°C/30 s, 72°C/30 s)/50 cycles, Step 3: (72°C/10 min)/1 cycle, Step 4: 4°C hold]. Pyrosequencing was performed using primer TSL101S (5′- AGAAGTTATTTTATAATTTTT-3′) on a Pyromark Q24 using PyroMark Gold Q24 Reagents (Qiagen, Valencia, CA).

On average, replicates deviated from the mean ± 1.66% for the tissue comparison study, and ± 1.83% for infant samples. Adult PBMC methylation levels averaged 47.39 ± 6.42%, adult whole blood methylation values averaged 46.61 ± 8.11%, adult saliva methylation values averaged 45.33 ± 6.46%, and infant saliva methylation levels averaged 40.34 ± 4.69%.

2.1.4 EEG acquisition and preprocessing

EEG acquisition information is detailed in Missana *et al.* (2017)[75]. In brief, EEG was recorded from 27 Ag/AgCl electrodes affixed to an elastic cap (EasyCap GmbH, Germany) using the 10–20 electrode placement system. The horizontal electrooculogram (EOG) was recorded from two electrodes (F9, F10), which are part of the cap located at the outer canthi of both eyes. The vertical EOG was recorded from an electrode on the

supraorbital ridge (FP2), which is part of the cap and an additional single electrode on the infraorbital ridge of the right eye. The data were sampled at a rate of 500 Hz, amplified using a Porti-32/M-REFA amplifier (Twente Medical Systems International), and online referenced to Cz.

EEG preprocessing was completed using EEGLab, v14.1.1[77]. Data were bandpass filtered (0.3 to 20 Hz), re-referenced to the average of all scalp electrodes, and segmented into stimulus-evoked epochs 100 ms before stimulus onset to 1000 ms post stimulus onset with pre-baseline correction. To assess ongoing variability, we also randomly extracted 1100 ms epochs that were not time-locked to the onset of a stimulus and did not overlap with stimulus-evoked epochs (i.e. from within the inter-stimulus interval). Epochs contaminated with excessive amplitude standard deviations (> 100 μV in ocular electrodes, > 80 μV in scalp electrodes) within a sliding window of width 200 ms and step 100 ms were discarded as artifacts. Participants with at least 30 artifact-free auditory-evoked trials (10 from each social-auditory condition) and 30 artifact-free ongoing trials (n = 70) were retained in the analysis. This rejection rate (27.1%) can be compared to that reported in a meta-analysis of 149 infant EEG studies that found an average rejection rate of 49.2%[78]. As an additional artifact rejection step, we then completed an Independent Component Analysis to remove components with clear ocular, muscular or electrical artifacts. On average 4.43 (range 2 to 10) components were removed. The number of components removed did not correlate with MSE (r = .17, p = .171) or SD (r = -.08, p = .519) metrics, and removed components did not show significant event-related potential (ERP) effects (Figure 2-1**,** Table 2-1), indicating that removed components were correctly identified as

artifacts. Because the number of data points included in MSE calculation can influence reliability of the estimates[63], we selected the 30 auditory-evoked (10 from each social-auditory condition) and 30 ongoing trials with total global field power (GFP)[42] closest to the median GFP for each participant for inclusion in downstream analyses (16470 data points per condition). To ensure that these preprocessing procedures did not obscure or eliminate relevant evoked response, we reproduced all results from Missana *et al.* (2017)[75] using these data re-referenced to the average of the mastoids (Figure 2-1, Table 2-1).

2.1.5 Quantification of brain signal variability

Brain signal variability can be quantified in many ways[37]. Here we consider two of the most commonly applied measures of brain signal variability – SD, a measure of the distributional width of a signal, and MSE, a measure of temporal irregularity.

Multiscale Entropy. We computed MSE on the residuals of the EEG signal (i.e. after subtracting the within-person average ERP) for scales 1 to 100 (500 to 5 Hz) for the 30 auditory-evoked and 30 ongoing trials for each scalp electrode using the algorithm described in Grandy et al. (2016)[63] for estimating MSE across discontinuous segments, modified to recalculate r for each scale. Parameter values were set to pattern length $m = 2$ and similarity criterion $r = .5$.

Here, we consider the area under the MSE curve (MSE_{AUC}) for each electrode for scales 1 to 100 (corresponding to 500 to 5 Hz) to obtain a comprehensive picture of the temperodynamic structure of our data. Average MSE curves are plotted in Figure 2-2 and average MSE_{AUC} values are listed in Table 2-2. We also consider entropy at scales 1 (MSE_1, 500 Hz), 50 (MSE_{50}, 10 Hz), and 100 (MSE_{100}, 5 Hz) to assess the impact of specific time

scales on our models. We find across all electrodes, scales 37 to 60 (8 to 13 Hz) show the highest correlation with MSE_{AUC}, suggesting these scales, in particular, may drive our results with MSE_{ACU}.

Standard Deviation Analysis. To quantify variance in the EEG signal, we calculated SD on the residuals of the EEG signal (i.e. after subtracting the within-person average ERP) for the 30 auditory-evoked and 30 ongoing trials for each scalp electrode using two methods commonly reported in the literature. Specifically, SD can be calculated across the time series as a measure of distributional width (SD_{CONT})[60], or across trials as a measure of the trial-by-trial reliability of the evoked response (SD_{TXT})[54]. These computation methods yield highly correlated SD values (all rs $\geq$ .99). To equalize data volume and computation across our brain signal variability metrics, we also consider the area under the course-grained SD curve (SD_{AUC}), and SD at scales 1 (SD_1, equivalent to SD_{CONT}), 50 (SD_{50}), and 100 (SD_{100}).

Finally, as we are particularly interested in understanding the unique contribution of entropy and variance of a signal on behavioral effects, we residualized SD from MSE[68] (MSE_{SDRes}). However, this computation yielded highly uncorrelated values across electrodes (Figure 2-3) such that including this measure for each electrode failed to load on to a single construct (mean loading = .01), regardless of whether considering the area under the MSE_{SDRes} curve, or MSE_{SDRes} at scales 1, 50 or 100. Attempts to identify patterns of correlation among electrodes to model separate constructs of this measure (e.g. frontal, central, posterior) failed to improve construct loadings. We therefore could not consider MSE_{SDRes} further in our current PLS-PM framework.

2.1.6 Infant behavior

Infant behavior was assessed via parental report with the IBQ-R[76], a widely used measure of infant behavior and temperament across 14 domains. Questionnaire data for 12 infants was not available. To separately consider social and non-social aspects of infant behavior, we created new Social and Non-Social IBQ-R constructs. We first identified unambiguously social and non-social items by subscore. Then, we conducted an item analysis using the psych package in R[79,80] and removed items until Cronbach's $\alpha > .70$ for all Social and Non-Social subscores or until the removal of additional items did not improve α. Subscores that did not achieve $\alpha > .60$ were not considered. Models 2 and 3 were run with Social and Non-Social Constructs both before and after item removal. Results did not appreciably change after item removal; results are presented after item removal. Individual items included in the Social and Non-Social IBQ-R constructs are listed in Table 2-3.

2.1.7 Experimental design and statistical analysis

To identify causative associations among our epigene-brain-behavior variables, we analyzed data using PLS-PM, a prediction-based multivariate method for simultaneously analyzing associations among multiple blocks of variables in which each block plays the role of a latent variable[71]. Traditionally, it is assumed that there is a system of linear associations between blocks. However, to account for potentially curvilinear associations among our biological and behavioral variables, we estimated all models using WarpPLS v6.0, the only software currently available to explicitly identify nonlinear functions connecting pairs of latent variables by performing nonlinear transformations on the

predictor latent variable scores prior to the calculation of path coefficients[81]. For all models, we estimated a reflexive outer model for all constructs using the PLS regression algorithm with WarpPLS v6.0[81]. Inner model path coefficients were estimated using the Warp2 algorithm, which tests for second-order polynomial associations among latent variables. If curvilinear associations are not found by best-fitting nonlinear functions that minimize sums of squared residuals on a bivariate basis[81], the algorithm defaults to identifying linear associations.

Outliers. After initial model fitting, values were considered outliers if the factor score fell more than 3 median absolute deviations from the median. We selected this relatively conservative criterion to balance outlier detection with subject retention. We first determined whether these outliers were driven by a single indicator within blocks. Methylation values for two subjects were identified as outliers in single replicates. These outlier replicates were removed and imputed with the mean of the other replicate values for these subjects. One subject was identified as an outlier across all three replicates; one subject was identified as an outlier in both MSE and SD factor scores; one subject was identified as an outlier in the behavioral factor scores but was not an outlier in any single behavioral indicator. These three subjects were removed and models were re-estimated. Results did not appreciably change with or without outliers; we therefore conservatively report on models excluding outliers (n = 55, 29 female).

Model Assessment. After removal of outliers, we identified indicators with negative loadings and reverse-coded these items. These items included Activity Level, Distress to Limitations, Fear, Perceptual Sensitivity, Sadness, Social Fear and Non-Social Fear.

Next, we checked for discriminant validity by identifying and removing any items that loaded higher onto another construct or did not significantly load onto its construct for each model. These included Duration of Orientation, Perceptual Sensitivity, Vocal Reactivity, Social Duration of Orientation, Non-Social Fear, Non-Social Duration of Orientation, and Non-Social High Pleasure. Removing these items did not appreciably change results; results are presented with these items removed.

Finally, we determined that the square root of the average variance extracted (AVE) was greater than the correlations between constructs. We report construct internal consistency and reliability as indexed through the composite reliability coefficient (recommended value > .60[82]), and explanatory power through R^2 values in for each model in Table 2-4. We report path coefficients (β), standard errors for path coefficients (*SE*), and *p*-values (*p*) estimated with delete-1 jackknifing for all significant effects. The oxytocinergic system, social behavior, and their related brain systems have all been shown to be sexually dimorphic[83]. We therefore tested for sex effects in our models by examining differences in path coefficients across males and females using multi-group analysis with pooled standard error.

Sample Size. After preprocessing and outlier removal, the final sample consisted of 55 participants with complete epigenetic, neural and behavioral data. To determine that we had sufficient power for our models with this sample size, we followed the recommendation of Chin & Newsted[84] to compute a power analysis based on the portion of the model with the largest number of predictors. In our models, IBQ-R constructs have the largest number of predictors – up to 3. An extensive literature review suggests a

moderate association (r = .3 to .5) between measures of neural variability and behavioral outcomes[42,47,48]. A two-tailed multiple regression power analysis[85] determined that 56 participants are needed to detect an effect size of 0.3 with 3 predictors, 95% power, and α = .05.

2.2 Results

2.2.1 Saliva is a reliable tissue for assaying *OXTR* methylation

Previous work has shown that *OXTR* methylation assayed from peripheral blood at CpG site -934 reflects the level of DNA methylation at this site in the brain[27,70] – the causal tissue for behavior. To expand this marker for use with infants, we first established that *OXTR* methylation levels in saliva, a peripheral tissue more appropriate for vulnerable populations, correspond to *OXTR* methylation levels in blood. Healthy adults provided both passive drool and intravenous blood samples for assessment of whole blood (n = 182) and/or peripheral blood mononuclear cells (PBMC, n = 142). Epigenetic analyses revealed significant correlations between *OXTR* methylation derived from saliva and whole blood ($r(180) = .75$ [95% CI: .68, .81], $p < .001$), and saliva and PBMC ($r(140) = .78$, [.70, .83], $p < .001$) at site -934 (Figure 2-4).

2.2.2 *OXTR* methylation is associated with brain signal entropy to influence infant behavior

This study is the first to directly compare the explanatory power of two commonly used measures of neural variability – MSE and SD – within one model. We hypothesized that infants with lower *OXTR* methylation (presumed increased sensitivity to endogenous oxytocin) would show increased brain signal variability during social perception, and

would also receive more positive social behavioral ratings. To test this hypothesis, we used a multivariate approach to simultaneously model the entire data structure including our epigene (*OXTR* methylation), brain (MSE, SD), and behavior (IBQ-R) measures using PLS-PM. The results of this model can be seen in Figure 2-5 and Table 2-4 (Model 1). First, we ensured that MSE_{AUC} and SD_{CONT} were identified as unique, distinguishable constructs in the model by confirming that the loadings for each electrode exceeded .5[71] for its own construct (average loading: MSE_{AUC} M = .70; SD_{CONT} M = .67), and that the cross-loadings for each electrode did not exceed .5 onto the other construct (average cross-loading: MSE_{AUC} M < .01; SD_{CONT} M < .01). We found a significant negative curvilinear association between *OXTR* methylation and MSE_{AUC} (β = -0.26, SE = 0.12, p = .014) such that infants with low *OXTR* methylation showed increased brain signal entropy. We simultaneously found a significant positive curvilinear association between MSE_{AUC} and IBQ-R (β = 0.35, SE = 0.19, p = .035) such that infants that showed greater entropy during social perception received more positive behavioral ratings. However, we did not find any significant associations between signal SD_{CONT} and *OXTR* methylation (β = 0.10, SE = 0.12, p = .197) or IBQ-R (β = -.07, SE = 0.17, p = .346). While all electrodes loaded significantly onto the MSE_{AUC} construct in our model, we obtained significantly higher loading coefficients (t = 3.12, p = .006) – indicating strongest associations in the model – for frontal and temporal electrodes (M = .74) compared to all other scalp electrodes (M = .65). A multi-group analysis revealed no significant differences in path coefficients across male and female participants (all two-tailed p values ≥ .753). Table 2-5 contains results for Model 1 using alternate MSE and SD calculation methods.

2.2.3 Evoked entropy during social perception is associated with infant social but not non-social behavior

Next, we tested the hypothesis that brain signal variability evoked during social perception would specifically account for individual differences in social, but not non-social, behaviors. To test this hypothesis, we classified items in the IBQ-R subscores into Social and Non-Social constructs (Table 2-3). The results of this model can be seen in Figure 2-6 and Table 2-4 (Model 2). We found the significant negative curvilinear association between *OXTR* methylation and MSE_{AUC} persisted (β = -0.27, *SE* = 0.17, *p* = .012), and no significant associations emerged for SD_{CONT} (*p*s ≥ .196). As hypothesized, we found that the significant positive curvilinear association between MSE_{ACU} and behavior persisted only for the Social IBQ-R construct (β = 0.27, *SE* = 0.13, *p* = .025). The association between MSE_{AUC} and the Non-Social IBQ-R construct was not significant (β = 0.19, *SE* = 0.18, *p*=.152). Significant social-behavioral indicators suggest that infants with lower *OXTR* methylation and higher MSE_{AUC} evoked during social perception vocalize, enjoy cuddling, and approach social situations more, show less fear in social situations, and soothe easier through social interaction. A multi-group analysis revealed no significant differences in path coefficients across male and female participants (all two-tailed *p* values ≥ .320). Table 2-6 contains results for Model 2 using alternate MSE and SD calculation methods.

2.2.4 Ongoing entropy does not show social-behavioral specificity

Finally, we examined whether these associations between *OXTR* methylation, brain signal variability, and infant social behavior occurred specifically due to the fact that

infants were engaged in social perception during brain signal measurement, or if general (ongoing) brain signal variability is associated with infant behavior regardless of perceptual context. To assess ongoing neural variability, we randomly extracted segments of brain signal from the inter-stimulus interval that were not time-locked to and did not overlap with stimulus presentation and re-ran the previous model with brain signal variability calculated on this ongoing signal. We found evoked and ongoing MSE_{AUC} are significantly correlated across all electrodes (*r*s range from .57 to .84, all *p*s < .001). We again found that the significant negative curvilinear association between *OXTR* methylation and MSE_{AUC} persisted (β = -0.33, *SE* = 0.13, *p* = .007), whereas no significant associations emerged for SD_{CONT} (*p*s ≥ .174). Interestingly, this analysis revealed a significant positive curvilinear association between MSE_{AUC} and both Social (β = 0.25, *SE* = 0.16, *p* = .014) and Non-Social (β = 0.36, *SE* = 0.19, *p* = .032) IBQ-R constructs, suggesting ongoing entropy, outside of a perceptual context, may reflect trait-level variability that is associated with general, non-context-specific infant behavior. Significant behavioral indicators demonstrate that infants who showed greater ongoing brain signal entropy soothe easier through both social and non-social means, are more likely to approach and show excitement for both social and non-social activities, show greater perceptual sensitivity to non-social stimuli, enjoy cuddling more, and show less fear in social situations. The results of this model can be seen in Figure 2-7 and Table 2-4 (Model 3). A multi-group analysis revealed no significant differences in path coefficients across male and female participants (all two-tailed p values ≥ .316). Table 2-7 contains results for Model 3 using alternate MSE and SD calculation methods.

2.3 Discussion

Using a multivariate, prediction-based model in a sample of infants, we show for the first time associations between early-life *OXTR* methylation, brain signal entropy, and parent-reported behavior. Specifically, infants with lower levels of *OXTR* methylation (and likely increased sensitivity to endogenous oxytocin) show increased brain signal entropy during social perception, which is associated with more positive ratings specific to social behaviors. Our results demonstrate that these associations are (1) measure-specific – entropy, but not signal variance, links *OXTR* methylation and infant behavior; and (2) context-sensitive – entropy evoked during social perception specifically explains social behavior only.

2.4 Figures

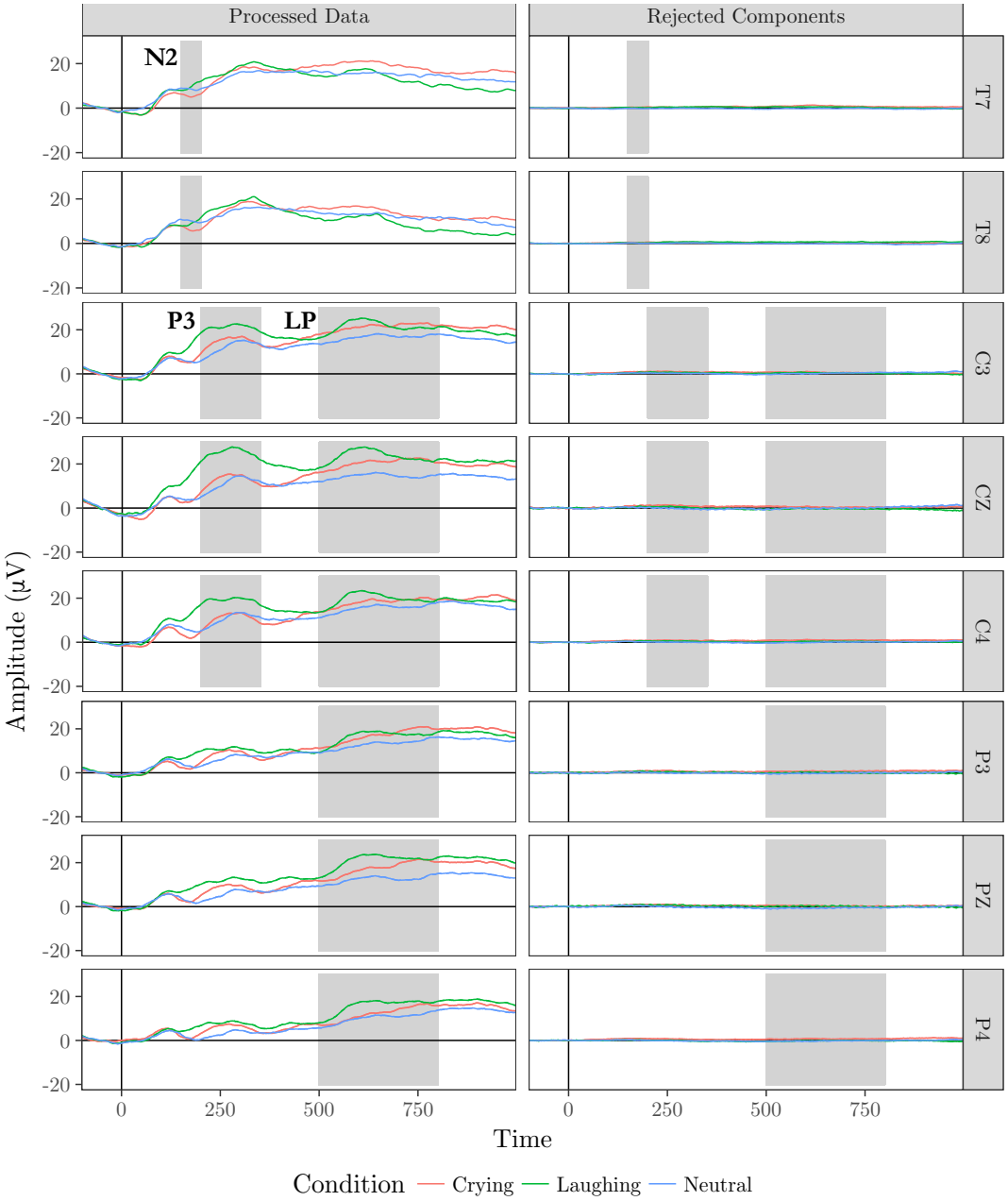

Figure 2-1. Replication of the original study results. To confirm that the preprocessing procedures used in our secondary data analysis (n = 55) did not obscure or eliminate relevant evoked response, we replicate results (left) of the original study, Missana *et. al.* (2017). We replicate the cry-sensitive ERP response (N2) at temporal electrodes, the laughter-sensitive ERP response (P3) at central electrodes, and the emotion-sensitive ERP response (LP) at central and parietal electrodes. We find no ERP in the rejected components (right).

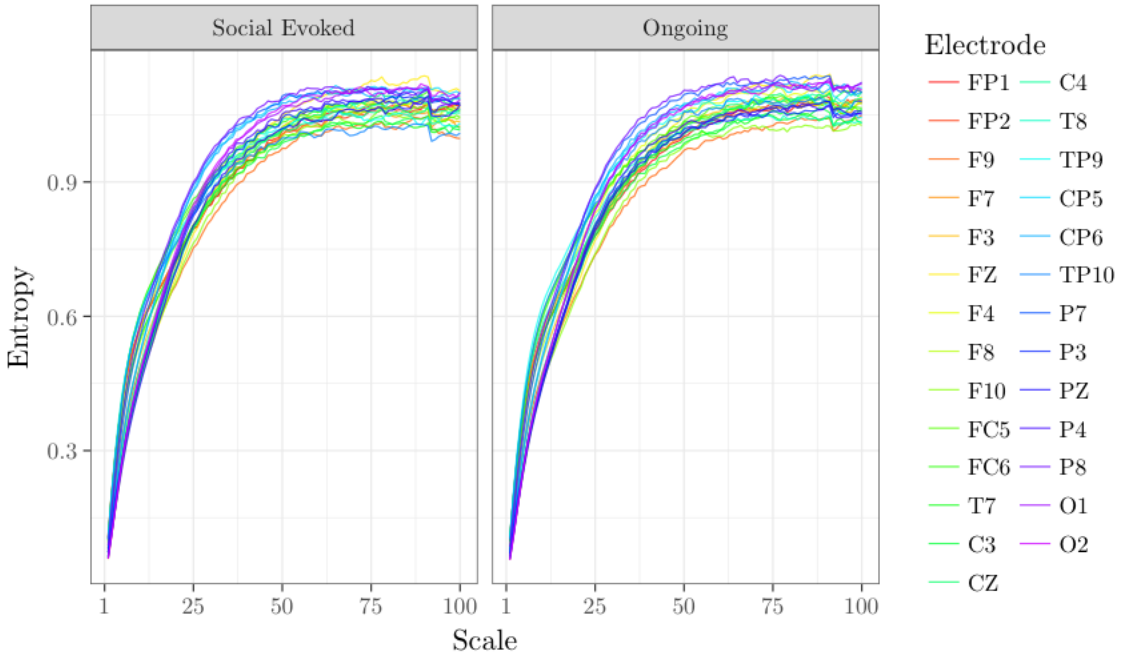

Figure 2-2. Group average multiscale entropy curves. The average multiscale entropy curves for scales 1 to 100 (500 to 5 Hz) are plotted for the social evoked (left) and ongoing (right) EEG signal for each electrode (n = 55).

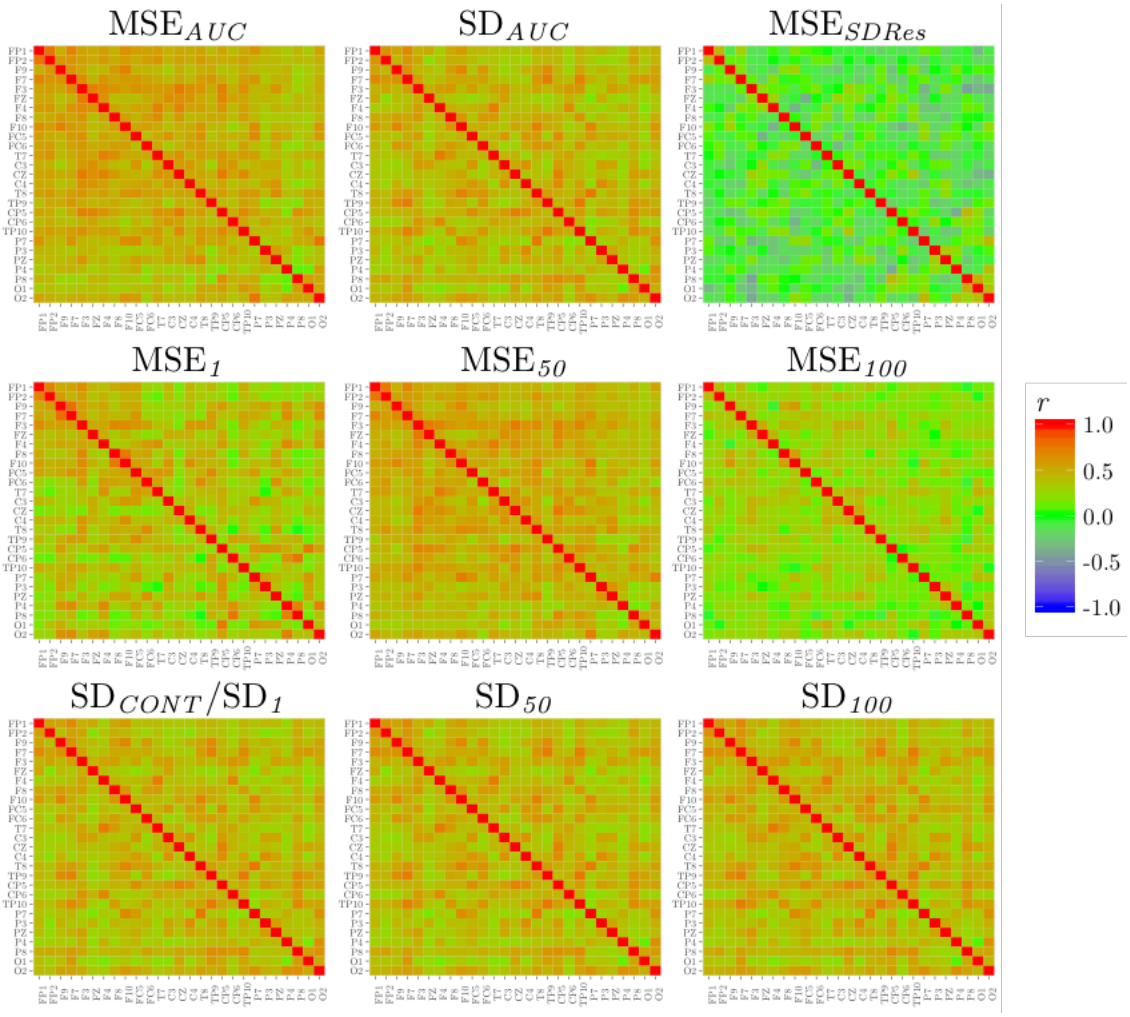

Figure 2-3. Correlations among electrodes across alternative brain signal variability computation methods. Correlation matrices showing the correlations among electrodes for each multiscale entropy (MSE) and standard deviation (SD) calculation method. In each correlation matrix, the electrodes from left to right and top to bottom are FP1, FP2, F9, F7, F3, FZ, F4, F8, F10, FC5, FC6, T7, C3, CZ, C4, T8, TP9, CP5, CP6, TP10, P7, P3, PZ, P4, P8, O1, and O2. MSE$_{AUC}$, area under the multiscale entropy curve; SD$_{AUC}$, area under the coarse-grained standard deviation curve; MSE$_{SDRes}$, standard deviation residualized from multiscale entropy; MSE$_{1}$, multiscale entropy of scale 1; MSE$_{50}$, multiscale entropy of scale 50; MSE$_{100}$, multiscale entropy of scale 100; SD$_{CONT}$/SD$_{1}$, standard deviation of the continuous time series, equivalent to standard deviation of scale 1; SD$_{50}$, standard deviation of scale 50; SD$_{100}$, standard deviation of scale 100; r, correlation coefficient.

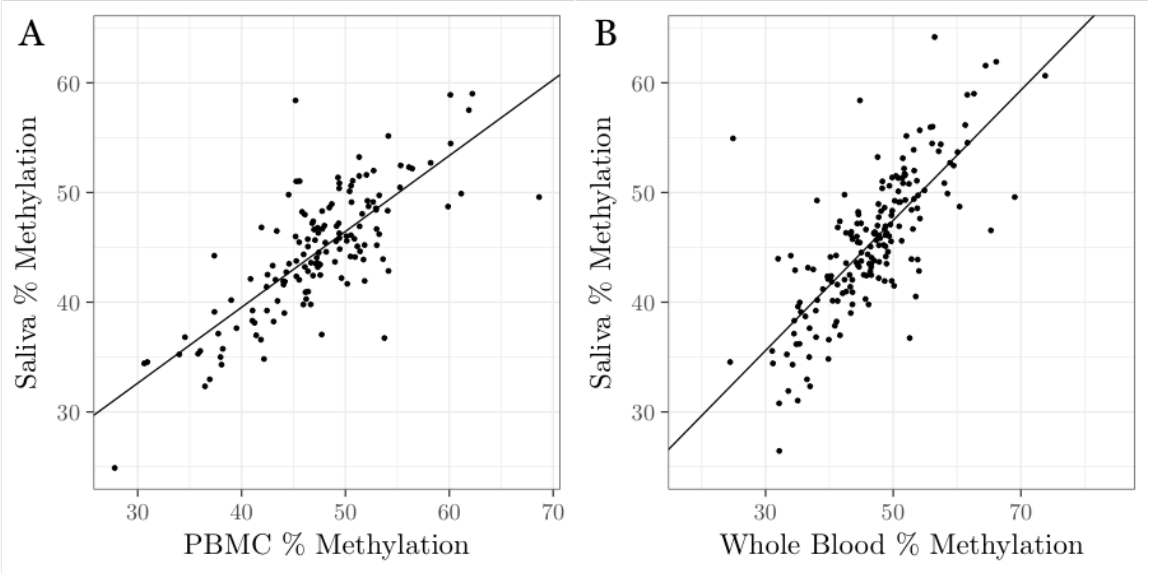

Figure 2-4. Saliva is a reliable tissue for assaying *OXTR* methylation. DNA methylation values at *OXTR* cytosine-phosphate-guanine (CpG) site -934 are significantly correlated between (A) saliva and peripheral blood mononuclear cells (PBMC) ($n = 142$, $r(140) = .78$, $p < .001$), and (B) saliva and whole blood ($n = 182$, $r(180) = .75$, $p < .001$).

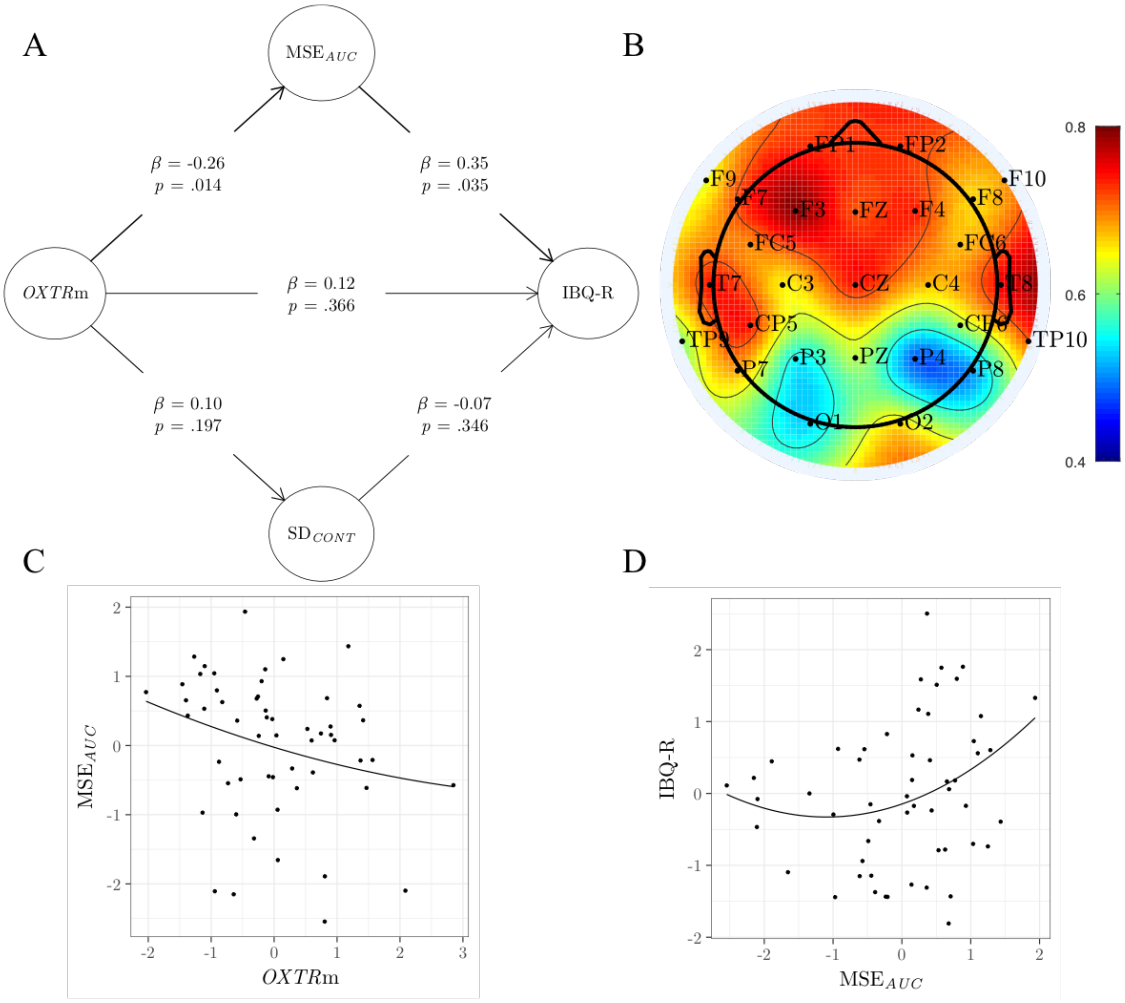

Figure 2-5. *OXTR* methylation is associated with brain signal entropy to influence infant behavior. (A) Results from the partial least squares path model (Model 1, n = 55) showing associations between *OXTR* methylation (*OXTR*m), area under the multiscale entropy curve (MSE$_{AUC}$) evoked during social perception, standard deviation of the continuous time series (SD$_{CONT}$) evoked during social perception, and ratings on the Revised Infant Behavioral Questionnaire (IBQ-R). β, path model coefficient; p, jackknifed p-value for coefficient. (B) Topographical map showing loadings of each electrode on the MSE$_{AUC}$ construct. (C) Plot of the significant association between MSE$_{AUC}$ and *OXTR*m standardized factor scores. (D) Plot of the significant association between MSE$_{AUC}$ and IBQ-R standardized factor scores.

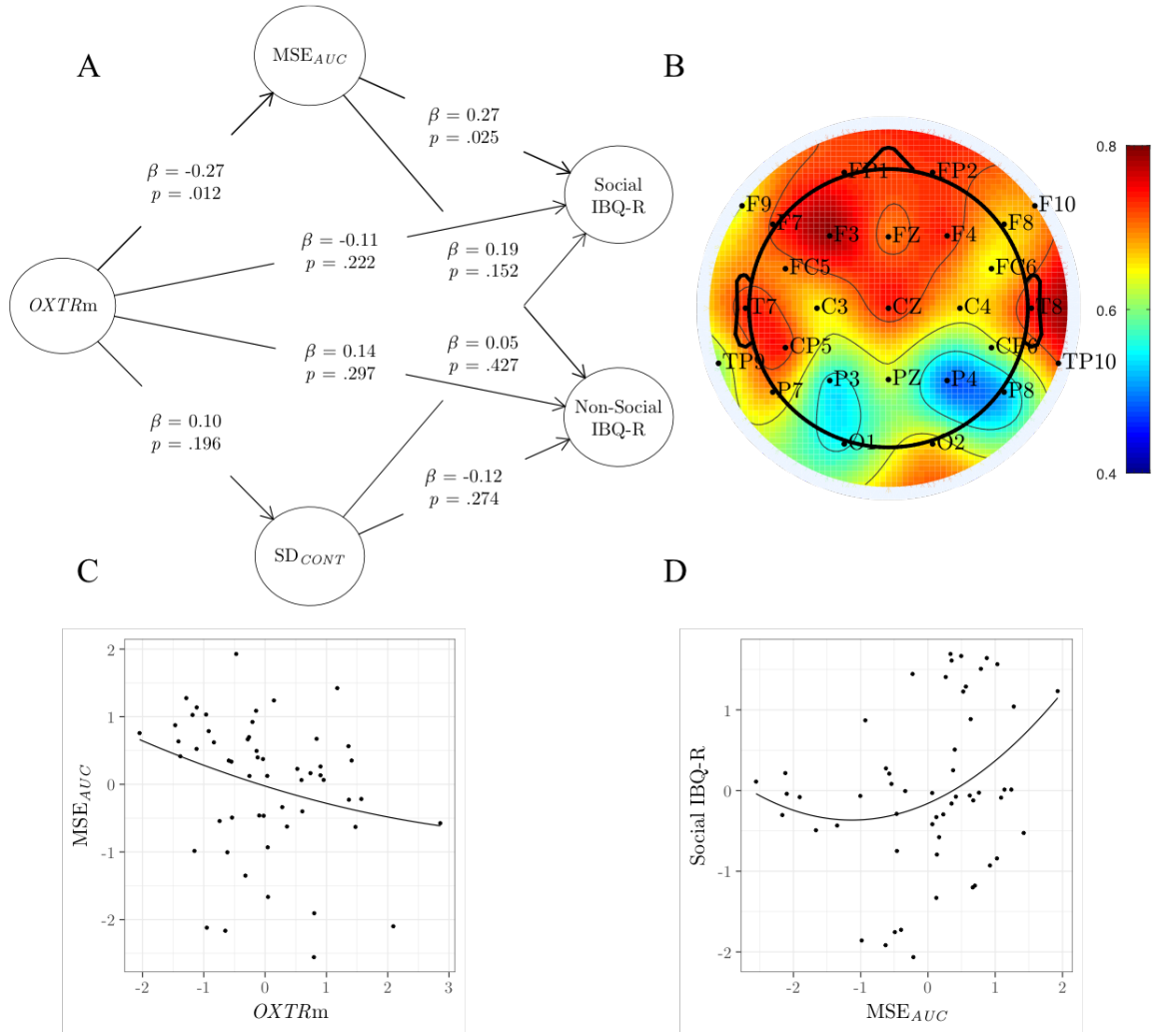

Figure 2-6. Evoked entropy during social perception is associated with infant social but not non-social behavior. (A) Results from the partial least squares path model (Model 2, n = 55) showing associations between *OXTR* methylation (*OXTR*m), area under the multiscale entropy curve (MSE$_{AUC}$) evoked during social perception, standard deviation of the continuous time series (SD$_{CONT}$) evoked during social perception, and ratings on the Social and Non-Social constructs of the Revised Infant Behavioral Questionnaire (IBQ-R). β, path model coefficient; p, jackknifed p-value for coefficient. (B) Topographical map showing loadings of each electrode on the MSE$_{AUC}$ construct. (C) Plot of the significant association between MSE$_{AUC}$ and *OXTR*m standardized factor scores. (D) Plot of the significant association between MSE$_{AUC}$ and Social IBQ-R standardized factor scores.

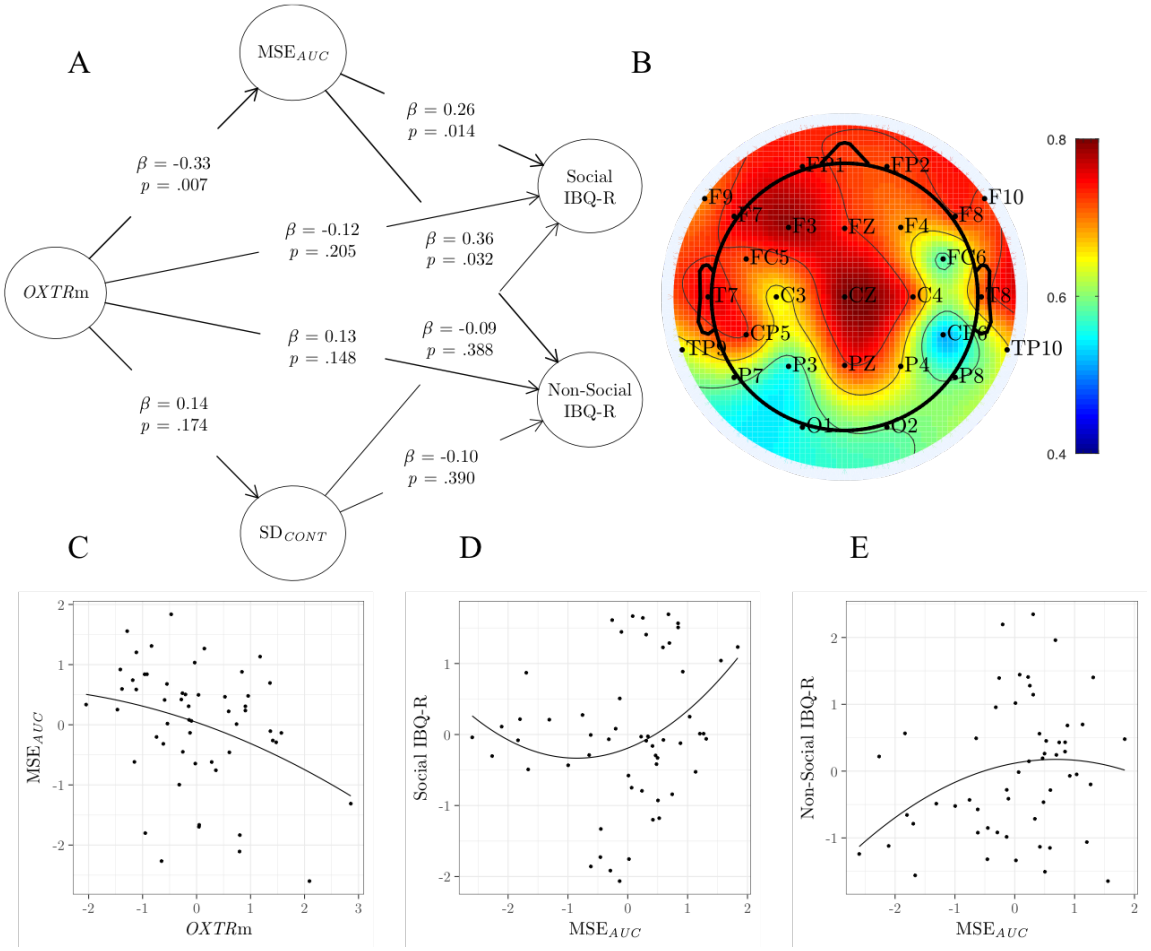

Figure 2-7. Ongoing entropy does not show social-behavioral specificity. (A) Results from the partial least squares path model (Model 3, n = 55) showing associations between *OXTR* methylation (*OXTR*m), ongoing area under the multiscale entropy curve (MSE$_{AUC}$), signal standard deviation of the continuous ongoing time series (SD$_{CONT}$), and ratings on the Social and Non-Social constructs of the Revised Infant Behavioral Questionnaire (IBQ-R). β, path model coefficient; p, jackknifed p-value for coefficient. (B) Topographical map showing loadings of each electrode on the MSE$_{AUC}$ construct. (C) Plot of the significant association between MSE$_{AUC}$ and *OXTR*m standardized factor scores. (D) Plot of the significant association between MSE$_{AUC}$ and Social IBQ-R standardized factor scores. (E) Plot of the significant association between MSE$_{AUC}$ and Non-Social IBQ-R standardized factor scores.

2.5 Tables

		ANOVA	Crying vs. Neutral	Crying vs. Laughing	Laughing vs. Neutral
Processed Data	N2	$F(2,138) = 4.43$, $p = .014$	$t(69) = -2.74$, $p = .008$	$t(69) = -2.72$, $p = .008$	$t(69) = 0.05$, $p = .960$
	P3	$F(2,138) = 16.14$, $p < .001$	$t(69) = 0.85$, $p = .396$	$t(69) = -4.93$, $p < .001$	$t(69) = 4.66$, $p < .001$
	LP	$F(2,138) = 4.55$, $p = .012$	$t(69) = 2.13$, $p = .037$	$t(69) = -0.95$, $p = .346$	$t(69) = 2.88$, $p = .005$
Rejected Components	N2	$F(2,138) = 0.91$, $p = .406$	$t(69) = 1.28$, $p = .206$	$t(69) = 0.7$, $p = .485$	$t(69) = 0.69$, $p = .495$
	P3	$F(2,138) = 2.21$, $p = .113$	$t(69) = 1.9$, $p = .062$	$t(69) = 0.98$, $p = .329$	$t(69) = 1.3$, $p = .197$
	LP	$F(2,138) = 0.72$, $p = .489$	$t(69) = 0.92$, $p = .360$	$t(69) = 1.02$, $p = .310$	$t(69) = 0.22$, $p = .826$

Table 2-1. Replication results. Analysis of variance (ANOVA) results replicating ERP N2, P3, and LP effects reported in the original study by Missana *et al*. (2017) using the novel preprocessing steps taken in this secondary data analysis. We find no significant differences across conditions in the ICA components rejected as artifacts during preprocessing.

Electrode	Social Evoked	Ongoing
FP1	89.61 (1.58)	89.20 (1.59)
FP2	89.46 (1.56)	89.92 (1.46)
F9	85.26 (1.55)	84.71 (1.69)
F7	89.04 (1.66)	89.49 (1.59)
F3	89.27 (1.72)	89.43 (1.70)
FZ	90.62 (1.38)	90.22 (1.48)
F4	91.43 (1.51)	92.38 (1.66)
F8	89.71 (1.55)	89.63 (1.53)
F10	86.56 (1.45)	84.51 (1.51)
FC5	91.11 (1.51)	92.11 (1.75)
FC6	92.39 (1.83)	91.82 (1.73)
T7	87.66 (1.83)	88.25 (1.85)
C3	86.21 (1.66)	86.31 (1.68)
CZ	89.00 (1.54)	88.87 (1.64)
C4	88.88 (1.79)	89.02 (1.70)
T8	91.71 (1.87)	89.52 (1.91)
TP9	90.44 (1.56)	93.29 (1.57)
CP5	94.04 (1.24)	93.00 (1.28)
CP6	93.38 (1.41)	93.48 (1.37)
TP10	88.46 (1.63)	92.67 (1.45)
P7	94.45 (1.51)	95.20 (1.50)
P3	90.18 (1.52)	87.76 (1.44)
PZ	88.10 (1.59)	87.66 (1.74)
P4	90.47 (1.50)	88.41 (1.65)
P8	95.20 (1.26)	95.77 (1.22)
O1	91.69 (1.27)	92.36 (0.99)
O2	92.23 (1.14)	92.14 (1.15)

Table 2-2. Average area under the multiscale entropy curve values. Mean and (standard error of the mean) area under the multiscale entropy curve values for each electrode and condition.

Construct	Subscore	α	Items
Social IBQ-R	Cuddliness	0.88	5, 6, 7, 105, 106, 107, 108, 123, 124, 125, 126, 127, 128, 129, 130, 131, 132
	Duration of Orientation	0.68	55, 101
	Fear	0.90	90, 150, 151, 152, 153, 154, 155, 156, 161, 162, 163, 164
	High Pleasure	0.72	58, 59, 60, 61, 65, 66, 67, 77, 78, 79, 80, 81, 165
	Soothability	0.71	174, 176, 177, 178, 179, 189, 190, 191
	Vocalization	0.73	8, 9, 10, 35, 42, 45, 52, 102, 103, 146, 147, 148
Non-Social IBQ-R	Approach	0.70	85, 86, 87, 88, 97, 98, 160
	Duration of Orientation	0.70	46, 47, 48, 49, 50, 51, 54, 91, 92
	Fear	0.78	157, 158
	Perceptual Sensitivity	0.78	4, 83, 95, 96, 133, 134, 135, 136, 137, 138, 139
	High Pleasure	0.78	82, 62, 63, 64, 68, 69, 70, 71, 72, 73, 74
	Soothability	0.68	183, 184, 186, 187

Table 2-3. Items included in the Social and Non-Social behavioral constructs. Individual items included in the Social and Non-Social Revised Infant Behavior Questionnaire (IBQ-R) constructs after item analysis. α, Cronbach's alpha.

Composite reliability coefficients						
Model	*OXTR*m	MSE_{AUC}	SD_{CONT}	IBQ-R	Social IBQ-R	Non-Social IBQ-R
1	0.87	0.96	0.96	0.82	-	-
2	0.87	0.96	0.96	-	0.73	0.78
3	0.87	0.97	0.95	-	0.73	0.74
R^2 coefficients						
Model	*OXTR*m	MSE_{AUC}	SD_{CONT}	IBQ-R	Social IBQ-R	Non-Social IBQ-R
1	-	0.07	0.01	0.11	-	-
2	-	0.07	0.01	-	0.10	0.07
3	-	0.11	0.02	-	0.11	0.11

Table 2-4. Model fit statistics. Composite reliability coefficients reflecting internal consistency and reliability and R^2 coefficients reflecting explanatory power for each construct and model. *OXTR*m, *OXTR* DNA methylation; MSE_{AUC}, area under the multiscale entropy curve; SD_{CONT}, standard deviation of the continuous time series; IBQ-R, Revised Infant Behavioral Questionnaire.

Model 1: Path Coefficients and Standard Errors				
			From:	
	To:	*OXTR*m	MSE	SD
MSE_{AUC} & SD_{CONT}	MSE	**-0.26 (0.12)***	-	-
	SD	0.10 (0.12)	-	-
	IBQ-R	0.12 (0.34)	**0.35 (0.19)***	-0.07 (0.17)
MSE_{AUC} & SD_{TXT}	MSE	**-0.26 (0.12)***	-	-
	SD	0.10 (0.12)	-	-
	IBQ-R	0.12 (0.34)	**0.35 (0.20)***	-0.06 (0.17)
MSE_{AUC} & SD_{AUC}	MSE	**-0.26 (0.12)***	-	-
	SD	0.15 (0.12)	-	-
	IBQ-R	0.12 (0.35)	**0.37 (0.21)***	-0.08 (0.22)
MSE_{1} & SD_{1}	MSE	**-0.28 (0.13)***	-	-
	SD	0.10 (0.12)	-	-
	IBQ-R	0.09 (0.27)	0.13 (0.59)	-0.03 (0.17)
MSE_{50} & SD_{50}	MSE	**-0.24 (0.12)***	-	-
	SD	*0.15 (0.12)*+*	-	-
	IBQ-R	0.12 (0.36)	**0.36 (0.18)***	-0.02 (0.18)
MSE_{100} & SD_{100}	MSE	*-0.20 (0.13)*+*	-	-
	SD	*0.19 (0.11)*+*	-	-
	IBQ-R	0.09 (0.26)	0.18 (0.22)	0.07 (0.37)

Table 2-5. Model 1 results using alternative brain signal variability computation methods. Path coefficients and (standard errors) are reported for iterations of Model 1 using alternative computation methods for multiscale entropy and standard deviation of the time series. *P*-values are estimated with delete-1 jackknifing. **Boldfaced*** effects are significant at the $p \leq .05$ level; *Italicized*+ effects approach significance at the $p < .10$ level. MSE_{AUC}, area under the multiscale entropy curve; SD_{CONT}, standard deviation of the continuous time series; SD_{TXT}, standard deviation across trials; SD_{AUC}, area under the coarse-grained standard deviation curve; MSE_{1}, multiscale entropy of scale 1; SD_{1}, standard deviation of scale 1; MSE_{50}, multiscale entropy of scale 50; SD_{50}, standard deviation of scale 50; MSE_{100}, multiscale entropy of scale 100; SD_{100}, standard deviation of scale 100.

Model 2: Path Coefficients and Standard Errors				
			From:	
	To:	*OXTR*m	MSE	SD
MSE_{AUC} & SD_{CONT}	MSE	**-0.27 (0.12)***	-	-
	SD	0.10 (0.12)	-	-
	Social IBQ-R	-0.11 (0.14)	**0.27 (0.13)***	0.05 (0.27)
	Non-social IBQ-R	0.14 (0.27)	0.19 (0.18)	-0.12 (0.20)
MSE_{AUC} & SD_{TXT}	MSE	**-0.27 (0.12)***	-	-
	SD	0.10 (0.12)	-	-
	Social IBQ-R	-0.04 (0.17)	**0.23 (0.11)***	0.10 (0.16)
	Non-social IBQ-R	0.04 (0.49)	0.22 (0.24)	0.03 (0.29)
MSE_{AUC} & SD_{AUC}	MSE	**-0.27 (0.12)***	-	-
	SD	*0.15 (0.12)*+*	-	-
	Social IBQ-R	-0.11 (0.14)	**0.29 (0.14)***	0.00 (0.13)
	Non-social IBQ-R	0.14 (0.27)	0.13 (0.20)	-0.19 (0.21)
MSE_{1} & SD_{1}	MSE	**-0.28 (0.13)***	-	-
	SD	0.10 (0.12)	-	-
	Social IBQ-R	-0.20 (0.17)	0.11 (0.34)	-0.21 (0.26)
	Non-social IBQ-R	0.14 (0.36)	0.10 (0.13)	-0.22 (0.15)
MSE_{50} & SD_{50}	MSE	**-0.25 (0.12)***	-	-
	SD	*0.15 (0.12)*+*	-	-
	Social IBQ-R	-0.10 (0.15)	**0.31 (0.13)***	0.03 (0.14)
	Non-social IBQ-R	0.15 (0.38)	0.08 (0.23)	-0.23 (0.22)
MSE_{100} & SD_{100}	MSE	*-0.20 (0.13)*+*	-	-
	SD	*0.19 (0.12)*+*	-	-
	Social IBQ-R	-0.12 (0.17)	0.21 (0.20)	-0.04 (0.30)
	Non-social IBQ-R	0.14 (0.38)	-0.08 (0.32)	-0.25 (0.17)

Table 2-6. Model 2 results using alternative brain signal variability computation methods. Path coefficients and (standard errors) are reported for iterations of Model 2 using alternative computation methods for multiscale entropy and standard deviation of the time series. *P*-values are estimated with delete-1 jackknifing. **Boldfaced*** effects are significant at the $p \leq .05$ level; *Italicized*+ effects approach significance at the $p < .10$ level. MSE_{AUC}, area under the multiscale entropy curve; SD_{CONT}, standard deviation of the continuous time series; SD_{TXT}, standard deviation across trials; SD_{AUC}, area under the coarse-grained standard deviation curve; MSE_{1}, multiscale entropy of scale 1; SD_{1}, standard deviation of scale 1; MSE_{50}, multiscale entropy of scale 50; SD_{50}, standard deviation of scale 50; MSE_{100}, multiscale entropy of scale 100; SD_{100}, standard deviation of scale 100.

Model 3: Path Coefficients and Standard Errors				
			From:	
	To:	*OXTR*m	MSE	SD
MSE_{AUC} & SD_{CONT}	MSE	**-0.33 (0.13)***	-	-
	SD	0.14 (0.15)	-	-
	Social IBQ-R	-0.12 (0.15)	**0.26 (0.12)***	-0.09 (0.31)
	Non-social IBQ-R	0.13 (0.12)	**0.36 (0.19)***	-0.10 (0.37)
MSE_{AUC} & SD_{TXT}	MSE	**-0.33 (0.13)***	-	-
	SD	0.14 (0.15)	-	-
	Social IBQ-R	-0.04 (0.16)	**0.25 (0.13)***	0.12 (0.14)
	Non-social IBQ-R	-0.02 (0.14)	**0.45 (0.25)***	-0.16 (0.80)
MSE_{AUC} & SD_{AUC}	MSE	**-0.33 (0.13)***	-	-
	SD	*0.19 (0.15)+*	-	-
	Social IBQ-R	-0.12 (0.15)	**0.26 (0.13)***	0.03 (0.29)
	Non-social IBQ-R	0.13 (0.12)	0.35 (0.23)	-0.09 (0.55)
MSE_{1} & SD_{1}	MSE	**-0.27 (0.14)***	-	-
	SD	0.14 (0.15)	-	-
	Social IBQ-R	-0.21 (0.18)	-0.17 (0.68)	-0.22 (0.36)
	Non-social IBQ-R	0.12 (0.31)	0.11 (0.15)	-0.15 (0.16)
MSE_{50} & SD_{50}	MSE	**-0.33 (0.13)***	-	-
	SD	0.19 (0.15)	-	-
	Social IBQ-R	-0.13 (0.15)	**0.24 (0.13)***	-0.08 (0.26)
	Non-social IBQ-R	0.10 (0.14)	0.27 (0.21)	-0.01 (0.23)
MSE_{100} & SD_{100}	MSE	*-0.23 (0.14)+*	-	-
	SD	*0.24 (0.14)+*	-	-
	Social IBQ-R	-0.13 (0.16)	**0.40 (0.14)***	-0.07 (0.12)
	Non-social IBQ-R	0.11 (0.22)	0.20 (0.22)	-0.10 (0.20)

Table 2-7. Model 3 results using alternative brain signal variability computation methods. Path coefficients and (standard errors) are reported for iterations of Model 3 using alternative computation methods for multiscale entropy and standard deviation of the time series. *P*-values are estimated with delete-1 jackknifing. **Boldfaced*** effects are significant at the $p \leq .05$ level; *Italicized*+ effects approach significance at the $p < .10$ level. MSE_{AUC}, area under the multiscale entropy curve; SD_{CONT}, standard deviation of the continuous time series; SD_{TXT}, standard deviation across trials; SD_{AUC}, area under the coarse-grained standard deviation curve; MSE_{1}, multiscale entropy of scale 1; SD_{1}, standard deviation of scale 1; MSE_{50}, multiscale entropy of scale 50; SD_{50}, standard deviation of scale 50; MSE_{100}, multiscale entropy of scale 100; SD_{100}, standard deviation of scale 100.

3 Study 2: Context- and modality-specific associations between oxytocinergic system function, neural noise, and infant social behavior

3.1 Methods

3.1.1 Participants

Sixty-five infants (31 female) were recruited from the greater Charlottesville area to participate in Study 2 at 4 months of age (M = 131.92 ± 11.59 days). The racial breakdown of infants was as follows: 77% Caucasian (n = 50), 20% mixed race (n = 13), and 3% Black (n = 2). Four infants were born pre-term (prior to 37 weeks gestation). The average birth weight was 3439.19 ± 525.73 grams. The average maternal age at birth was 31.68 ± 4.82 years. Forty-nine infants were delivered vaginally, 15 via elective cesarean, and 1 via emergency cesarean. Labor was induced via Pitocin in 23.08% (n = 15) births.

Eleven infants (4 female; 9 Caucasian, 2 mixed race, 1 Black; 0 pre-term) returned within 1 week (M = 5.23 ± 2.00 days) to assess the test-retest reliability of our measures. Thirty-seven infants (18 female; 29 Caucasian, 8 mixed race; 4 pre-term) returned at 8 months of age (M = 241.70 ± 15.13) to assess the developmental trajectory of our measures. On average, 111.92 ± 10.23 days passed between the 4- and 8-month visits.

The primary caregiver accompanied the infant to all appointments and provided written informed consent for a protocol approved by the University of Virginia Health and Human Sciences Institutional Review Board. At each visit, infants provided a DNA sample, participated in an eye-tracking paradigm, were video-recorded during a free-play interaction with their caregiver, and underwent EEG. Caregivers completed the Short Revised Infant Behavior Questionnaire (IBQ-RS) at each visit, and provided a DNA

sample at the 4-month visit. Visits lasted no longer than two hours and families were paid $50 for each visit.

3.1.2 DNA sample collection and epigenetic analysis

All infants (with the exception of one 8-month-old) provided a saliva sample at each visit for the assessment of *OXTR* methylation. Saliva was collected with CS-2 sponges (DNA Genotek, Ottawa) at least 30 minutes after the last feeding and stored in OG-250 kits (DNA Genotek, Ottawa) at room temperature until DNA isolation. The primary caregiver provided a saliva sample at the first visit at least 30 minutes after the last meal. Saliva was collected using OG-500 kits (DNA Genotek, Ottawa) and stored at room temperature until DNA isolation.

DNA isolation and downstream epigenetic analysis proceeded exactly as described in Study 1. Technical replicates deviated an average of ± 2.10% from the mean.

3.1.3 Eye-tracking paradigm

To assess the extent to which social stimuli captured attention, infants participated in an eye-tracking paradigm in which they viewed videos of children playing in a naturalistic environment[86]. Stimuli were provided courtesy of researchers at the Center for Autism Research at the Children's Hospital of Philadelphia and included 16 silent video clips of 8 sibling pairs of school-aged, Caucasian children playing with various toys (e.g. cards, Jenga) at a table or on the floor. Filming took place in naturalistic playroom settings were background objects (e.g. paintings, light switches, toys) were visible. Each sibling pair was filmed once engaging in joint play and once engaging in parallel play. Videos lasted 16 s and were presented to the infants in a randomized order. Between each video,

infants' attention was re-oriented to the center of the screen with a colorful, dynamically spinning object (soccer ball, stars, sun, acorn, painter's pallet) and was paired with an attention-getting sound (bells, beeps, boings). The order and pairing of these attention-getters was randomized. Once the infant fixated on the attention-getter for 500 ms, the next video began. If the infant failed to fixate after 5000 ms, the next video began. If the infant failed to fixate for 6 attention-getters in a row, the paradigm automatically stopped to avoid losing infant attention and compliance for the remaining visit tasks.

Stimuli were presented using PsychToolBox[87] v3.0.14 for MATLAB. Eye-tracking was recorded with Tobii Pro SDK v1.6 for MATLAB and a Tobii X60 eye tracker mounted to a 43 cm computer screen. The infant was seated on the caregiver's lap throughout the protocol. The caregiver wore darkened glasses to ensure the eye tracker registered only the infant's pupils and was instructed not to talk or interact with the infant so as to not interfere with data acquisition. The infant was first adjusted to be positioned 60 cm from the eye-tracker and screen. Then the infant underwent a 5-point calibration procedure in which a colorful, dynamic animation (flower, beachball, or ladybug) expanded and contracted and was paired with an attention-getting sound. If any points failed to calibrate, the calibration procedure was repeated up to two times for those points at which point the eye-tracking paradigm commenced.

Gaze data preprocessing was carried out using custom MATLAB scripts following Tobii recommendations[88], including gap fill-in using linear interpolation for gaps up to 75 ms, average eye computation from binocular data, and median filtering with a length of 7 points (100 ms)[89]. Areas of interest (AOIs) were drawn around faces within the videos in

Tobii Pro Studio and provided by researchers at the Center for Autism Research at the Children's Hospital of Philadelphia. We converted AOIs to frame-wise x and y coordinates corresponding to the display area for eye gaze analysis with custom MATLAB scripts.

Attention to social stimuli was defined as the Proportion of Total Fixation Duration to Faces relative to Total Fixation Time to the entire screen. Calculating a proportional fixation duration in this manner accounts for individual differences in overall looking behavior and does not require the implementation of an exclusionary gaze time threshold that would reduce sample size and may produce selection biases[86]. We also calculated Average Time to First Fixation to Faces to assess how quickly social information captured infant's attention, and Total Fixation Count to Faces to assess the extent of visual exploration of social information.

Eye-tracking data was not available for eight 4-month-olds and seven 8-month-olds either due to a failure of the eye-tracker to register the infant's eyes or technical error. On average, 4-month-olds viewed 8.06 ± 4.12 videos and their looking behavior was accurately recorded for 56.37% of the total duration that videos were presented. On average, 8-month-olds viewed 9.71 ± 4.64 videos and their looking behavior was accurately recorded for 40.87% of the total duration that the videos were presented.

3.1.4 EEG paradigm

Infants participated in an EEG paradigm (Figure 3-1) consisting of four conditions, resulting in a 2 x 2 design with the factors context (social or non-social) and modality (visual or auditory).

Visual stimuli. Visual social stimuli consisted of dynamic color videos of women rotating their heads and smiling. Stimuli were obtained from the Amsterdam Dynamic Facial Expression Set (http://aice.uva.nl/research-tools/adfes-stimulus-set/adfes-stimulus-set.html) and consisted of six Caucasian actors each turning towards or away from the camera to the left or right and then smiling for a total of 24 videos.

Visual non-social stimuli consisted of dynamic color videos of common objects (e.g. cups, vegetables, ribbon) rotating. Stimuli were obtained from the Amsterdam Library of Object Images (http://aloi.science.uva.nl/), a database of objects photographed in multiple viewing directions. Objects were first cropped and placed on a background matching the social stimuli, then selected such that the non-social stimulus set were matched to the social stimulus set on luminance (M_{social} = 177.16, $M_{non\text{-}social}$ = 178.24, t = 0.13, p = 0.898, contrast (M_{social} = 52.95, $M_{non\text{-}social}$ = 53.73, t = 0.16, p = 0.875), and spatial frequency (M_{social} = 13743.58, $M_{non\text{-}social}$ = 12067.46, t = -1.92, p = 0.068) using custom MATLAB scripts adopted from the SHINE[90] toolbox. The final set consisted of 12 unique objects, each rotating to the left and to the right for a total of 24 videos.

Each visual block had a total duration of 18 s and consisted of six unique 2400-ms videos presented at a visual angle of 8° in a randomized order and with a randomized inter-stimulus interval ranging from 500 to 1000 ms. White noise generated in MATLAB was presented as auditory stimuli during visual blocks.

Auditory stimuli. Auditory non-social stimuli consisted of sounds of water from nature (e.g. rain, surf) and household products (e.g. bubbling, splashing) downloaded from http://www.findsounds.com. Auditory social stimuli consisted of naturalistic infant-

directed speech, recorded from seven English-speaking mothers as they spoke to their preverbal children in their homes[91], downloaded from the Child Language Data Exchange System (https://childes.talkbank.org/access/Eng-NA/Brent.html). Clips containing single-word utterances (e.g. "*shoes*," "*open*," "*hot*") or short phrases (e.g. "*oh my goodness*," "*uh oh*," "*bye-bye*") were extracted from the recordings. Clips containing incoherent speech or background noises were discarded and stimuli were selected such that the social stimulus set matched the non-social stimulus set on mean fundamental frequency (M_{social} = 311.16, $M_{non\text{-}social}$ = 335.29, t = -1.29, p = .200), standard deviation of fundamental frequency (M_{social} = 66.85, $M_{non\text{-}social}$ = 57.82, t = 0.95, p = .343), and duration (M_{social} = 0.87, $M_{non\text{-}social}$ = 0.97, t = -1.35, p = .179) using Praat v6.0.36[92] and custom MATLAB scripts.

The final auditory stimulus set consisted of 60 unique social and 60 unique non-social auditory clips. Clips were grouped by condition into six 10-clip, 18 s blocks such that no word or water-sound type repeated within a block. The inter-stimulus interval between clips ranged from 500 to 10000 ms, randomized across participants. The order of clips within a block and the presentation order of blocks was randomized across participants. Static videos generated in MATLAB were presented as visual stimuli during auditory blocks.

Paradigm. Stimuli were presented with PsychToolBox[87] v3.0.14 in MATLAB. Blocks were pseudo-randomized such that visual and auditory blocks alternated. An attention-getting stimulus was presented within the inter-block interval to regain the infant's attention to the computer screen, at which point the experimenter initiated the beginning of the next block. Infants were seated on their caregiver's lap approximately 100

cm from a computer monitor throughout the experiment. Caregivers were instructed not to talk or interact with the infant so as to not interfere with data acquisition. The experimenter viewed the infant via live stream from the control area and could pause the experiment between blocks to regain the infant's attention or compliance if necessary. The EEG session ended when the infant became fussy or inattentive or after 24 blocks. On average, infants completed 7.30 blocks of the paradigm.

3.1.5 EEG acquisition and preprocessing

EEG was recorded from 32 Ag/AgCl active actiCAP slim electrodes (Brain Products GmbH, Germany) affixed to an elastic cap using the 10-20 electrode placement system. The horizontal electrooculogram (EOG) was recorded from two electrodes (F7, F8), which are part of the cap located at the outer canthi of both eyes. The vertical EOG was recorded from two electrodes (FP1, FP2), which are part of the cap on the supraorbital ridge of both eyes. The infant's head circumference was first obtained to determine the correct cap size. Capping and gel application took place in a child-friendly waiting room so that the infant would not acclimate to the testing area prior to recording. Impedances were assessed via the actiCAP Control Box (Brain Products GmbH, Germany) prior to recording.

EEG was amplified with a BrainAmp DC Amplifier (Brain Products GmbH, Germany) and recorded using BrainVision Recorder software with a sampling rate of 5000 Hz, online referenced to FCz, and online band-pass filtered between 0.1 to 1000 Hz. Data were analyzed offline using EEGLab v14.1.1[93], ERPLab v7.0.0[93] and custom MATLAB scripts. Data were resampled at 500 Hz, band-pass filtered between 0.3 to 20 Hz, and re-

referenced to the average of all scalp electrodes. Visual stimuli were segmented into stimulus-evoked epochs 100 ms pre-stimulus onset to 1000 ms post-stimulus onset with pre-baseline correction. Auditory stimuli were segmented into stimulus-evoked epochs 100 ms pre-stimulus onset to 500 ms post-stimulus onset with pre-baseline correction. Epochs contaminated with excessive amplitude standard deviations (> 100 μV in ocular channels, > 80 μV in scalp electrodes) within a sliding window of width 200 ms and step 100 ms were discarded as artifacts. Participants with at least 20 artifact-free visual segments and 40 artifact-free auditory segments were retained in the analyses. Four 4-month-olds and one 8-month-old were excluded for an insufficient number of artifact-free segments. EEG data failed to save due to a technical error for an additional 4-month-old. EEG data for sixty (92.3%) 4-month-olds and thirty-six (97.3%) 8-month-olds was retained.

We then used an Independent Component Analysis (ICA) to remove components with ocular, muscular or electrical artifacts. On average, 3.48 (range 2 to 8) components were removed. The number of components removed did not correlate with MSE within the visual ($r = .13$, $p = .330$) or auditory ($r = -.15$, $p = .249$) domain and did not show significant ERP effects (Figure 3-2), indicating that the components identified as artifacts did not contain relevant brain activity.

To include an equivalent number of data points for each condition in the MSE computation[63], we selected the 20 visual segments (10 social) and the 40 auditory segments (20 social) with a total global field power (GFP)[42] closest to the median GFP for each participant for inclusion in downstream analyses (5000 data points per condition). To ensure that these preprocessing procedures did not obscure or eliminate relevant brain

activity, we examined the ERP (Figure 3-2) using these data re-referenced to Cz (visual) or the average of the mastoids (auditory).

3.1.6 Quantification of brain signal variability

We computed MSE on the residuals of the average-referenced post-stimulus onset EEG signal (i.e. after subtracting the within-person average ERP) using pattern length m = 2 and similarity criterion r = .5 (recalculated at each scale) across segments[63]. We then calculated the area under the MSE curve (MSE_{AUC}) for each electrode for scales 1 to 50 (corresponding to 500 to 10 Hz). Average MSE curves are plotted in Figure 3-3 and average area under the curve values are listed in Table 3-1.

3.1.7 Statistical analysis

To identify causative associations among our epigene-brain-behavior variables, we analyzed data in the partial least squares path modeling (PLS-PM) framework using WarpPLS v6.0[81] to model curvilinear associations between our latent constructs. The aim of the present study was to identify whether there are context- and modality- specific associations between *OXTR* methylation, brain signal entropy evoked during perception, and infant behavior. Specifically, we hypothesized that infants that show greater entropy to social relative to non-social stimuli in both modalities would show enhanced social behavior. We therefore included Social – Non-social MSE-AUC differences scores for each electrode across visual and auditory modalities separately in the model. To assess modality-specific behavioral associations in our model, we included three metrics of social attention from the eye-tracking paradigm as a Visual Behavior construct: Average Time to First Fixation to Faces, Total Fixation Count to Faces, and Proportion of Total Fixation

Duration to Faces. We included the seven items that constitute the Vocalization subscore of the IBQ-RS (Table 3-2) as a Vocal Behavior construct. IBQ-RS data was unavailable for four 4-month-old infants. These missing data were imputed via arithmetic mean imputation. Each technical replicate (3) of the *OXTR* methylation analysis was included in the *OXTR* methylation construct.

Sample size. The target sample size for the test-retest reliability analysis was determined via power analysis tables provided by Bujang and Baharum[94] which specify that 10 subjects are sufficient to detect an interclass correlation coefficient (*ICC*) of .70 based on two observations with 80% power.

The target sample size for the PLS-PM analysis assessing associations between our genetic, neural, and behavioral measures was determined via a power analysis using effect sizes established in Study 1 and following recommendations of Chin & Newsted[84]. In our models, behavioral constructs have the largest number of predictors – 3. A two-tailed multiple regression power analysis[85] determined that 58 participants are needed to detect an effect size of 0.29 with 3 predictors, 95% power, and $\alpha = .05$. We therefore include data for the 4-month-olds ($n = 60$) in our epigene-brain-behavior association models. Data for the 8-month-olds ($n = 35$) was included in analyses assessing the developmental trajectory of MSE.

3.2 Results

3.2.1 Methylation values do not vary by age, race, or delivery method

Methylation levels at 4 months averaged 42.02 ± 4.53%. Methylation levels at 8 months averaged 41.61 ± 4.71%. There was no significant difference in methylation across

age groups $t(35) = -0.21$, $p = .831$. There was no significant difference in the variance of methylation values across age groups ($F(64,35) = 0.92$, two-tailed p-value = .772).

Parental methylation levels averaged 47.08 ± 7.19%. Although parental methylation levels were not significantly correlated with infant methylation values at 4 months ($r = .18$, $p = .146$) or at 8 months ($r = -.27$, $p = .104$), there was a significant change in parent-infant correlation with development. Infant and parent methylation values were significantly more correlated at 4 than at 8 months (Fisher r-to-$z = 2.12$, two-tailed p-value = .030).

Methylation levels may vary by race[95]. However, we find no differences in *OXTR* methylation levels ($t(63) = -0.59$, $p = .557$) among Caucasian infants ($M = 41.84$) and non-Caucasian infants ($M = 42.63$). *OXTR* methylation levels may also be impacted by labor and delivery factors[96]. However, we find no differences in *OXTR* methylation levels ($t(63) = 1.32$, $p = .192$) among infants who were delivered vaginally ($M = 42.45$) or via cesarean ($M = 40.73$), or among infants who did ($M = 42.91$) or did not ($M = 41.76$) receive Pitocin during delivery ($t(63) = 0.86$, $p = .391$).

3.2.2 Multiscale entropy is a reliable measure in infancy

A subset of 4-month-old infants returned within one week of their first appointment to determine the test-retest reliability of brain signal entropy. EEG data for one 4-month-old at retest was excluded for an insufficient number of artifact-free segments. Test-retest reliability was assessed for average MSE_{AUC} across all conditions via interclass correlation coefficient (*ICC*). *ICC* estimates and their 95% confident intervals were calculated using the irr v0.84.1[97] statistical package in R v3.4.4[80] based on a single rating ($k = 1$), absolute-

agreement, 2-way mixed-effects model. MSE was found to show good reliability within one week (*ICC* = .73, p = .004). MSE test-retest reliability curves for each condition are plotted in Figure 3-4.

3.2.3 Entropy shows modality-specific associations with infant behavior within the auditory domain

We modeled context- and modality-specific associations between *OXTR* methylation, brain signal evoked by social relative to non-social stimuli, and infant visual (attention to faces) and verbal (vocalization) social behavior in 4-month-old infants. We find, as in Study 1, a negative association between *OXTR* methylation and auditory-evoked MSE (β = -0.25, p = .026) such that 4-month-olds that have lower levels of *OXTR* methylation (i.e. presumed increased ability to use endogenous oxytocin) show increased brain signal entropy to social relative to non-social auditory stimuli. Brain signal entropy to social auditory stimuli is positively associated with infant verbal behavior (β = 0.19, p = .031), but is not associated with infant visual behavior (β = -0.09, p = .349). There is no association between *OXTR* methylation and visually-evoked MSE (β = 0.14, p = .182), nor between visually-evoked MSE and visual (β = 0.07, p = .311) or verbal (β = 0.14, p = .408) behavior at 4 months of age. Topographical loadings for auditory-evoked MSE load strongest onto left temporal electrodes. The results of this model can be seen in Figure 3-5 and Table 3-3.

3.2.4 Multiscale entropy increases across development

Previous work has suggested that MSE increases with development[41,42]. To assess whether MSE shows a developmental trajectory in our sample, we computed a paired-

sample t-test using the infants that participated in both the 4- and 8-month visits. We find overall MSE is significantly higher ($t(32) = 3.47$, $p = .002$) at 8-months ($M = 32.25$) than at 4-months ($M = 29.91$). We also computed *ICC* estimates to assess absolute agreement in MSE estimates across 4- and 8-month visits. We find, contrary to comparisons within 1 week, there is no longer absolute agreement among MSE measures after 4 months (*ICC* = -.18, $p = .889$). There was no significant difference in the variance of MSE values across age groups ($F(59,35) = 1.48$, two-tailed p-value = .218). MSE curves showing this age-related change across all conditions are plotted in Figure 3-6.

3.3 Discussion

Results of this novel, longitudinal dataset replicate and extend upon the work presented in Study 1. We find infants with lower levels of *OXTR* methylation (and likely increased sensitivity to endogenous oxytocin) show increased brain signal entropy during social perception, corroborating results from Study 1. We also show that brain signal entropy increases from 4 to 8 months of age, suggesting a brain signal entropy reports upon neurodevelopmental processes early in life. However, results of the present study suggest a modality-specific association between brain signal variability and infant social behavior. Specifically, we find 4-month-old infants that show increased entropy to social, relative to non-social stimuli within the auditory domain vocalize more frequently. However, the extent to which brain signal entropy distinguished between social and non-social visual perception was not associated with their verbal behavior. Neither entropy within visual nor auditory modalities was associated with the infant's visual attention to social stimuli at 4 months of age. These results replicate Study 1, which consisted solely of social auditory

stimuli. Together, these studies highlight the importance of social auditory perception for the developing infant.

3.4 Figures

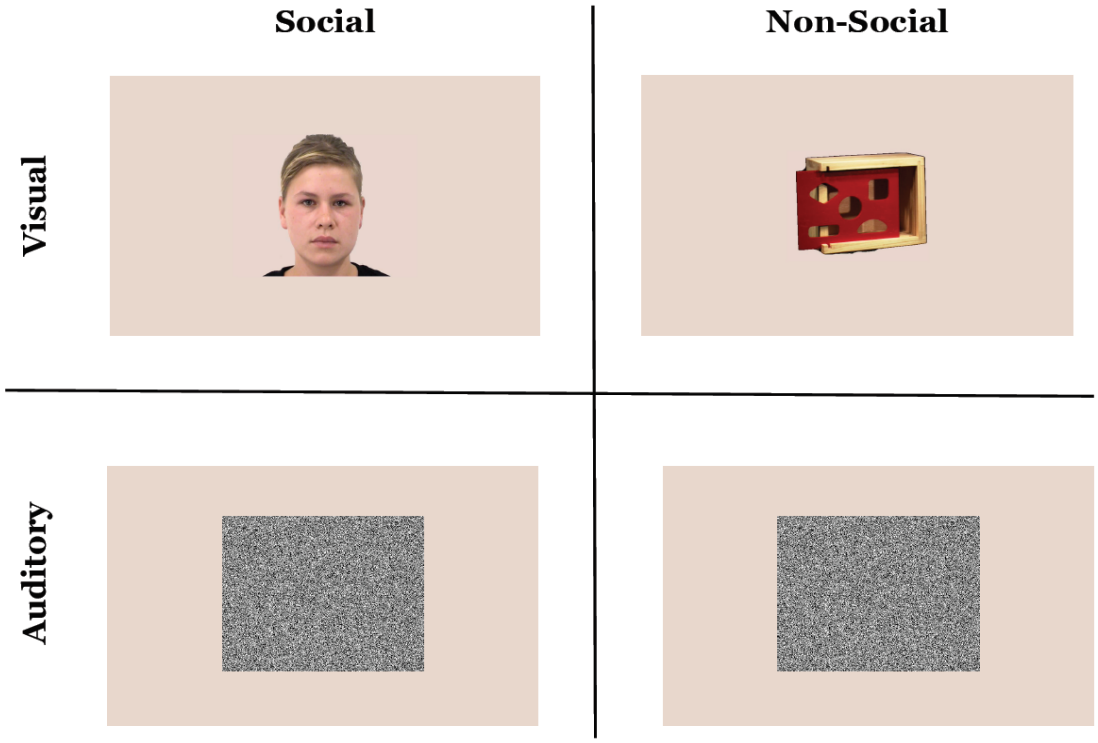

Figure 3-1. Example stimuli from the EEG paradigm. The EEG paradigm had a 2 x 2 design with the factors context (social or non-social) and modality (visual or auditory). Visual social stimuli consisted of videos of women smiling. Visual non-social stimuli consisted of videos of common objects rotating. During visual perception, white noise was played in the auditory domain. Auditory social stimuli consisted of infant-directed speech. Auditory non-social stimuli consisted of recordings of water sounds. During auditory perception, a video of static noise was played in the visual domain.

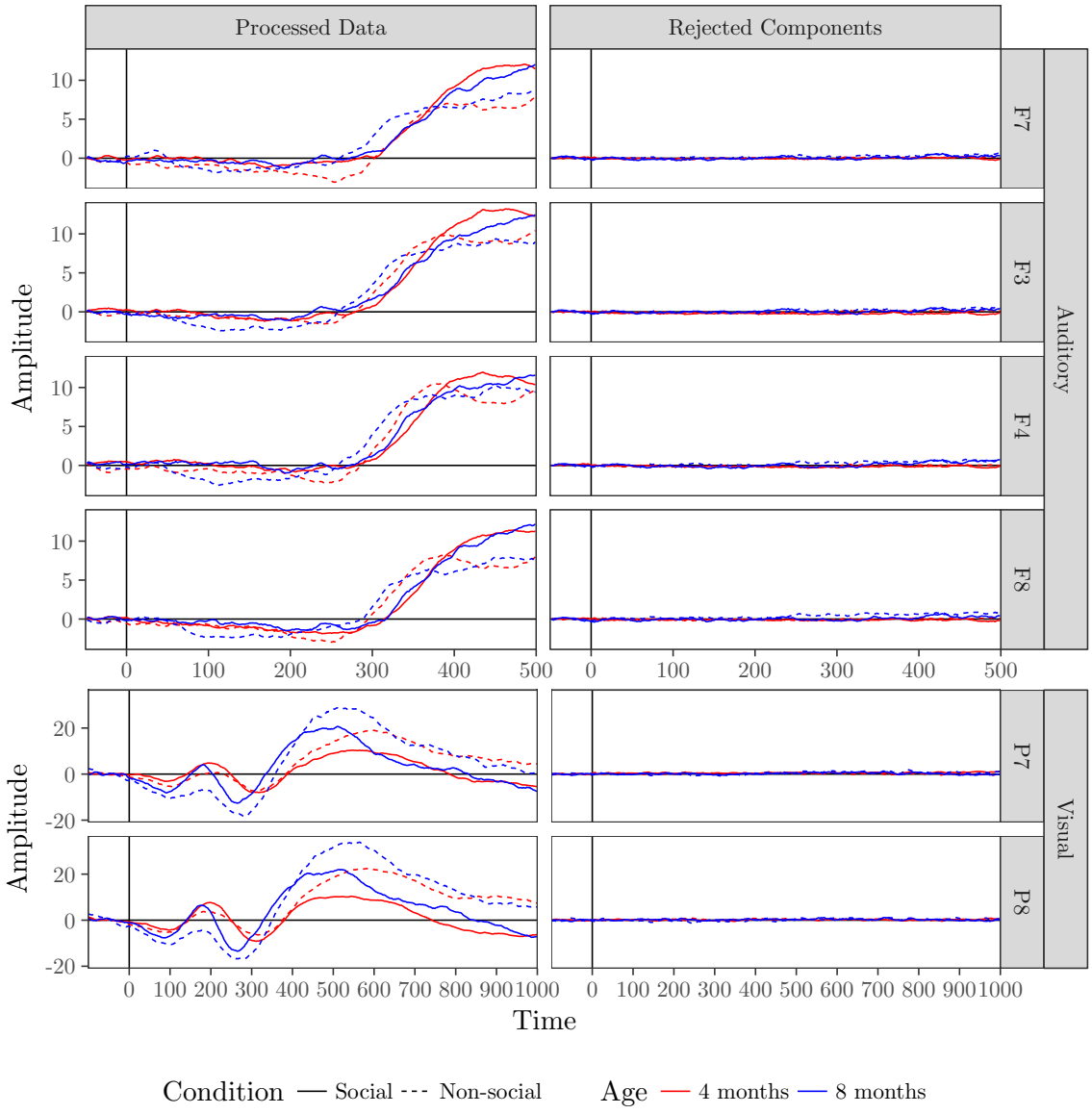

Figure 3-2. Auditory and visual event-related potentials. Auditory event-related potentials (ERPs) were examined at electrodes F7, F3, F4, and F8, which show a positive-going component at approximately 300 ms (top left). Visual ERPs were examined at electrodes P7 and P8, which show a negative-going component at approximately 290 ms (bottom left). These ERPs indicate that infants attended to and processed the stimuli. We find no ERPs in the rejected components (right), indicating that the preprocessing procedures did not obscure or eliminate relevant evoked response. Solid lines, ERPs for social stimuli. Dashed lines, ERPs for non-social stimuli. Red, ERPs at 4-months (n = 60). Blue, ERPs at 8-months (n = 36).

A

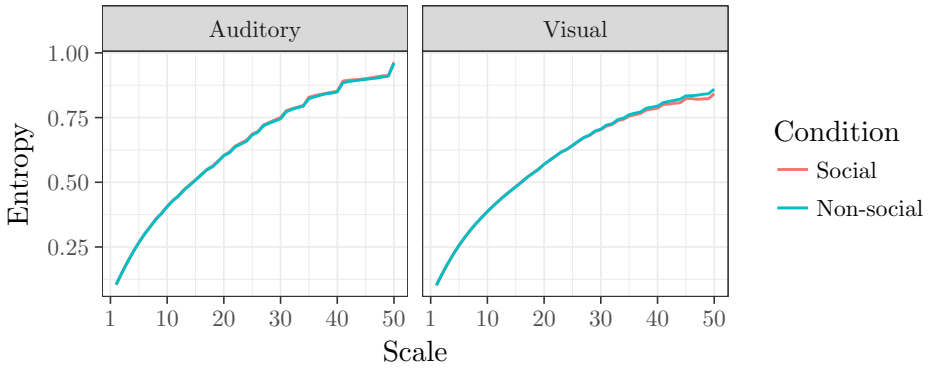

B

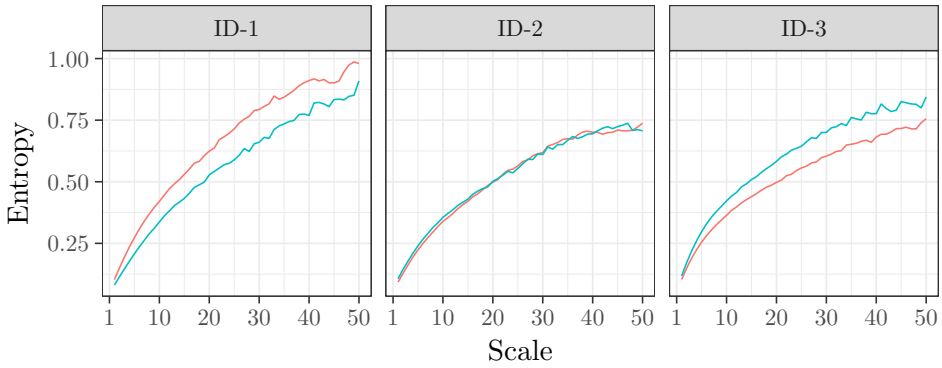

Figure 3-3 Average and individual difference multiscale entropy curves for each condition. (A) At the group level, multiscale entropy does not differ across social (pink) and non-social (blue) conditions in either auditory (left) or visual (right) modality (n = 60 4-month-olds). (B) However, individual infants show different levels of entropy across social and non-social conditions. Here, the multiscale entropy curves for three infants are depicted. One infant (left) shows greater brain signal entropy to social relative to non-social stimuli; one infant (middle) does not show differences in brain signal entropy across social and non-social conditions; one infant (right) shows greater brain signal entropy to non-social relative to social stimuli. These individual differences may be accounted for by differences in the endogenous oxytocinergic system, and may account for differences in infant social behavior.

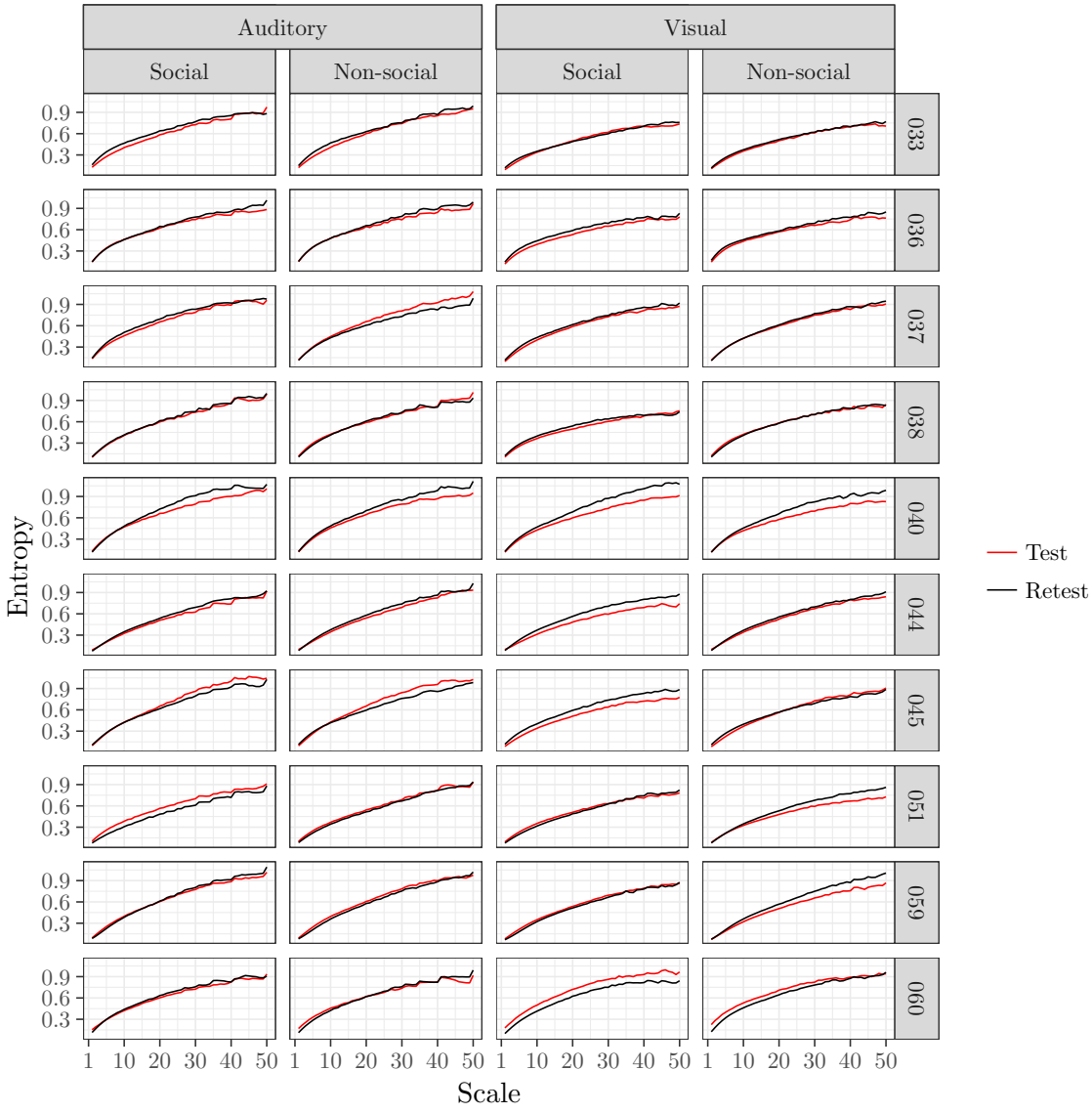

Figure 3-4. Multiscale entropy is a reliable measure in infancy. Average multiscale entropy curves for scales 1 to 50 (500 to 10 Hz) are plotted for each condition for ten infants who underwent EEG at 4 months of age (test visit, red), and repeated the procedure within 1 week (retest visit, black). We find good reliability across visits.

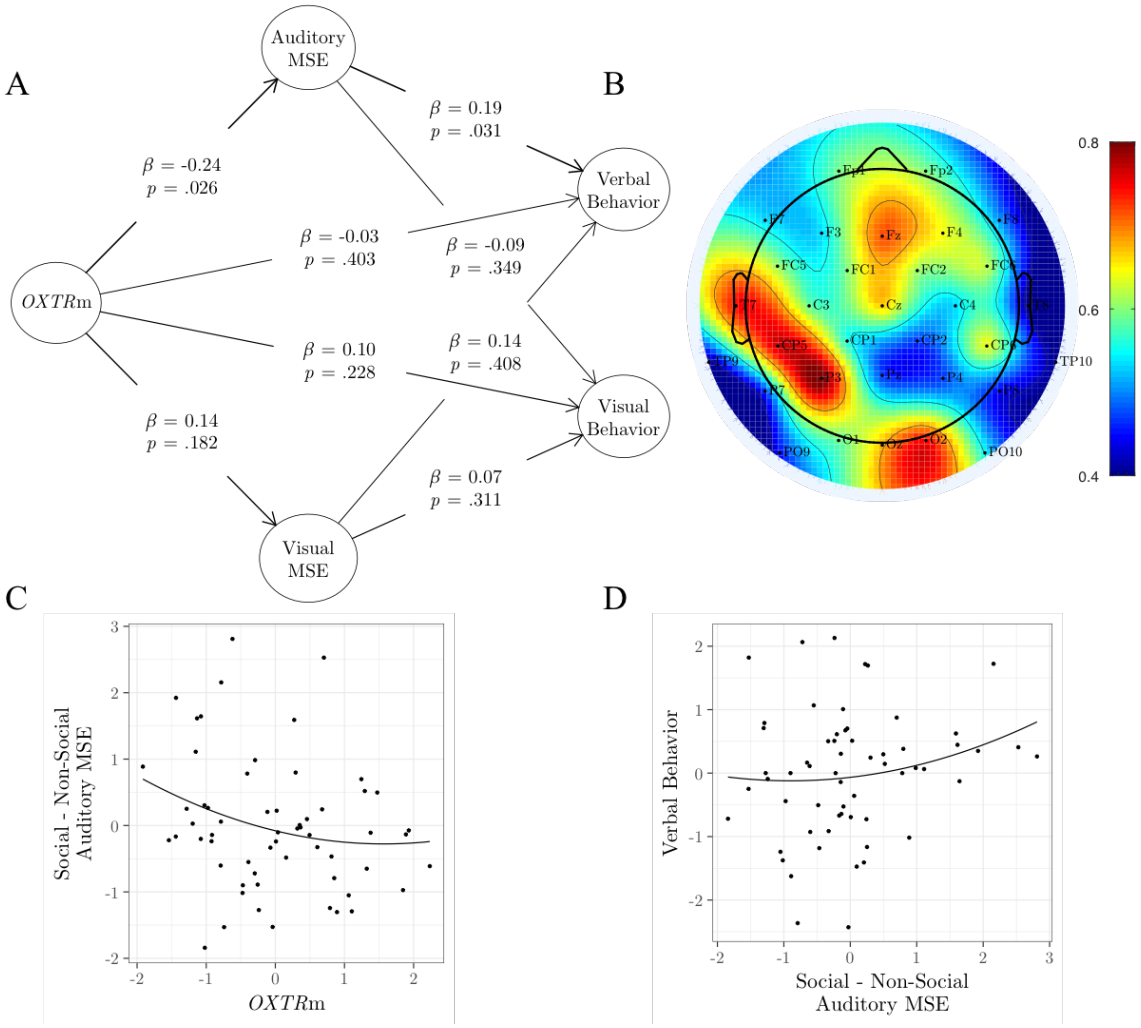

Figure 3-5. Entropy shows modality-specific associations with infant behavior within the auditory domain. (A) Results from the partial least squares path model (n = 60) showing associations between *OXTR* methylation (*OXTR*m), multiscale entropy evoked during social relative to non-social auditory perception (Auditory MSE), multiscale entropy evoked during social relative to non-social visual perception (Visual MSE), infant verbal behavior and infant visual behavior. β, path model coefficient; p, jackknifed p-value for coefficient. (B) Topographical map showing loadings of each electrode on the MSE Auditory construct. (C) Plot of the significant association between Auditory MSE and *OXTR*m standardized factor scores. (D) Plot of the significant association between Auditory MSE and infant verbal behavior standardized factor scores.

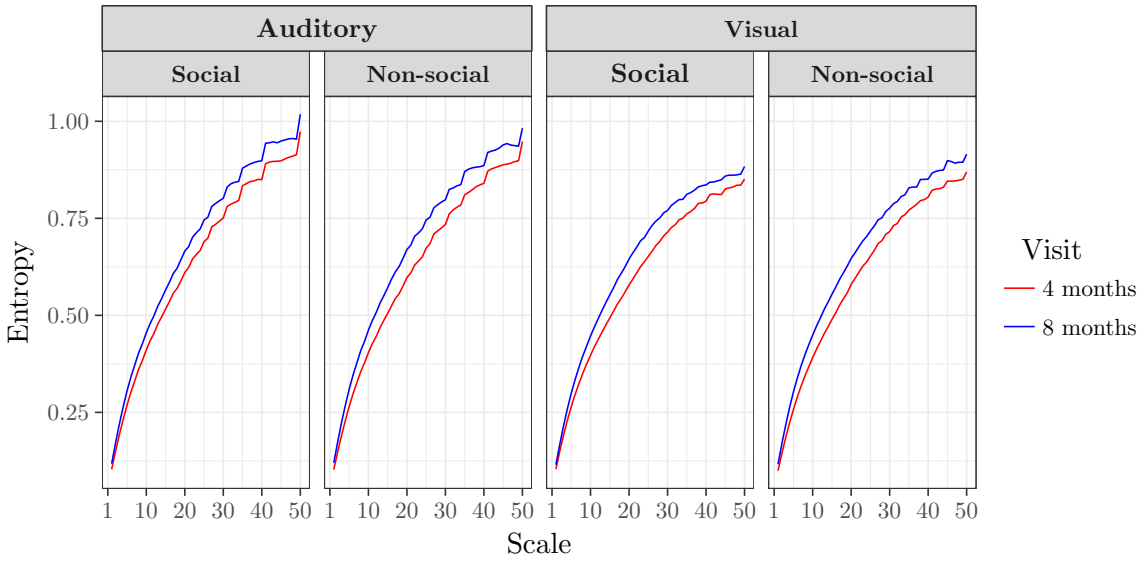

Figure 3-6. Entropy significantly increases from 4 to 8 months of age. Average multiscale entropy curves for scales 1 to 50 (500 to 10 Hz) are plotted for each condition and visit. Entropy is significantly higher at 8 months of age (n = 36, blue) than at 4 months of age (n = 60, red).

3.5 Tables

	Auditory		Visual	
Electrode	Social	Non-Social	Social	Non-Social
FP1	30.38 (0.68)	29.83 (0.67)	29.32 (0.73)	27.89 (0.78)
FP2	30.72 (0.81)	30.84 (0.90)	29.71 (0.95)	28.76 (0.80)
F7	31.71 (0.88)	32.25 (0.65)	29.56 (0.69)	30.46 (0.82)
F3	32.69 (0.74)	31.74 (0.87)	30.30 (0.72)	29.83 (0.87)
Fz	30.42 (0.67)	29.75 (0.76)	29.21 (0.74)	28.83 (0.77)
F4	32.12 (0.74)	31.00 (0.76)	29.88 (0.85)	29.32 (0.83)
F8	30.74 (0.74)	31.15 (0.72)	29.98 (0.71)	30.43 (0.87)
FC5	33.09 (0.80)	32.39 (0.72)	30.29 (0.80)	30.26 (0.90)
FC1	30.57 (0.71)	30.91 (0.68)	29.96 (0.71)	28.84 (0.87)
FC2	30.20 (0.66)	30.14 (0.60)	28.16 (0.78)	28.44 (0.80)
FC6	32.40 (0.80)	32.09 (0.72)	30.07 (0.94)	29.65 (0.73)
T7	31.69 (0.77)	31.73 (0.80)	30.15 (0.82)	31.10 (0.82)
C3	32.78 (0.73)	31.20 (0.65)	28.95 (0.80)	29.08 (0.88)
Cz	30.01 (0.64)	30.53 (0.71)	28.59 (0.68)	28.50 (0.71)
C4	33.18 (0.74)	31.63 (0.65)	29.71 (0.73)	29.18 (0.78)
T8	33.00 (0.68)	33.18 (0.71)	31.08 (0.87)	30.70 (0.79)
TP9	30.64 (0.76)	30.11 (0.68)	29.26 (0.91)	27.46 (0.88)
CP5	33.33 (0.70)	33.77 (0.76)	30.31 (0.72)	31.51 (0.72)
CP1	30.16 (0.76)	29.81 (0.68)	27.82 (0.92)	27.53 (0.93)
CP2	29.20 (0.70)	28.20 (0.74)	27.11 (0.79)	26.12 (1.01)
CP6	34.24 (0.80)	33.78 (0.66)	32.10 (0.73)	31.99 (0.73)
TP10	29.97 (0.75)	31.95 (0.83)	28.63 (0.84)	28.47 (0.87)
P7	33.70 (0.79)	33.59 (0.78)	31.05 (0.73)	30.37 (0.72)
P3	32.56 (0.73)	31.70 (0.63)	29.56 (0.68)	30.59 (0.81)
Pz	29.34 (0.69)	28.87 (0.72)	26.40 (0.88)	26.55 (0.86)
P4	31.59 (0.79)	31.03 (0.67)	29.30 (0.64)	30.11 (0.81)
P8	33.52 (0.71)	33.55 (0.65)	31.21 (0.89)	30.51 (0.70)
PO9	31.03 (0.73)	30.37 (0.75)	29.19 (0.85)	28.01 (0.81)
PO10	30.04 (0.83)	31.02 (0.76)	28.04 (0.87)	27.10 (0.78)
O1	31.90 (0.66)	31.73 (0.73)	29.79 (0.62)	29.78 (0.62)
Oz	31.38 (0.68)	31.71 (0.79)	28.72 (0.55)	29.37 (0.70)
O2	30.59 (0.62)	32.04 (0.79)	28.93 (0.59)	29.06 (0.71)

Table 3-1. Average multiscale entropy values. Mean (and standard error) area under the multiscale entropy curve values for each electrode and condition.

How often did your baby make talking sounds when s/he was ready for more food?
How often did your baby squeal or shout when excited?
When being dressed or undressed, how often did the baby coo or vocalize?
How often did your baby make talking sounds when riding in a car?
How often did your baby make talking sounds when riding in a shopping cart?
When hair was washed how often did the baby vocalize?
How often did your baby make talking sounds when you talked to her/him?

Table 3-2. Vocalization items from the Short Revised Infant Behavior Questionnaire. Individual items from the vocalization subscale of the Short Revised Infant Behavior Questionnaire were included in the infant verbal behavior construct.

Composite reliability coefficients				
*OXTR*m	Auditory MSE	Visual MSE	Verbal Behav	Visual Behav
0.82	0.75	0.79	0.84	0.9
R^2 coefficients				
*OXTR*m	Auditory MSE	Visual MSE	Verbal Behav	Visual Behav
-	.06	.02	.06	.03

Table 3-3. Model fit statistics. Composite reliability coefficients reflecting internal consistency and reliability and R^2 coefficients reflecting explanatory power for each construct and model. *OXTR*m, *OXTR* DNA methylation; MSE, multiscale entropy Social – Non-Social difference score; Verbal Behav, Vocalization subscore of the Short Revised Infant Behavioral Questionnaire (IBQ-RS); Visual Behav, visual attention to faces during the eye-tracking paradigm.

4 Study 3: Age-related changes in the context-specific associations between oxytocinergic system function, neural variability, and social signal detection in adulthood

4.1 Methods

4.1.1 Participants

One hundred four Caucasian young adults (60 female) aged 17 to 28 (M = 18.91 ± 1.34) years recruited from the University of Virginia's Psychology Department Participant Pool participated in Study 3 for partial course credit.

4.1.2 DNA sample collection and epigenetic analysis

Eight ml of blood was collected in a Mononuclear Cell Preparation Tube (BD Biosciences, San Jose, CA) by a professional phlebotomist. Peripheral blood mononuclear cells (PBMC) were immediately isolated from blood and stored at room temperature until downstream DNA isolation and epigenetic analysis. DNA isolation was carried out using reagents and protocol supplied in the Gentra Puregene Blood Kit (Qiagen, Valencia, CA). Samples from Study 2 and Study 3 were subjected to bisulfite treatment, PCR, and pyrosequencing together as a batch so that methylation levels could be compared across our infant and adult samples. Samples were processed in a randomized order. Adult methylation values averaged 49.77 ± 6.13%.

4.1.3 Social signal detection paradigms

Participants completed two measures assessing social signal detection abilities within the visual domain. The first is a biological motion perceptual threshold task in which participants were asked to discriminate point-light displays of biological motion embedded

within a noisy display (Figure 4-1). The second is the Reading the Mind in the Eyes Test (RMET) in which participants were asked to discriminate subtle emotions from photographs depicting only the eye region of the face.

Biological Motion Perceptual Threshold Task. Participants first completed a familiarization procedure in which they were shown five 1000-ms point-light displays of biological motion presented without noise (climbing, skipping rope, drop-kicking, overhand throwing, underhand throwing) and five 1000-ms point-light displays of scrambled versions of the biological motion presented without noise[98]. Participants were asked to verbalize if the display depicted a person, and if so, what the person was doing. If an incorrect response was given, the researcher corrected the participant. Plausible alternatives to the biological motion displays (e.g. "*bowling*" instead of "*underhand throwing*") were accepted as correct responses.

Then, participants were familiarized to the two-alternative, forced-choice perceptual threshold detection task. Participants were shown two displays back-to-back, one containing a display of biological motion embedded among additional noise points, and one containing a display of scrambled motion embedded among additional noise points, and asked to identify which display contained the biological motion via 1/2 key press. The point-light displays were identical to those used in the familiarization procedure. Which display contained the biological motion, the action presented, and the position of the point-light display within the noise display was randomized across trials. During this familiarization phase, the point-light displays were colored blue and the noise points were colored black (Figure 4-1). Each display was presented for 1000 ms and displays within a

trial were separated by a 500 ms interval. Stimuli were presented with PsychToolBox[87] v3.0.14 for MATLAB. Participants were given an unlimited amount of time to enter their response, and then initiated the next trial via key press. Participants completed 5 trials of the familiarization phase.

Participants then completed 2 blocks of 50 trials in the test phase in which all parameters were identical to the familiarization phase except both the point-light displays and the noise points were colored black. The level of noise was varied over trials according to an adaptive procedure (QUEST[99]) to derive 75% correct threshold estimates[100].

The Reading the Mind in the Eyes Test. In this task[101], participants were shown 40 greyscale photographs of the eye-region of the face of different actors and actresses, and asked to discern which of four words best described what the person in the photograph is thinking or feeling. Performance on this task has been shown to discriminate adults with high functioning autism from neurotypical controls[101], is inversely associated with the degree to which neurotypical controls display autistic-like traits[101], and improves after the administration of exogenous oxytocin[102].

4.1.4 Social communication measures

Participants completed two measures designed to assess autistic-like traits in neurotypical adults, the Autism Spectrum Quotient Questionnaire (AQ)[14] and the Broad Autism Phenotype Questionnaire (BAPQ)[103]. The AQ is a 50-item self-report measure in which participants are asked to rate the degree to which they agree or disagree with statements regarding behaviors and preferences across 5 domains associated with autism: social skill, communication, attention switching, attention to detail, and imagination. The

BAPQ is a 36-item self-report measure in which participants are asked to rate how frequently statements of personality and behavioral traits apply to them across 3 domains associated with autism: aloof personality, rigid personality, and pragmatic language skills. To assess verbal behavior association with social communication abilities, we include the AQ Communication subscale and the BAPQ Pragmatic Language Skills subscale. Individual items included in each of these subscales are listed in Table 4-1. Traditionally, a higher score on these measures indicates the endorsement of a greater number of traits associated with autism. In our analyses, these subscores were reverse-coded so that a higher number indicated enhanced social-communication abilities.

4.1.5 EEG paradigm

Adults in Study 3 completed 24 blocks of the same EEG paradigm described in Study 2, except the social auditory stimuli were replaced with naturalistic adult-directed speech, recorded from eleven English-speaking females as they engaged in an unscripted telephone conversation with another native English speaker, downloaded from http://talkbank.org/access/CABank/CallHome/eng.html. Clips containing single-word utterances (e.g. "*wow*," "*fourteen*," "*listen*") or short phrases (e.g. "*I don't know*," "*that's right*," "*no way*") were extracted from the recordings. Clips containing incoherent speech or background noises were discarded and stimuli were selected such that the social stimulus set matched the non-social stimulus set on mean fundamental frequency (M_{social} = 305.62, $M_{non\text{-}social}$ = 335.29, t = -1.60, p = .113), standard deviation of fundamental frequency (M_{social} = 73.29, $M_{non\text{-}social}$ = 57.82, t = 1.64, p = .103), and duration (M_{social} = 0.88, $M_{non\text{-}social}$ = 0.97, t = -1.48, p = .142) using Praat[92] and custom MATLAB scripts.

4.1.6 EEG acquisition and preprocessing

EEG was recorded from 32 Ag/AgCl active BioSemi electrodes affixed to an elastic cap (BioSemi, Wilmington, NC) using the 10-20 electrode placement system. The horizontal electrooculogram (EOG) was recorded from an electrode placed at the outer canthus of the right eye. The vertical EOG was recorded from an electrode placed on the supraorbital ridge of the right eye. The participant's head circumference was first obtained to determine the correct cap size. Electrode offsets were maintained within ± 20 μV.

EEG was amplified with an ActiveTwo AD-box (BioSemi, Wilmington, NC) and recorded using ActiView605-Hires software with a sampling rate of 1025 Hz and online band-pass filtered between 0.1-100 Hz. Participants were seated approximately 100 cm from a computer monitor and instructed to remain still and keep their eyes on the screen. Participants were given the opportunity to pause and rest their eyes between trials. The participant initiated the start of the next trial via key press.

Data were analyzed offline using EEGLab v14.1.1[93], ERPLab v7.0.0[93] and custom MATLAB scripts. Data were resampled at 500 Hz, band-pass filtered between 0.3-20 Hz, and re-referenced to the average of all scalp electrodes. Visual stimuli were segmented into stimulus-evoked epochs 100 ms pre-stimulus onset to 1000 ms post-stimulus onset with pre-baseline correction. Auditory stimuli were segmented into stimulus-evoked epochs 100 ms pre-stimulus onset to 500 ms post-stimulus onset with pre-baseline correction. Epochs contaminated with excessive amplitude standard deviations (> 40 μV in ocular channels, > 20 μV in scalp electrodes) within a sliding window of width 200 ms and step 100 ms were discarded as artifacts. Participants with at least 20 artifact-free visual segments and 40

artifact-free auditory segments were retained in the analysis. Seven participants were excluded for an insufficient number of artifact-free segments.

We then used Independent Component Analysis (ICA) to remove components with ocular, muscular or electrical artifacts. On average, 3.35 (range 1 to 7) components were removed. The number of components removed did not correlate with MSE within the visual ($r = .02$, $p = .828$) or auditory ($r = -.08$, $p = .455$) domain and did not show significant ERP effects (Figure 4-2), indicating that the components identified as artifacts did not contain relevant brain activity.

To include an equivalent number of data points for each condition in the MSE computation[63], we selected the 20 visual segments (10 social) and the 40 auditory segments (20 social) with a total global field power (GFP)[42] closest to the median GFP for each participant for inclusion in downstream analyses (5000 data points per condition). These numbers were selected so that the results of the present adult study would be directly comparable to the infant data in Study 2. To ensure that these preprocessing procedures did not obscure or eliminate relevant brain activity, we examined the ERP (Figure 4-2**)** using these data re-referenced to Cz (visual) or the average of the mastoids (auditory).

To assess the reliability of brain signal entropy in adults, we repeated the GFP selection step to select 40 visual segments (20 social) and 80 auditory segments (40 social). We then examined the split-half reliability by comparing MSE from the first half (10 visual and 20 auditory per context) and the second half (10 visual and 20 auditory per context) of the experiment.

4.1.7 Quantification of brain signal variability

We computed MSE on the residuals of the average-referenced post-stimulus onset EEG signal (i.e. after subtracting the within-person average ERP) using pattern length m = 2 and similarity criterion r = .5 (recalculated at each scale) across segments[63]. We then calculated the area under the MSE curve for each electrode for scales 1 to 50 (corresponding to 500 to 10 Hz). Group-average MSE curves are plotted in Figure 4-3 and average area under the curve values are listed in Table 4-2.

4.1.8 Statistical analysis

To identify causative associations among our epigene-brain-behavior variables, we analyzed data in the partial least squares path modeling (PLS-PM) framework using WarpPLS v6.0[81] to model curvilinear associations between our latent constructs. The aim of the study was to identify whether there are age-related changes in the context- and modality-specific associations between *OXTR* methylation, brain signal entropy evoked during perception, and behavior seen in infancy. We included Social – Non-social MSE_{AUC} differences scores for each electrode across visual and auditory modalities separately in the model. We included the AQ Communication and BAPQ Pragmatic Language Skills subscores in the Verbal Behavior construct. These subscores were reverse-coded so that a higher number indicated enhanced social-communication abilities. The Total Items Correct on the RMET, and the mean and quantile estimates from each of two blocks of the Biological Motion Perceptual Threshold Task were included in the Visual Behavior construct. Each technical replicate (3) of the *OXTR* methylation analysis was included in the *OXTR* methylation construct.

Outliers. After initial model fitting, values were considered outliers if the factor score residuals fell more than 3 median absolute deviations from the median. We selected this relatively conservative criterion to balance outlier detection with subject retention. One subject was identified as an outlier for the Visual Behavior construct, and one subject was identified as an outlier for the Verbal Behavior construct. These two subjects were removed and models were re-estimated. Results did not appreciably change with or without outliers; we therefore conservatively report on models excluding outliers (n = 95, 32 female).

Model Assessment. After removal of outliers, we checked for discriminant validity by identifying and removing any items that loaded higher onto another construct or did not significantly load onto its construct for each model. These included T8 for both Auditory and Visual MSE constructs and RMET for the Visual Behavior construct. Removing these items did not appreciably change results; results are presented with these items removed.

Sample size. The target sample size for the PLS-PM analysis assessing associations between our epigenetic, neural, and behavioral measures was determined via a power analysis using effect sizes established in Study 2 and following recommendations of Chin & Newsted[84]. In our models, behavioral constructs have the largest number of predictors – 3. A two-tailed multiple regression power analysis[85] determined that 94 participants are needed to detect an effect size of 0.19 with 3 predictors, 95% power, and α = .05.

4.2 Results

4.2.1 Entropy is reliable in adulthood

ICC estimates and their 95% confident intervals were calculated using the irr v0.84.1[97] statistical package in R v3.4.4[80] based on a single rating (k = 1), absolute-

agreement, 2-way mixed-effects model. MSE was found to show good reliability (*ICC* = .84, $p < .001$) across the first and second halves of the experiment. See Figure 4-4 for first and second split-half reliability MSE curves.

4.2.2 Entropy during social perception is significantly higher in adulthood than infancy

We then compared MSE across age groups using a one-way between-subjects ANOVA. We find a significant main effect of age group $F(2,190) = 308.40$, $p < .001$. Post hoc comparisons using the Tukey HSD test in R[80] indicated that MSE is significantly higher for 8- than 4-month-olds, and that the adults have significantly higher MSE than both 4- and 8-month-olds (Figure 4-5). There was no significant difference in the variance of MSE values between adults and 4-month-olds ($F(96,59) = 0.74$, two-tailed p-value = .189), or between adults and 8-month-olds ($F(96,35) = 1.09$, two-tailed p-value = .790), indicating that, although MSE is higher in adulthood, we do not find a ceiling effect; there are significant individual differences in brain signal entropy within an adult sample that may be accounted for by individual differences in molecular makeup, or that may account for individual differences in behavioral phenotype.

4.2.3 Entropy shows modality-specific associations with adult behavior in both the auditory and visual domains

We modeled context- and modality-specific associations between *OXTR* methylation, brain signal evoked by social relative to non-social stimuli, and visual (social signal detection) and verbal (social communication abilities) social behavior in young adults. Unlike in Studies 1 and 2, we failed to find an association between *OXTR*

methylation and MSE in either the auditory (β = 0.13, p = .133) or the visual (β = 0.06, p = .260) modalities. However, we did find significant negative associations between *OXTR* methylation and both verbal (β = -0.17, p = .049) and visual (β = -0.18, p = .031) social behavior such that participants with lower levels of *OXTR* methylation (i.e. presumed increased sensitivity to endogenous oxytocin) performed better on the social signal detection tasks and reported enhanced social communication abilities.

We found modality-specific associations between Social – Non-social MSE. Greater entropy during social auditory relative to non-social auditory perception was significantly associated with improved social-communication skills (β = 0.32, p = .001), but auditory-evoked MSE was unrelated to visual social behavior (β = 0.02, p = .447). Conversely, greater entropy during social visual relative to non-social visual perception was positively associated with visual social signal detection abilities (β = 0.14, p = .039), but visual-evoked MSE was unrelated to verbal behavior (β = -0.10, p = .13). Auditory MSE loadings were highest for bilateral frontal and parietal electrodes. Visual MSE loadings were highest for frontal and occipital electrodes. The results of this model can be seen in Figure 4-6 and Table 4-3.

4.3 Discussion

Expanding our work into a healthy young adult sample, we found continued support for modality- and context-specific associations between brain signal entropy during social perception and social behavioral outcomes. As in our infant samples, adults that showed increased brain signal entropy during auditory social perception reported enhanced verbal abilities. However, an association between brain signal entropy during visual social

perception and visual sensitivity to social cues also emerged in our adult sample only, suggesting a developmental trajectory for the differential reliance on modality-specific social cues. These data also provide the first evidence that individuals who display a more entropic brain response during social perception find social information more salient – we find a positive association between social visual brain signal entropy and biological motion perceptual threshold such that those who displayed a more entropic response were able to detect a point-light walker among a greater number of noise points.

Unlike in our infant samples, we failed to find direct associations between *OXTR* methylation and brain signal entropy. However, we replicated results of Study 2 and others[41,42] showing a developmental trajectory for brain signal entropy. Our adult sample displayed significantly higher levels of brain signal entropy than our infant samples across all conditions and modalities. Together, these results highlight a role for brain signal entropy as a marker of differential social-developmental processes that persist into adulthood and may be involved with ascribing salience to social information.

4.4 Figures

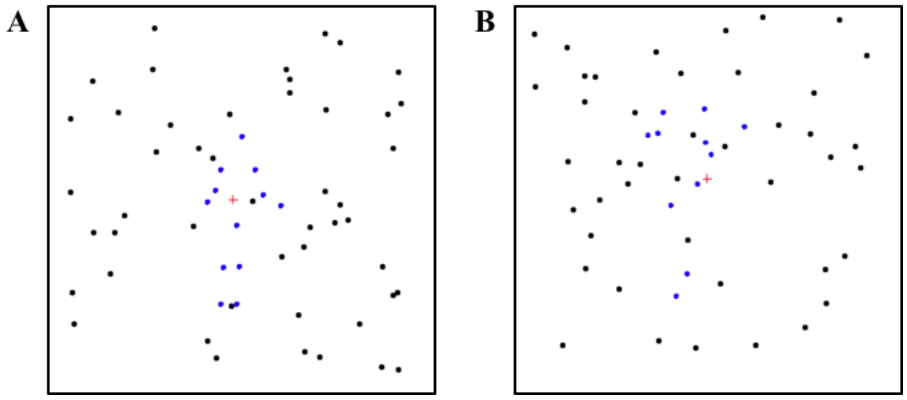

Figure 4-1. Biological motion perceptual threshold task. (A) A point-light display of biological motion (blue, jumping rope) is masked among additional noise points. (B) A point-light display of scrambled motion (blue) is masked among additional noise points. Participants were shown two displays back-to-back and asked to indicate which display contained the biological motion. During the familiarization stage, point-light displays were colored blue, as above. During the test phase, all points were colored black. The number of additional noise points varied over trials according to an adaptive procedure to derive 75% correct threshold estimates.

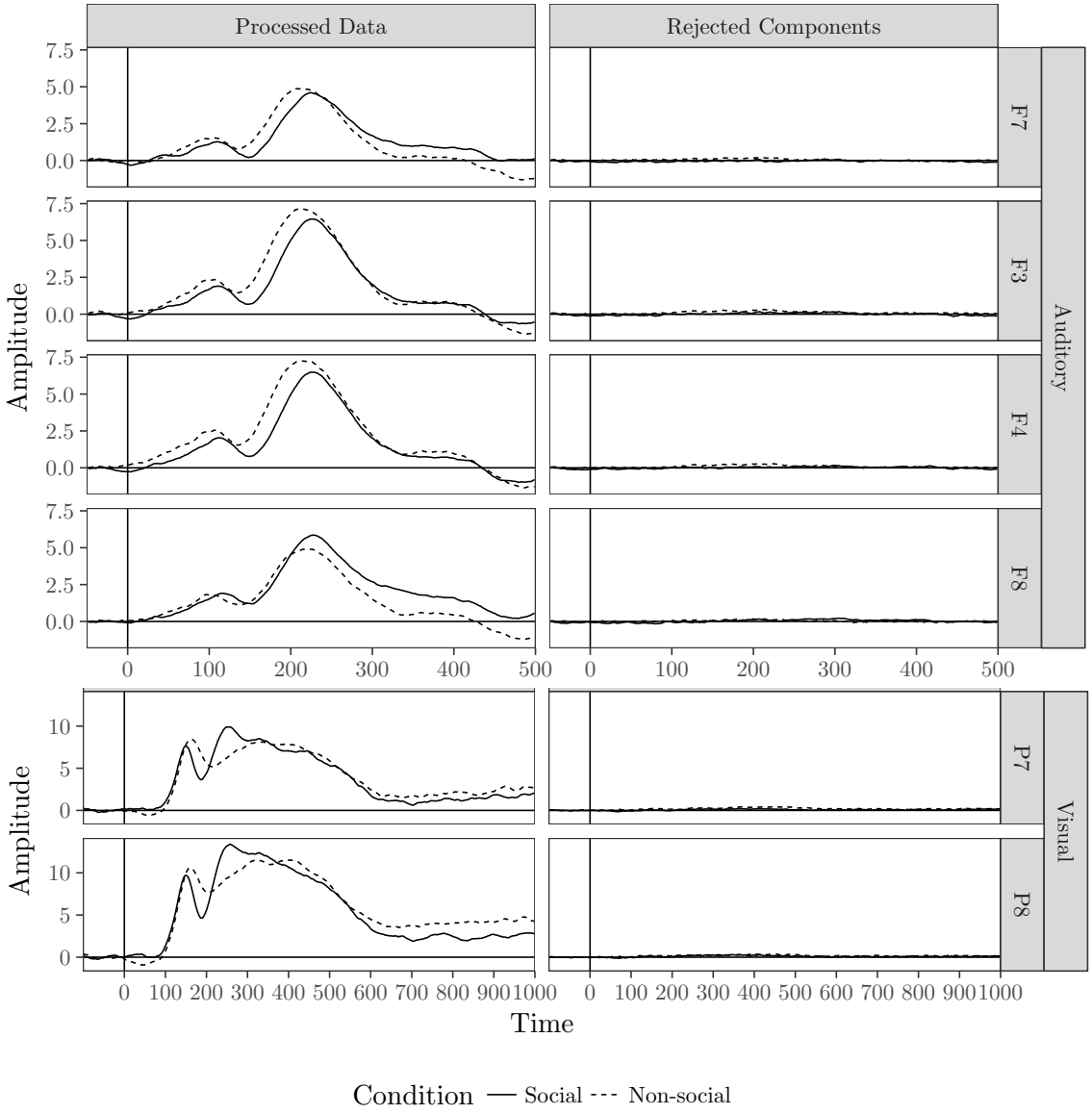

Figure 4-2. Auditory and visual event-related potentials. Auditory event-related potentials (ERPs) were examined at electrodes F7, F3, F4, and F8, which show a positive-going component at approximately 150 ms (top left). Visual ERPs were examined at electrodes P7 and P8, which show a negative-going component at approximately 170 ms (bottom left). These ERPs indicate that participants (n = 95) attended to and processed the stimuli. We find no ERPs in the rejected components (right), indicating that the preprocessing procedures did not obscure or eliminate relevant evoked response. Solid lines, ERPs for social stimuli. Dashed lines, ERPs for non-social stimuli.

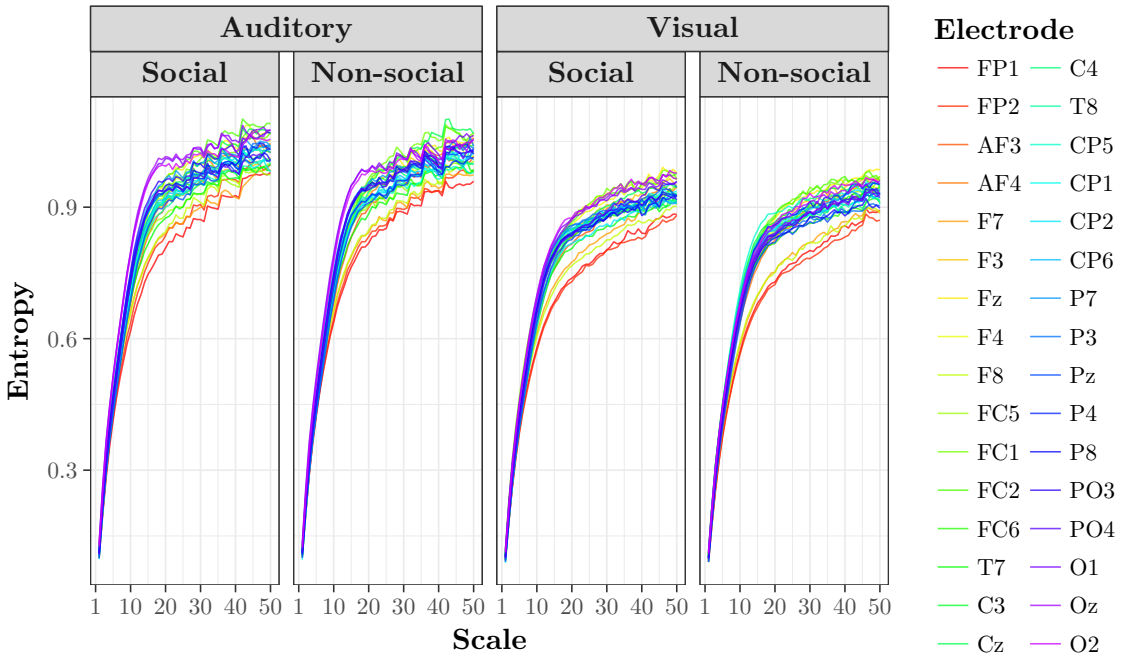

Figure 4-3. Group average multiscale entropy curves. The average multiscale entropy curves for scales 1 to 50 (500 to 10 Hz) are plotted for each condition and electrode (n = 95).

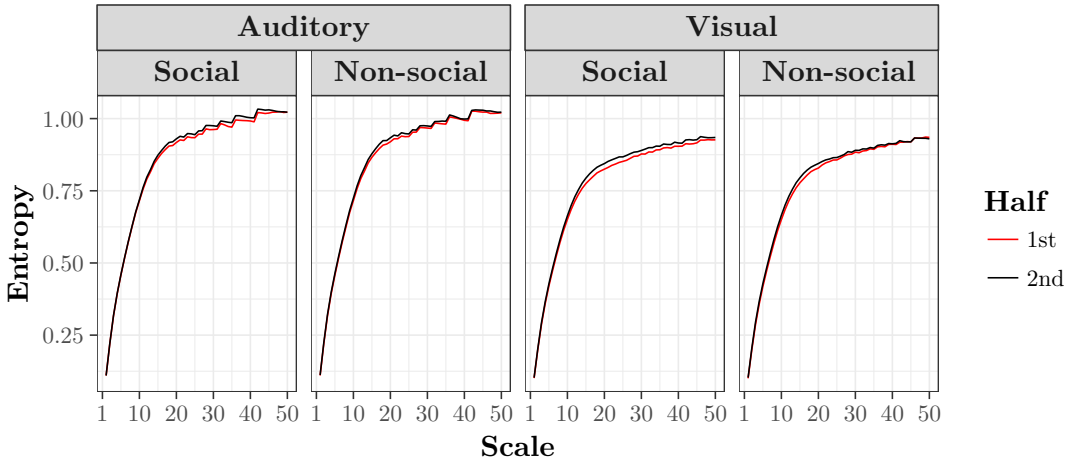

Figure 4-4. Multiscale entropy is a reliable measure in adulthood. Average multiscale entropy curves for scales 1 to 50 (500 to 10 Hz) are plotted for each split-half of the experiment (n = 95) We find good reliability across split-halves.

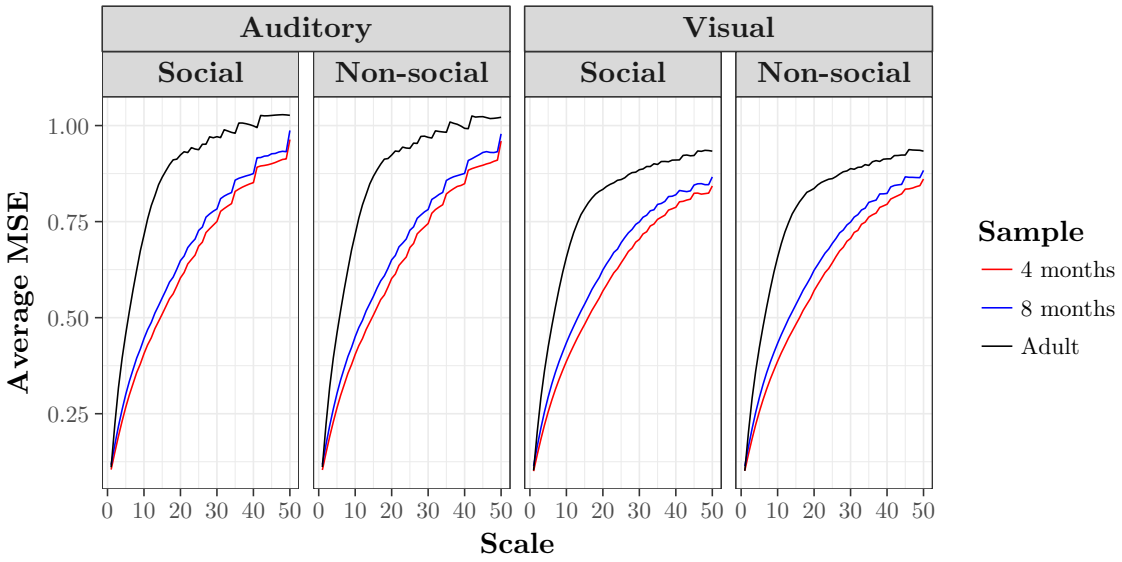

Figure 4-5. Entropy is significantly higher in adulthood than in infancy. Average multiscale entropy curves for scales 1 to 50 (500 to 10 Hz) are plotted for each condition and age group. Entropy is significantly higher in adulthood ($n = 95$, black), than at 8 months of age ($n = 36$, blue) or at 4 months of age ($n = 60$, red).

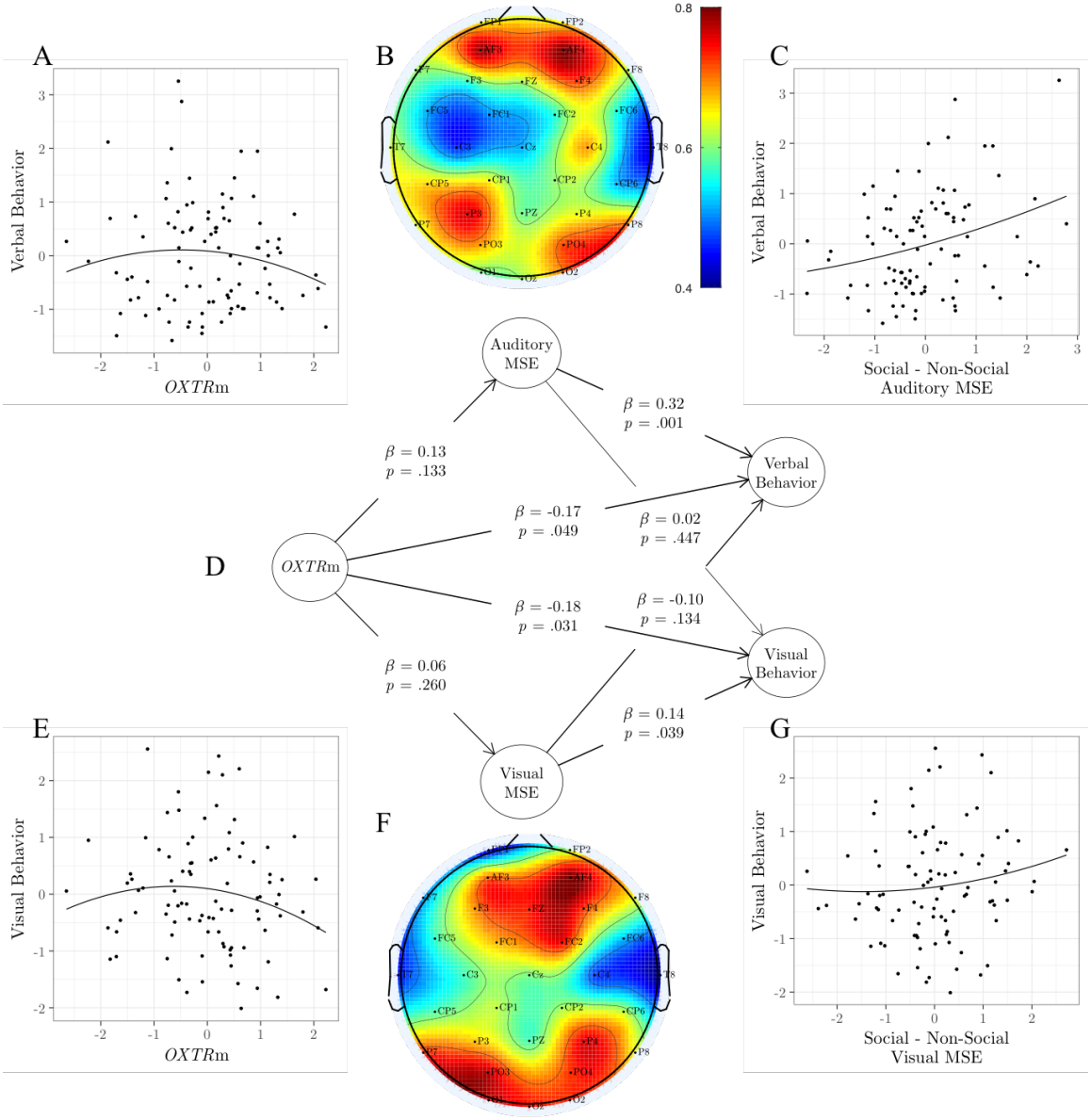

Figure 4-6. Entropy shows modality-specific associations with adult behavior in both the auditory and visual domains. (D) Results from the partial least squares path model ($n = 95$) showing modality-specific associations between multiscale entropy (MSE) evoked during social relative to non-social auditory perception. β, path model coefficient; p, jackknifed p-value for coefficient. (B) Topographical map showing loadings of each electrode on the MSE Auditory construct. (F) Topographical map showing loadings of each electrode on the MSE Visual construct. (A,E) Plots of the significant association between *OXTR* methylation (*OXTR*m) and social behavior standardized factor scores. (C,G) Plots of the significant, modality-specific associations between MSE and social behavior standardized factor scores.

4.5 Tables

AQ	Other people frequently tell me that what I've said is impolite, even though I think it is I enjoy social chit-chat. *** When I talk, it isn't always easy for others to get a word in edgeways. I frequently find that I don't know how to keep a conversation going. I find it easy to "read between the lines" when someone is talking to me. *** I know how to tell if someone listening to me is getting bored. *** When I talk on the phone, I'm not sure when it's my turn to speak. I am often the last to understand the point of a joke. I am good at social chit-chat. *** People often tell me that I keep going on and on about the same thing.
BAPQ	I find it hard to get my words out smoothly. It's hard for me to avoid getting sidetracked in conversation. I am "in-tune" with the other person during conversation. *** My voice has a flat or monotone sound to it. I feel disconnected or "out of sync" in conversations with others. *** People ask me to repeat things I've said because they don't understand. I have been told that I talk too much about certain topics. I speak too loudly or softly I can tell when someone is not interested in what I am saying. *** I leave long pauses in conversation. I lose track of my original point when talking to people. I can tell when it is time to change topics in conversation. ***

Table 4-1. Social communication items. Individual items included in the Autism Spectrum Quotient Questionnaire (AQ) Communication subscale, and the Broad Autism Phenotype Questionnaire (BAPQ) Pragmatic Language Skills subscale.

	Auditory		Visual	
Electrode	Social	Non-social	Social	Non-social
FP1	38.20 (0.71)	38.55 (0.60)	34.96 (0.61)	34.81 (0.63)
FP2	39.41 (0.64)	39.10 (0.64)	34.57 (0.58)	34.30 (0.66)
AF3	41.60 (0.57)	41.31 (0.55)	37.80 (0.51)	38.78 (0.51)
AF4	42.48 (0.50)	42.63 (0.49)	38.52 (0.56)	38.13 (0.58)
F7	39.26 (0.55)	39.60 (0.51)	36.59 (0.56)	35.59 (0.61)
F3	41.64 (0.55)	43.08 (0.51)	39.08 (0.58)	39.69 (0.55)
Fz	43.59 (0.47)	43.18 (0.47)	39.87 (0.49)	39.94 (0.60)
F4	43.42 (0.56)	42.78 (0.48)	39.74 (0.57)	39.15 (0.54)
F8	39.92 (0.63)	39.88 (0.65)	35.94 (0.65)	35.56 (0.57)
FC5	40.85 (0.54)	41.54 (0.51)	39.10 (0.59)	39.09 (0.58)
FC1	43.17 (0.48)	44.02 (0.48)	40.05 (0.62)	40.26 (0.51)
FC2	44.29 (0.46)	43.58 (0.51)	39.78 (0.57)	40.27 (0.55)
FC6	42.38 (0.50)	41.76 (0.52)	38.45 (0.61)	37.87 (0.65)
T7	40.68 (0.48)	40.95 (0.52)	37.42 (0.63)	38.46 (0.54)
C3	41.62 (0.60)	43.26 (0.51)	38.70 (0.67)	39.44 (0.61)
Cz	42.96 (0.51)	43.61 (0.45)	38.52 (0.52)	39.32 (0.47)
C4	42.92 (0.51)	42.55 (0.54)	38.74 (0.61)	38.86 (0.64)
T8	41.55 (0.52)	42.07 (0.46)	38.62 (0.62)	38.66 (0.55)
CP5	42.86 (0.47)	41.74 (0.52)	38.63 (0.62)	40.18 (0.63)
CP1	41.89 (0.53)	41.73 (0.51)	38.40 (0.57)	38.53 (0.61)
CP2	41.69 (0.52)	41.92 (0.48)	37.42 (0.54)	38.97 (0.51)
CP6	42.32 (0.61)	42.16 (0.48)	38.80 (0.65)	38.83 (0.58)
P7	43.61 (0.51)	43.40 (0.46)	38.74 (0.61)	39.31 (0.57)
P3	42.80 (0.59)	43.06 (0.56)	39.11 (0.61)	38.00 (0.67)
Pz	41.39 (0.54)	41.57 (0.55)	37.98 (0.54)	37.59 (0.56)
P4	42.49 (0.48)	41.90 (0.51)	38.43 (0.60)	39.38 (0.53)
P8	42.75 (0.54)	43.00 (0.51)	38.25 (0.57)	37.88 (0.57)
PO3	43.79 (0.50)	43.04 (0.52)	38.55 (0.63)	38.56 (0.58)
PO4	42.32 (0.52)	42.91 (0.51)	38.75 (0.56)	38.37 (0.53)
O1	45.42 (0.48)	44.72 (0.51)	40.14 (0.58)	38.83 (0.60)
Oz	45.40 (0.56)	44.39 (0.55)	40.13 (0.59)	39.53 (0.53)
O2	44.70 (0.52)	44.21 (0.48)	40.45 (0.52)	39.92 (0.56)

Table 4-2. Average multiscale entropy values. Mean (and standard error) area under the multiscale entropy curve values for each electrode and condition.

Composite reliability coefficients				
*OXTR*m	Auditory MSE	Visual MSE	Verbal Behav	Visual Behav
0.98	0.86	0.87	0.89	0.85
R^2 coefficients				
*OXTR*m	Auditory MSE	Visual MSE	Verbal Behav	Visual Behav
-	.02	.00	.13	.05

Table 4-3. Model fit statistics. Composite reliability coefficients reflecting internal consistency and reliability and R^2 coefficients reflecting explanatory power for each construct and model. *OXTR*m, *OXTR* DNA methylation; MSE, multiscale entropy Social – Non-Social difference score; Verbal Behav, social communication abilities; Visual Behav, social signal detection abilities.

5 General Discussion

5.1 Brain signal entropy is a powerful indicator of behavioral and developmental outcomes

Across three studies, we provide evidence that brain signal entropy during social perception links early-life individual differences in the endogenous oxytocinergic system and social behavioral outcomes. The current findings critically extend a growing body of research highlighting brain signal entropy as a powerful indicator of behavioral and developmental outcomes when compared to other measures of neural variability[53,67,68,104]. In our analyses, we compared the explanatory power of two measures of brain signal variability – standard deviation (SD) and multiscale entropy (MSE) in Study 1 – and find that only MSE shows significant links between *OXTR* methylation and infant behavior. SD, a measure of overall distributional width, has been an effective measure for identifying group-level differences between healthy and clinical populations[54,55,65] or young and old adults[60,74]. However, we may have found significant results with MSE and not SD in our sample of healthy infants because MSE is sensitive to temporal dependencies in a time series (Figure 1-5) and is measured across multiple time scales. These distinctions may enable MSE to index neurodevelopmental changes that occur very early in life or are indicative of individual differences within even the healthy range of the continuum of human social behavior. Investigations of individual time scales (Study 1) reveal a particular importance for entropy at time scales within the alpha band (8 to 13 Hz) impacting behavioral outcomes. Prior research suggests that entropy in these coarser time scales is

driven by long-range integration between distributed neuronal populations and associated with early life development[46].

In addition to understanding what measures of neural variability are capable of explaining developmental or behavioral differences, it is also important to understand when neural variability is exploited to benefit perception or behavior. Neural activity can be categorized into two primary states: spontaneous ongoing brain activity, considered the default state of the brain, and evoked brain activity that occurs in response to specific stimulation. It is thought that ongoing variability predominates in the brain, and evoked variability represents a relatively small proportion of overall variability that operates on top of ongoing variability to enable relevant behaviors[37], perhaps by optimizing sensory encoding and enhancing subsequent representations[105]. Our MSE results are in line with this understanding of neural variability. Infants that show greater ongoing MSE (Study 1) receive more positive behavioral ratings across social and non-social contexts, perhaps reflecting a more dynamic, flexible neural system in general (trait) among these infants. However, infants that show higher MSE during social perception, specifically, (state) might show enhanced social behaviors (Studies 1 and 2) because they are able to build better perceptual and cognitive representations of complex social stimuli, enabling particular sensitivity and flexibility to social stimuli. Results from our adults in Study 3 also support a role for brain signal entropy in increasing sensitivity to social information. We found a positive association between signal entropy and biological motion perceptual threshold such that those who displayed a more entropic response specifically during visual social perception were more sensitive to these visual social cues.

Ongoing and evoked activity are understood to be intricately linked[49], and indeed we find evoked and ongoing MSE are significantly correlated across all electrodes (Study 1). These findings corroborate other research[105] showing that brain signal entropy reflects both trait-like differences across individuals and state-like variability within an individual.

5.2 The relative importance of auditory and visual social information across development

In Study 2, we find a modality-specific effect at 4 months of age such that only social auditory, and not visual, perception is associated with *OXTR* methylation and infant verbal behavior. However, in our adult sample, while behavioral associations still showed modality specificity, brain signal entropy in both the visual and auditory modalities emerged as significant paths. Greater entropy during social auditory perception in adults was associated with enhanced social communication abilities, and greater entropy during social visual perception in adults was associated with increased ability to discriminate point-light displays of biological motion.

Converging lines of research suggest that infants initially rely primarily on auditory cues for social perception[106]. For example, 5-month-old infants consistently respond differentially to positive and negative voices but not faces[107], suggesting infants are more sensitive to voices than faces in early infancy. In a social referencing paradigm in which infants use the emotional expression of their mother to regulate their own behavior, mother's vocalized fear alone, but not fearful face alone, towards an object was sufficient for 12-month-old infants to avoid the object[108].

This auditory dominance in infancy is unsurprising. As with many mammals, the auditory system develops much earlier than the visual system[109], and in humans visual acuity does not reach adult levels until the third year of life[110]. Conversely, by adulthood, both visual and auditory stimuli act as important social cues. For example, visual information, whether facial movements[111] or gestures[112], enhances the audibility of speech, and adults use information in both faces and voices to make reliable judgments about conspecifics[113].

Our context-specific results support the hypothesis that neural variability is exploited to benefit perception or behavior in a developmentally-appropriate manner. Perhaps infants show higher brain signal entropy during social auditory perception because their perceptual experience with that stimulus class enables better cognitive representations, which positively impacts their own vocalization behaviors.

5.3 Tissue considerations for epigenetic associations with measures of moment-to-moment brain signal variability

It is notable that only our adult data failed to show direct paths between *OXTR* methylation and brain signal entropy. These results are contrary to data from our two infant studies, which demonstrated that infants with lower levels of *OXTR* methylation (presumed increased access to endogenous oxytocin) showed enhanced brain signal entropy during social perception. These results are also contrary to our prior adult work, which found individual differences in *OXTR* methylation were associated with differential blood oxygen level dependent (BOLD) neural response within networks involved in social perception[28,30].

A potential explanation for this discrepancy lies within the tissue assayed across samples; we assayed *OXTR* methylation for our infant samples from saliva, whereas we assayed *OXTR* methylation for our adult sample from peripheral blood mononuclear cells. Although we established a significant correlation in *OXTR* methylation levels across these tissue types in a large adult sample in Study 1 (Figure 2-4), there may be divergent developmental and/or temporodynamical differences in these tissues that were not captured by our correlational assay in adults. For example, a study of salivary cellular content across age groups found that children's saliva contained a significantly higher proportion of buccal epithelial cells than adults' saliva[114]. This difference may be significant for using saliva as a proxy for brain (the causal tissue for behavior) in epigenetic research because both buccal epithelial cells and neurons are derived from the ectodermal layer during development[115].

Emerging evidence from our labs suggest that *OXTR* methylation derived from saliva, but not blood, shows significant cyclical variation in menstruating and pregnant women (data unpublished). Therefore, salivary *OXTR* methylation levels may report on dynamic changes within the oxytocinergic system that occur with early-life development or that are capable of accounting for variance in moment-to-moment brain signal fluctuations during social perception. Conversely, blood *OXTR* methylation levels may reflect more systemic, trait levels that can account for individual differences in established brain network patterns in adulthood. Future longitudinal work that tracks associations between *OXTR* methylation and brain signal entropy from infancy to adulthood in the same

tissue is necessary to distinguish whether developmental or methodological factors account for this discrepancy.

5.4 Implications

Our results have important implications for our understanding of neurodevelopmental disorders such as autism. Across all three studies, we find the highest loadings for socially-evoked MSE over frontal and temporal electrodes, indicating variability in these regions most accounts for our epigene-brain-behavior associations. These regions are directly implicated in the oxytocinergic signaling pathway[116] and are critical for supporting social-cognitive processes[117] that emerge early in infancy[8]. Individuals with autism – a neurodevelopmental disorder marked by social impairment – show atypical neural development, particularly in frontal and temporal lobes[118]. These differences are thought to be reflected in altered brain signal entropy that occurs in autism[53,119] even before diagnostic behaviors emerge[59,104]. Differences within the oxytocinergic system are also implicated in autism, including increased *OXTR* methylation in both the brain and blood at site -934[27]. Results of the present studies may provide the foundation for a unifying, mechanistic account of social neurodevelopment. Optimal levels of brain signal entropy are linked to enhanced social-behavioral outcomes – an association that persists from infancy to adulthood and may be driven by early-life epigenetic differences within the oxytocinergic system.

5.5 Conclusions

Understanding how the brain develops to form accurate models of the external world and generate appropriate behavioral responses is a significant and critical question of widespread multidisciplinary interest. Social information is particularly complex and

dynamic, and the ability to perceive, interpret, elicit, and respond to social information is critical for an infant's ability to survive, learn, and form critical social relationships[120]. The failure to form adequate social relationships is one of the greatest risk factors for mortality, akin to smoking fifteen cigarettes a day[121]. Therefore understanding the neurobiological factors that support successful social functioning across the lifespan is an important goal with widespread multidisciplinary interest[122].

Our results suggest a mechanism by which early-life individual differences in the endogenous oxytocinergic system may drive unique neurodevelopmental trajectories affecting social abilities throughout the lifespan. These results hold implications for identifying individuals at risk for atypical development before behavioral manifestations of disorder occur and suggest potential biomarkers with probable diagnostic, therapeutic, and prognostic value.

6 References

1. Wang, S. & Adolphs, R. Social Saliency. in *Computational and Cognitive Neuroscience of Vision* (ed. Zhao, Q.) 171–193 (Springer, 2017). doi:10.1007/978-981-10-0213-7_8
2. Reid, V. M. *et al.* The Human Fetus Preferentially Engages with Face-like Visual Stimuli. (2017). doi:10.1016/j.cub.2017.05.044
3. Goren, C. C., Sarty, M. & Wu, P. Y. K. Visual following and pattern discrimination of face-like stimuli by newborn infants. *Pediatrics* **56,** 544–549 (1975).
4. Johnson, M. H., Dziurawiec, S., Ellis, H. & Morton, J. Newborns' preferential tracking of face-like stimuli and its subsequent decline. *Cognition* **40,** 1–19 (1991).
5. McKone, E., Crookes, K. & Kanwisher, N. The Cognitive and Neural Development of Face Recognition in Humans. in *The Cognitive Neurosciences* (ed. Gazzaniga, M. S.) 467–482 (MIT Press, 2009).
6. DeCasper, A. J. & Fifer, W. P. Of human bonding: newborns prefer their mothers' voices. *Science (80-.).* **208,** 1174–6 (1980).
7. Vouloumanos, A., Hauser, M. D., Werker, J. F. & Martin, A. The tuning of human neonates' preference for speech. *Child Dev.* **81,** 517–527 (2010).
8. Grossmann, T. The development of social brain functions in infancy. *Psychol. Bull.* **141,** 1266–1287 (2015).
9. Johnson, M. H., Grossmann, T. & Cohen, K. K. Mapping functional brain development: Building a social brain through interactive specialization. *Dev. Psychol.* **45,** 151–159 (2009).

10. Chita-Tegmark, M. Social attention in ASD: A review and meta-analysis of eye-tracking studies. *Res. Dev. Disabil.* **48,** 79–93 (2016).

11. Klin, A., Lin, D. J., Gorrindo, P., Ramsay, G. & Jones, W. Two-year-olds with autism orient to non-social contingencies rather than biological motion. *Nature* **459,** 257–261 (2009).

12. Klin, A. *et al.* Visual Fixation Patterns During Viewing of Naturalistic Social Situations as Predictors of Social Competence in Individuals With Autism. *Arch. Gen. Psychiatry* **59,** 809 (2002).

13. Jones, W. & Klin, A. Attention to eyes is present but in decline in 2-6-month-old infants later diagnosed with autism. *Nature* **504,** 427–31 (2013).

14. Baron-Cohen, S., Wheelwright, S., Skinner, R., Martin, J. & Clubley, E. The Autism-Spectrum Quotient (AQ): Evidence from Asperger Syndrome/High-Functioning Autism, Males and Females, Scientists and Mathematicians. *J. Autism Dev. Disord.* **31,** 5–17 (2001).

15. Hoekstra, R. A., Bartels, M., Verweij, C. J. H. & Boomsma, D. I. Heritability of autistic traits in the general population. *Arch. Pediatr. Adolesc. Med.* **161,** 372–377 (2007).

16. Parish-Morris, J. *et al.* Visual attention to dynamic faces and objects is linked to face processing skills: A combined study of children with autism and controls. *Front. Psychol.* **4,** 185 (2013).

17. Pavlova, M. A. Biological motion processing as a hallmark of social cognition. *Cereb. Cortex* **22,** 981–995 (2012).

18. Puglia, M. H. & Morris, J. P. Neural response to biological motion in healthy adults varies as a function of autistic-like traits. *Front. Neurosci.* **11,** (2017).

19. MacDonald, K. & MacDonald, T. M. The peptide that binds. *Harv. Rev. Psychiatry* **18,** 1–21 (2010).

20. Carter, C. S. Oxytocin Pathways and the Evolution of Human Behavior. *Annu. Rev. Psychol* **65,** 17–39 (2014).

21. Ross, H. E. & Young, L. J. Oxytocin and the neural mechanisms regulating social cognition and affiliative behavior. *Front. Neuroendocrinol.* **30,** 534–547 (2009).

22. Feldman, R., Weller, A., Zagoory-Sharon, O. & Levine, A. Evidence for a neuroendocrinological foundation of human affiliation: Plasma oxytocin levels across pregnancy and the postpartum period predict mother-infant bonding. *Psychol. Sci.* **18,** 965–970 (2007).

23. Guastella, A. J., Mitchell, P. B. & Dadds, M. R. Oxytocin Increases Gaze to the Eye Region of Human Faces. *Biol. Psychiatry* **63,** 3–5 (2008).

24. Shamay-Tsoory, S. G. *et al.* Intranasal Administration of Oxytocin Increases Envy and Schadenfreude (Gloating). *Biol. Psychiatry* **66,** 864–870 (2009).

25. Shamay-Tsoory, S. G. & Abu-Akel, A. The Social Salience Hypothesis of Oxytocin. *Biol. Psychiatry* **79,** 194–202 (2016).

26. Gimpl, G., Fahrenholz, F. & Gene, C. The Oxytocin Receptor System: Structure, function, and regulation. *Physiol. Rev.* **81,** 629–683 (2001).

27. Gregory, S. G. *et al.* Genomic and epigenetic evidence for oxytocin receptor deficiency in autism. *BMC Med.* **7,** 62 (2009).

28. Puglia, M. H., Lillard, T. S., Morris, J. P. & Connelly, J. J. Epigenetic modification of the oxytocin receptor gene influences the perception of anger and fear in the human brain. *Proc. Natl. Acad. Sci.* **112,** 3308–3313 (2015).

29. Kusui, C. *et al.* DNA Methylation of the Human Oxytocin Receptor Gene Promoter Regulates Tissue-Specific Gene Suppression. *Biochem. Biophys. Res. Commun.* **289,** 681–686 (2001).

30. Puglia, M. H., Connelly, J. J. & Morris, J. P. Epigenetic regulation of the oxytocin receptor is associated with neural response during selective social attention. *Transl. Psychiatry* **8,** 116 (2018).

31. Owen, S. F. *et al.* Oxytocin enhances hippocampal spike transmission by modulating fast-spiking interneurons. *Nature* **500,** 458–62 (2013).

32. Marlin, B. J., Mitre, M., D'amour, J. A., Chao, M. V & Froemke, R. C. Oxytocin enables maternal behaviour by balancing cortical inhibition. *Nature* **520,** 499–504 (2015).

33. Maier, P., Kaiser, M. E., Grinevich, V., Draguhn, A. & Both, M. Differential effects of oxytocin on mouse hippocampal oscillations in vitro. *Eur. J. Neurosci.* **44,** 2885–2898 (2016).

34. Mühlethaler, M., Charpak, S. & Dreifuss, J. J. Contrasting effects of neurohypophysial peptides on pyramidal and non-pyramidal neurones in the rat hippocampus. *Brain Res.* **308,** 97–107 (1984).

35. Faisal, A. A., Selen, L. P. J. & Wolpert, D. M. Noise in the nervous system. *Nat. Rev. Neurosci.* **9,** 292–303 (2008).

36. Ward, L. M., Doesburg, S. M., Kitajo, K., MacLean, S. E. & Roggeveen, A. B. Neural synchrony in stochastic resonance, attention, and consciousness. *Can. J. Exp. Psychol. Can. Psychol. expérimentale* **60,** 319 (2006).

37. Garrett, D. D. *et al.* Moment-to-moment brain signal variability: A next frontier in human brain mapping? *Neurosci. Biobehav. Rev.* **37,** 610–624 (2013).

38. Stein, R. B., Gossen, E. R. & Jones, K. E. Neuronal variability: noise or part of the signal? *Nat. Rev. Neurosci.* **6,** 389–397 (2005).

39. Garrett, D. D., McIntosh, A. R. & Grady, C. L. Moment-to-moment signal variability in the human brain can inform models of stochastic facilitation now. *Nat. Rev. Neurosci.* **12,** 612–612 (2011).

40. Heisz, J. J., Gould, M. & McIntosh, A. R. Age-related shift in neural complexity related to task performance and physical activity. *J. Cogn. Neurosci.* **27,** 605–613 (2015).

41. Lippé, S., Kovacevic, N. & McIntosh, A. R. Differential maturation of brain signal complexity in the human auditory and visual system. *Front. Hum. Neurosci.* **3,** 48 (2009).

42. McIntosh, A. R., Kovacevic, N. & Itier, R. J. Increased brain signal variability accompanies lower behavioral variability in development. *PLoS Comput. Biol.* **4,** e1000106 (2008).

43. Vakorin, V. A. *et al.* Exploring Age-Related Changes in Dynamical Non-Stationarity in Electroencephalographic Signals during Early Adolescence. *PLoS One* **8,** e57217 (2013).

44. Garrett, D. D., Kovacevic, N., McIntosh, A. R. & Grady, C. L. The modulation of BOLD variability between cognitive states varies by age and processing speed. *Cereb. Cortex* **23,** 684–693 (2013).

45. Polizzotto, N. R., Takahashi, T., Walker, C. P. & Cho, R. Y. Wide range multiscale entropy changes through development. *Entropy* **18,** 12 (2016).

46. Zhang, D. *et al.* Neurodevelopment in newborns: a sample entropy analysis of electroencephalogram. *Physiol. Meas.* **30,** 491–504 (2009).

47. Garrett, D. D., Kovacevic, N., McIntosh, A. R. & Grady, C. L. The Importance of Being Variable. *J. Neurosci.* **31,** 4496–4503 (2011).

48. Mills, T., Taylor, M. J. & McIntosh, A. R. Brain Noise Is Task Dependent and Region Specific. *J Neurophysiol* **104,** 2667–2676 (2010).

49. Shew, W. L., Yang, H., Petermann, T., Roy, R. & Plenz, D. Neuronal Avalanches Imply Maximum Dynamic Range in Cortical Networks at Criticality. *J. Neurosci.* **29,** 15595–15600 (2009).

50. Fuchs, E., Ayali, A., Robinson, A., Hulata, E. & Ben-Jacob, E. Coemergence of regularity and complexity during neural network development. *Dev. Neurobiol.* **67,** 1802–1814 (2007).

51. Mišić, B. *et al.* Coordinated information generation and mental flexibility: Large-scale network disruption in children with autism. *Cereb. Cortex* **25,** 2815–2827 (2015).

52. Takahashi, T. Complexity of spontaneous brain activity in mental disorders. *Prog. Neuro-Psychopharmacology Biol. Psychiatry* **45,** 258–266 (2013).

53. Catarino, A., Churches, O., Baron-Cohen, S., Andrade, A. & Ring, H. Atypical EEG complexity in autism spectrum conditions: A multiscale entropy analysis. *Clin. Neurophysiol.* **122,** 2375–2383 (2011).

54. Dinstein, I. *et al.* Unreliable Evoked Responses in Autism. *Neuron* **75,** 981–991 (2012).

55. Milne, E. Increased intra-participant variability in children with autistic spectrum disorders: Evidence from single-trial analysis of evoked EEG. *Front. Psychol.* **2,** 51 (2011).

56. Takahashi, T. *et al.* Enhanced brain signal variability in children with autism spectrum disorder during early childhood. *Hum. Brain Mapp.* **37,** 1038–1050 (2016).

57. Ghanbari, Y. *et al.* Joint Analysis of Band-Specific Functional Connectivity and Signal Complexity in Autism. *J. Autism Dev. Disord.* **45,** 1–17 (2013).

58. Kulisek, R. *et al.* Nonlinear analysis of the sleep EEG in children with pervasive developmental disorder. *Neuro Endocrinol. Lett.* **29,** 512–517 (2008).

59. Bosl, W., Tierney, A., Tager-Flusberg, H. & Nelson, C. EEG complexity as a biomarker for autism spectrum disorder risk. *BMC Med.* **9,** 18 (2011).

60. Garrett, D. D., Kovacevic, N., McIntosh, A. R. & Grady, C. L. Blood Oxygen Level-Dependent Signal Variability Is More than Just Noise. *J. Neurosci.* **30,** 4914–4921 (2010).

61. Costa, M., Goldberger, A. L. & Peng, C.-K. Multiscale Entropy Analysis of Complex Physiologic Time Series. *Phys. Rev. Lett.* **89,** 068102 (2002).

62. Nikulin, V. V & Brismar, T. Comment on 'Multiscale Entropy Analysis of Complex Physiologic Time Series'. *Phys. Rev. Lett.* **92,** 89803 (2004).

63. Grandy, T. H., Garrett, D. D., Schmiedek, F. & Werkle-Bergner, M. On the estimation of brain signal entropy from sparse neuroimaging data. *Sci. Rep.* **6,** 23073 (2016).

64. Costa, M., Goldberger, A. L. & Peng, C. K. Multiscale entropy analysis of biological signals. *Phys. Rev. E* **71,** 021906 (2005).

65. Haigh, S. M., Heeger, D. J., Dinstein, I., Minshew, N. & Behrmann, M. Cortical Variability in the Sensory-Evoked Response in Autism. *J. Autism Dev. Disord.* **45,** 1176–1190 (2015).

66. McIntosh, A. R. *et al.* The development of a noisy brain. *Archives Italiennes de Biologie* **148,** 323–337 (2010).

67. Miskovic, V., Owens, M., Kuntzelman, K. & Gibb, B. E. Charting moment-to-moment brain signal variability from early to late childhood. *Cortex.* **83,** 51–61 (2016).

68. Shafiei, G. *et al.* Dopamine Signaling Modulates the Stability and Integration of Intrinsic Brain Networks. *Cereb. Cortex* **29,** 397–409 (2019).

69. Jack, A., Connelly, J. J., Morris, J. P. & James, P. DNA methylation of the oxytocin receptor gene predicts neural response to ambiguous social stimuli. *Front. Hum. Neurosci.* **6,** 280 (2012).

70. Perkeybile, A. M. *et al.* Early nurture epigenetically tunes the oxytocin receptor. *Psychoneuroendocrinology* (2018). doi:10.1016/J.PSYNEUEN.2018.08.037

71. *Handbook of Partial Least Squares*. (Springer Berlin Heidelberg, 2010). doi:10.1007/978-3-540-32827-8

72. Ravand, H. Partial Least Squares Structural Equation Modeling with R. *Pract. Assessment, Res. Eval.* **21,** 1–16 (2016).

73. McIntosh, A. R. & Lobaugh, N. J. Partial least squares analysis of neuroimaging data: Applications and advances. *Neuroimage* **23,** S250-63 (2004).

74. Grady, C. L. & Garrett, D. D. Understanding variability in the BOLD signal and why it matters for aging. *Brain Imaging Behav.* **8,** 274–283 (2014).

75. Missana, M., Altvater-Mackensen, N. & Grossmann, T. Neural correlates of infants' sensitivity to vocal expressions of peers. *Dev. Cogn. Neurosci.* **26,** 39–44 (2017).

76. Gartstein, M. A. & Rothbart, M. K. Studying infant temperament via the Revised Infant Behavior Questionnaire. *Infant Behav. Dev.* **26,** 64–86 (2003).

77. Delorme, A. & Makeig, S. EEGLAB: An open source toolbox for analysis of single-trial EEG dynamics including independent component analysis. *J. Neurosci. Methods* **134,** 9–21 (2004).

78. Stets, M., Stahl, D. & Reid, V. M. A meta-analysis investigating factors underlying attrition rates in infant ERP studies. *Dev. Neuropsychol.* **37,** 226–252 (2012).

79. Revelle, W. R. psych: Procedures for Personality and Psychological Research. (2017).

80. R Core Team. R: A language and environment for statistical computing. (2016).

81. Kock, N. WarpPLS. (2018).

82. Bagozzi, R. P. & Yi, Y. On the evaluation of structural equation models. *J. Acad.*

Mark. Sci. **16,** 74–94 (1988).

83. Carter, C. S., Grippo, A. J., Pournajafi-Nazarloo, H., Ruscio, M. G. & Porges, S. W. Oxytocin, vasopressin and sociality. *Prog. Brain Res.* **170,** 331–336 (2008).

84. Chin, W. W. & Newsted, P. R. Structural Equation Modeling Analysis with Small Samples Using Partial Least Squares. in *Statistical strategies for small sample research* (ed. Hoyle, R.) 307–341 (Sage Publications, 1999).

85. Faul, F., Erdfelder, E., Buchner, A. & Lang, A.-G. Statistical power analyses using G*Power 3.1: tests for correlation and regression analyses. *Behav. Res. Methods* **41,** 1149–60 (2009).

86. Chevallier, C. *et al.* Measuring social attention and motivation in autism spectrum disorder using eye-tracking: Stimulus type matters. *Autism Res.* **8,** 620–628 (2015).

87. Brainard, D. H. The Psychophysics Toolbox. *Spat. Vis.* **10,** 443–446 (1997).

88. Olsen, A. *The Tobii I-VT Fixation Filter Algorithm Description*. (2012).

89. Leppänen, J. M., Forssman, L., Kaatiala, J., Yrttiaho, S. & Wass, S. Widely applicable MATLAB routines for automated analysis of saccadic reaction times. *Behav. Res. Methods* **47,** 538 (2015).

90. Willenbockel, V. *et al.* Controlling low-level image properties: the SHINE toolbox. *Behav Res Methods* **42,** 671–684 (2010).

91. Brent, M. R. & Siskind, J. M. The role of exposure to isolated words in early vocabulary development. *Cognition* **81,** B33–B44 (2001).

92. Boersma, P. & Weenink, D. Praat: doing Phonetics by Computer. (2017).

93. Lopez-Calderon, J. & Luck, S. J. ERPLAB: an open-source toolbox for the analysis

of event-related potentials. *Front. Hum. Neurosci.* **8,** 213 (2014).

94. Bujang, M. A. & Baharum, N. *A simplified guide to determination of sample size requirements for estimating the value of intraclass correlation coefficient: a review*. *Archives of Orofacial Sciences The Journal of the School of Dental Sciences, USM Arch Orofac Sci* **12,** (2017).

95. Zhang, F. F. *et al.* Significant differences in global genomic DNA methylation by gender and race/ethnicity in peripheral blood. *Epigenetics* **6,** 623–629 (2011).

96. Kenkel, W. M. *et al.* Behavioral and epigenetic consequences of oxytocin treatment at birth. *Sci. Adv.* **5,** eaav2244 (2019).

97. Gamer, M., Lemon, Singh, J. & Fellows Puspendra Singh, I. irr: Various Coefficients of Interrater Reliability and Agreement. (2019).

98. Grossman, E. D., Blake, R. & Kim, C.-Y. Learning to See Biological Motion: Brain Activity Parallels Behavior. *J. Cogn. Neurosci.* **16,** 1669–1679 (2004).

99. Watson, A. B. & Pelli, D. G. *QUEST: A Bayesian adaptive psychometric method*. *Perception & Psychophysics* **33,** (1983).

100. Jung, E. L., Zadbood, A., Lee, S.-H., Tomarken, A. J. & Blake, R. Individual differences in the perception of biological motion and fragmented figures are not correlated. *Front. Psychol.* **4,** 795 (2013).

101. Baron-Cohen, S., Wheelwright, S., Hill, J., Raste, Y. & Plumb, I. The 'Reading the Mind in the Eyes' Test revised version: a study with normal adults, and adults with Asperger syndrome or high-functioning autism. *J. Child Psychol. Psychiatry.* **42,** 241–51 (2001).

102. Domes, G., Heinrichs, M., Michel, A., Berger, C. & Herpertz, S. C. Oxytocin Improves 'Mind-Reading' in Humans. *Biol. Psychiatry* **61,** 731–733 (2007).

103. Hurley, R. S. E., Losh, M., Parlier, M., Reznick, J. S. & Piven, J. The broad autism phenotype questionnaire. *J. Autism Dev. Disord.* **37,** 1679–1690 (2007).

104. Bosl, W. J., Tager-Flusberg, H. & Nelson, C. A. EEG Analytics for Early Detection of Autism Spectrum Disorder: A data-driven approach. *Sci. Rep.* **8,** 6828 (2018).

105. Waschke, L., Wöstmann, M. & Obleser, J. States and traits of neural irregularity in the age-varying human brain. *Sci. Rep.* **7,** 17381 (2017).

106. Walker-Andrews, A. S. Infants' perception of expressive behaviors: Differentiation of multimodal information. *Psychol. Bull.* **121,** 437–456 (1997).

107. Fernald, A. Human Maternal Vocalizations to Infants as Biologically Relevant Signals : An Evolutionary Perspective. (2008).

108. Mumme, D. L., Fernald, A. & Herrera, C. Infants' Responses to Facial and Vocal Emotional Signals in a Social Referencing Paradigm. *Child Dev.* **67,** 3219–3237 (1996).

109. Gottlieb, G. Ontogenesis of sensory function in birds and mammals. *biopsychology Dev.* **67,** (1971).

110. Catford, G. V & Oliver, A. Development of visual acuity. *Arch. Dis. Child.* **48,** 47–50 (1973).

111. Sumby, W. H. & Pollack, I. Visual Contribution to Speech Intelligibility in Noise. *J. Acoust. Soc. Am.* **26,** 212–215 (1954).

112. Hubbard, A. L., Wilson, S. M., Callan, D. E. & Dapretto, M. Giving Speech a Hand:

Gesture Modulates Activity in Auditory Cortex During Speech Perception. (2008). doi:10.1002/hbm.20565

113. Rezlescu, C. *et al.* Dominant Voices and Attractive Faces: The Contribution of Visual and Auditory Information to Integrated Person Impressions. *J. Nonverbal Behav.* **39,** 355–370 (2015).

114. Theda, C. *et al.* Quantitation of the cellular content of saliva and buccal swab samples. *Sci. Rep.* **8,** 6944 (2018).

115. Smith, A. K. *et al.* DNA extracted from saliva for methylation studies of psychiatric traits: Evidence tissue specificity and relatedness to brain. *Am. J. Med. Genet. Part B Neuropsychiatr. Genet.* **168,** 36–44 (2015).

116. Meyer-Lindenberg, A., Domes, G., Kirsch, P. & Heinrichs, M. Oxytocin and vasopressin in the human brain: social neuropeptides for translational medicine. *Nat. Rev. Neurosci.* **12,** 524–538 (2011).

117. Adolphs, R. The social brain: neural basis of social knowledge. *Annu. Rev. Psychol.* **60,** 693–716 (2009).

118. Hoppenbrouwers, M., Vandermosten, M. & Boets, B. Autism as a disconnection syndrome: A qualitative and quantitative review of diffusion tensor imaging studies. *Res. Autism Spectr. Disord.* **8,** 387–412 (2014).

119. Chu, Y.-J. *et al.* The Potential Application of Multiscale Entropy Analysis of Electroencephalography in Children with Neurological and Neuropsychiatric Disorders. *Entropy* **19,** 428 (2017).

120. Nelson III, C. A., Furtado, E. A., Fox, N. A. & Zeanah Jr., C. H. The Deprived

Human Brain. *Am. Sci.* **97,** 222 (2009).

121. Holt-Lunstad, J., Smith, T. B. & Layton, J. B. Social relationships and mortality risk: A meta-analytic review. *PLoS Med.* **7,** e1000316 (2010).

122. Fabiani, M. It was the best of times, it was the worst of times: A psychophysiologist's view of cognitive aging. *Psychophysiology* **49,** 283–304 (2012).